CalVal Envisat
CLS.DOS/NT/08.006
Version : 1rev0, December 21, 2007
Nomenclature : SALP-RP-MA-EA-21516-CLS

Ramonville, December 21, 2007

Envisat RA2/MWR ocean data validation and cross-calibration activities. Yearly report 2007.

Contract No 60453/00 - lot2.C

	AUTHORS	COMPANY	DATE	INITIALS
WRITTEN BY	Y. Faugere	CLS		
	N. Granier	CLS		
	A. Ollivier	CLS		
APPROVED BY	J.Dorandeu	CLS		
QUALITY VISA	DT/AQM	CLS		
APPLICATION AUTHORISED BY				

CLS - 8-10 Rue Hermès - Parc Technologique du Canal - 31520 Ramonville St-Agne - FRANCE
Telephone 33 5 61 39 47 00 / Fax 33 5 61 75 10 14

DISTRIBUTION LIST

COMPANY	NAMES	COPIES
CLS/DOS	J.DORANDEU	1 electonic copy
	V.ROSMORDUC	1 electonic copy
	P.ESCUDIER	1 electonic copy
DOC/CLS	DOCUMENTATION	1 electonic copy
CNES	P.LELOUP	1 CD
CNES	P.BOUBE	1 CD
CNES	D.CHERMAIN	1 CD
CNES	N.PICOT	1 electonic copy
CNES	J.LAMBIN	1 electonic copy
CNES	A.LOMBARD	1 electonic copy

CHRONOLOGY ISSUE

Control Initials	ISSUE	DATE	REASON FOR CHANGE
	1/0	2007/12/03	Creation

LIST OF ACRONYMS

ECMWF	European Center for Medium range Weather Forecasts
GDR-A	Geophysical Data Record version A (before cycle 41 for Envisat mission)
GDR-B	Geophysical Data Record version B (after cycle 41 for Envisat mission)
MSL	Mean Sea Level
MWR	MicroWave Radiometer
POE	Precise Orbit Estimation
SLA	Sea Level Anomalies
SSB	Sea State Bias
USO	Ultra Stable Oscillator

List of Tables

List of Figures

Contents

APPLICABLE DOCUMENTS / REFERENCE DOCUMENTS

1 Introduction

This report is an overview of Envisat validation and cross calibration studies carried out at CLS during year 2007. It is basically concerned with long-term monitoring of the Envisat altimeter system over ocean.

Envisat GDR data are routinely ingested in the Calval 1-Hz altimeter database maintained by the CLS Spatial Oceanography Division in the frame of the CNES Segment Sol Altimétrie et Orbitographie (SSALTO) and funded by ESA through F-PAC activities (SALP contract N° 60453/00 - lot2.C). In this frame, besides continuous analyses in terms of altimeter data quality, Envisat GDR Quality Assessment Reports (e.g. Faugere et al. 2004) are routinely produced in conjunction with data dissemination.

Data from GDR cycles 9 through 62 spanning five years have been used for this analysis. All relevant altimeter parameters deduced from Ocean 1 retracking, radiometer parameters and geophysical corrections are evaluated and tested.

Some of the results described here were presented in the the OSTST meeting (Hobart, March 2007), at the Envisat Symposium (Montreux, April 2007) and at the Quality Working Group (QWG) meeting (Barcelona, May and October 2007).

The work performed in terms of data quality assessment also includes cross-calibration with Jason-1 and ERS-2. This kind of comparisons between coincident altimeter missions provides a large number of estimations and consequently efficient long-term monitoring of instrument measurements. This enables the detection of instrument drifts and inter-mission biases essential to obtain a consistent multi-satellite data set. The full reprocessing of Jason-1 products in b version was completed mid-2007. Therefore, the Envisat/Jason-1 cross-calibration results were reprocessed this year.

After a preliminary section describing the data used, the report is split into 5 main sections: first, data coverage and measurement validity issues are presented. Second, monitoring of the main altimeter and radiometer parameters is performed, describing the major impact in terms of data accuracy. Then, performances are assessed and discussed with respect to the major sources of errors. Then, Envisat Sea Surface height (SSH) bias and MSL issues are analysed. Finally, an additional part presents the particular investigations that have been performed during this year.

2 Quality overview

Ra-2 instrumental status: The USO anomaly which was affecting Ra-2 data since cycle 46 disappeared during a 6 month period, cycle 56 to 61. This anomaly, which remains unexplained, reappeared on cycle 62. Since August 2006, a temporary procedure has been implemented by ESA to correct the effect of the USO anomaly. Using the proposed auxiliary files, Envisat Ra-2 data remain at the same high level of accuracy.
On the 27th of June 2007 (cycle 60) an on-board patch solving the S-Band anomaly has been successfully uploaded. Since then, no occurrence of the anomaly has been detected. This anomaly impacted about 3% of the available data on average before the upload of the patch. The S-band waveform will be hopefully reconstructed in the future versions of GDR.

Missing measurements: The unavailability of data over ocean for year 2007 is about 5.6% in average. This ratio, slightly higher than the two previous years, is due to several long RA-2 events resulting in a significant number of missing passes.
The MWR availability is stable, lower than 2% except for cycles 58 and 60 where the ratio of unavailability is greater than 5% due to ground segment anomalies.

Long term monitoring of RA-2 and MWR parameters: The ocean-1 altimeter and radiometer parameters are consistent with expected values. They have a very good stability and high performances, compared to Jason-1. A very good availability on every surface and very low editing ratios over ocean are observed since the beginning of the mission. The high frequency content of Ku-band Ra-2 parameters is very stable. A slight drift of 0.02dB/year is suspected on Sigma0 and is under investigation.

The MWR performances are still very good. Since the beginning of the mission, the instrumental parameters at 36.5 GHz have been drifting. Moreover from cycle 46 onwards, a 1.5 cm of amplitude annual signal seems to appear on the mean MWR-ECMWF time series.

SSH performance: The current standards (orbit configuration, instrumental and geophysical correction) used since September 2005 in the IPF/CMA, allow Envisat product to have a high geophysical quality. Using the provided temporary USO correction, Envisat Ra-2 data remain at the same high level of accuracy even during USO anomaly periods. The crossover analysis show that Envisat's performances are similar to Jason-1's. The SLA performance is very good, at the same level as Jason-1. The time invariant errors, observed on the crossover mean, are mainly due to gravity induced orbit errors and are well corrected by the use of a Grace Gravity model. The time varying errors have to be analysed further to confirm a possible error in the tide correction.

Mean Sea Level: The Envisat Mean Sea Level trend estimated at CLS is different from Jason-1 over the whole Envisat period. This issue has been widely investigated this year. Two potential sources of error impacting the Envisat MSL trend have been identified, the ionosphere correction and the orbit. But if the update of the ionosphere correction allows us to reduce the inconsistency with Jason-1, the use of other orbits, though homogeneous over the whole time series, is not conclusive. This study highlight moreover serious inconsistencies between MSL trend estimated from ascending and descending passes. Finally, on the two last years, Envisat and Jason-1 have the same MSL trend, which is positive.

3 Data used and processing

3.1 Data used

Envisat Geophysical Data Records (GDRs) from cycle 10 to cycle 62 have been used to derive the results presented in this report. This corresponds to a nearly five-year time period spanning from September 30th 2002 to October 29th 2007. The routine production started on September 2003 with cycle 15. In parallel, a backward reprocessing of cycles 14 to 9 was implemented. With only 7 days of available data, cycle 9 has not been used in this work. 11 GDR cycles have been produced this year: cycles 52 to 62 as part of the current processing.

The Envisat GDR data are generated using two softwares: the IPF, from Level0 to Level1B, and the CMA, from Level1B to Level2. As shown by table 1 several IPF processing chain and CMA Reference Software have been used to produce the 54 cycles of GDR. Tables 2 and 3 describe the main evolutions respectively associated with the IPF and CMA version.

Cycles	IPF version	CMA version
9 to 10	4.58	6.3
11 to 12	4.57	6.3
13 to 14	4.56	6.3
15 to 21	4.54	6.1
22 to 24	4.56	6.2
25 to 26	4.56	6.3
27 to 28	4.57	6.3
29 to 40	4.58	6.3
38 to 40 (reprocessed)	5.02	7.1
41 to 51 until pass 7	5.02	7.1
51 to 58 until pass 843	5.03	8.0
58 to 62	5.06	9.0

Table 1: *I*PF/CMA Processing version

Version	Changes
IPF 4.56	-Extrapolation of AGC value to the Waveform center (49.5) for both Ku- and S-Band -Correction for an error found in the evaluation of S band AGC
IPF 4.57	No impact on data
IPF 4.58	-Addition of a Pass Number Field in FD Level
IPF 5.02	-MWR Side Lobe correction upgrade -USO clock period units correction -Rain Flag tunning to compensate for the increase of the S band Sigma0 -Monthly IF estimation -DORIS Navigator CFI upgrade (RA-2 and MWR) -S-band anomaly flag
IPF 5.03	-Correction for an error found in the Channel 2 brightness temperature -Correction off error in the window delay (for the 80 and 20 MHz bandwidths) -S-band anomaly flag upgrade, now properly implemented
	-Correction of Rx-Fine parameter
	-MWR second channel corrected (SL correction)
IPF 5.06	none

Table 2: *I*PF changes impacting the Envisat GDR

The change from IPF 4.58/CMA6.3 to IPF 5.02/CMA7.1 strongly impacted the data. The Sea-State bias table has been recomputed ([34]) accounting for the impact of the new orbit and the new geophysical corrections (MOG2D, GOT00 ocean tide correction with the S2 component corrected once only, new wind speed algorithm from Abdalla, 2006 [1]). The new SSB correction is shifted in average by +2.0 cm in comparison with the previous one. New standards are used for the computation of the Envisat Precise Orbit Estimation. One of the main evolutions is the use of the GRACE gravity model EIGEN CG03C. This new model implies a strong reduction of the geographically correlated radial orbit errors. In order to take into account the dynamical effects and wind forcing, a new correction is computed from the MOG2D (Carrere and Lyard, 2003 [6]) barotropic model forced by pressure (without S1 and S2 constituents) and wind. The use of such a correction in the SSH strongly improves the performances. All the corresponding evolutions are detailed in [16].

Version	Changes
CMA 6	-MSS CLS01 -Rain flag -Updated OCOG retracker thresholds Ice1/Sea Ice Conf file -Sea State Bias Table file -GOT00.2 Ocean Tide Sol 1 Map file -FES 2002 Ocean Tide Sol 2 Map file -FES 2002 Tidal Loading Coeff Map
CMA 7.1	-Improving the mispointing estimation -Addition of square of the SWH in Ku and S band -Addition of GOT2000.2 loading tide -FES2004 tide and loading tide -New DEM AUX file (MACESS) merge of ACE land elevation data and Smith and Sandwell ocean bathymetry -New orbit -New SSB -new wind table -Mog2D -new S1S2 wave model in dry troposphere -GOT00.2 includes two extra waves, S1 and S2 -GIM model ionospheric correction added in the products
CMA 9	correction of an anomaly in the relative orbit field inside the product file name
	.../...

Version	Changes

Table 3: *C*MA changes impacting the Envisat GDR

3.2 Processing

To perform this quality assessment work, conventional validation tools are used including editing procedures, crossover analysis, collinear differences, and a large number of statistical monitoring and visualization tools. All these tools are integrated and maintained as part of the CNES SSALTO (Segment Sol Altimétrie et Orbitographie) ground segment and F-PAC (French Processing and Archiving Centre) tools operated at CLS premises. Each cycle is carefully routinely analyzed before data release to end users. The main data quality features are reported in a cyclic quality assessment report available on http://www.aviso.oceanobs.com/html/donnees/calval/validation_report/en/welcome_uk.html. The purpose of this document is to report the major features of the data quality from the Envisat mission.

As for all other existing altimeters, the Envisat GDR data are ingested in the Calval 1-Hz altimeter database maintained by the CLS Spatial Oceanography Division. This allows us to cross-calibrate and cross-compare Envisat data to other missions. In this study data from Jason-1 (GDRs cycles 27 to 214), ERS-2 (OPRs Cycle 78 to 108) are used. Jason-1 is the most suitable for Envisat cross calibration as it is available throughout the Envisat mission and has been extensively calibrated to T/P (Dorandeu et al., 2004b [13]). In 2007, Jason-1 GDRs cycles 1 to 135 were reprocessed in the GDR-B version in order to have an homogeneous data set [4]. Consequently, the cross-calibration between Envisat and Jason-1 were entirely reprocessed.

Comparisons between Jason-1 and Envisat altimeter and radiometer parameters have been carried out using 10-day dual crossovers for SSH comparison and 3-hour dual crossovers for altimeter and radiometer comparisons. The geographical distribution of the dual crossovers with short time lags strongly changes from one Envisat cycle to another. Indeed, contrary to Envisat which is sun-synchronous, Jason-1 observes the same place at the same local time every 12 cycles (120-day). Following the method detailed in Stum et al. (1998) [58], estimates of the differences are computed using a 120 day running window to keep a constant geographical coverage. ERS-2, flying on same ground track as Envisat only 30 minutes apart, has had a coverage limited to the North Atlantic since the failure of the on-board register in June 2003 (EOHelp message of 4 July 2003). To improve the significance of the Envisat/ERS-2 comparison, long term monitoring of altimeter parameters difference is performed on this restricted area all over the Envisat period using a repeat-track method.

Most of this work has been carried out using parameters available in the GDR products. However, a few updates have been necessary to complete the analyses:

- a method has been developped to detect data corrupted by S-Band anomaly. It has been applied until cycle 53. From cycle 54 onwards the product flag, available since cycle 51, has been used (see 4.3.1).
- a method has been developped to detect data corrupted by sea ice (see 4.3.2)
- filtered dual frequency ionosphere correction: A 300-km low pass filter is applied along track on the dual frequency ionosphere correction to reduce the noise of the correction.
- The new geophysical correction associated with version CMA7 have been updated on the whole dataset in order to have the most homogeneous time series: wind table and SSB, Mog2D , new S1S2 wave

model in dry troposphere, GOT00.2 with two extra waves, FES2004, S1 and S2

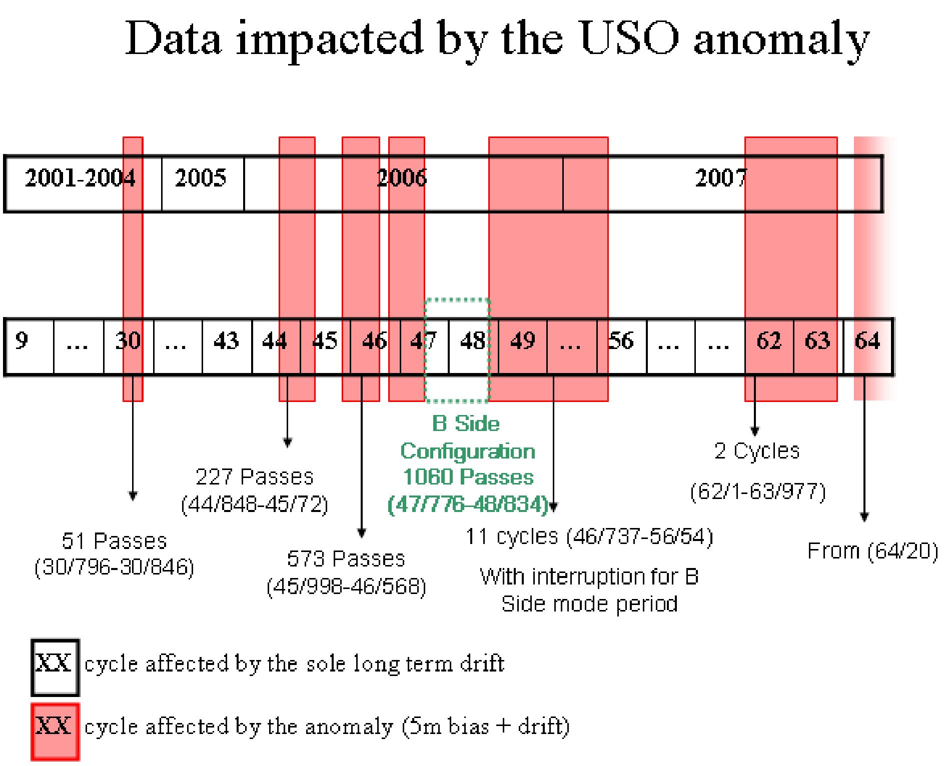

Figure 1: *Chronology of USO Correction anomaly.*

- A correction to the range is also applied. It is based on the Ultra-Stable Oscillator (USO) clock period variation correction depending on the cycle (see Figure 1):

For cycle 9 to 40, (outside of the anomaly periods): The USO clock period, which performs the computation of the Ra-2 window time delay, is affected by a drift due to the ageing of the device. The method to correct the USO clock period is described in Celani (2002 [8]). The correction is regularly updated in the IPF ground processing via an Auxiliary data file. However, due to an anomaly in the ADF format, the correction was not taken into account (Martini, 2003 [43]) in the products for cycles lower or equal 40. ESA supplies auxiliary files to allow users correcting their own database (Martini, 2003 [43]) (http://earth.esa.int/pcs/envisat/ra2/auxdata/). The distributed auxiliary correction containting the drift + bias have to be used. The distributed auxiliary correction is smoothed here over a 1-month period to filter peaks and short period variations. The supplied correction has to be subtracted from the original altimetric range (EOP-GOQ and PCF team, 2005) and consequently added to SSH

For cycle 41 to 45, (outside of the anomaly periods): The USO drift + bias is taken into account in the products. No additionnal auxiliary correction has to be used.

From cycle 46 onwards and all the previous anomaly periods: On the 1st of February 2006 (12:05:36), at the end of cycle 44, for an unknown reason a change of behaviour of the USO device occured. This anomaly has created a 5.5m jump on the range parameter and oscillations of about 20-30cm of amplitude at the orbital period. The anomaly becomes permanent on cycle 46 to 56. On the 1st of March 2007, the USO recovers in a non-anomalous mode. Between cycles 56 and 61, Ra2 data will not be affected by the anomaly. On the 27th of September 2007 (cycle 62), a new change of behaviour of the Ultra Stable Oscillator (USO) clock frequency occurred. The anomaly and associated correction is detailled in [43]. The quality assessment of these data has been performed using the USO temporary correction provided by ESA. Users are strongly advised not to use the range parameter in Ku and S Band without this correction during the anomaly periods.

- pressure values used for computing the inverse barometer and the dry troposphere corrections have been derived from the ECMWF rectangular grids. Indeed, errors due to the bathymetry, up to several centimeters near the coasts, significantly impact the accuracy the so-called gaussian grids used as input of the Envisat (and Jason-1) ground processing (e.g. Dorandeu et al., 2004b [13]).

- Jason-1 doesn't fly at the same altitude as Envisat which means that ionosphere corrections are not comparable (note that this has no impact on the other parameters (wind, waves, ...). Moreover, ERS-2 has a mono-frequency altimeter on-board. Therefore it is not possible to use these satellites to assess the Envisat ionosphere path delay. Thus the JPL GPS-based global Ionospheric Maps (GIM) containing the vertical ionospheric total electron content are used here. Note that since cycle 41 onwards, this GIM ionosphere correction is available in the GDR products. Note that GIM maps contain the vertical ionospheric total electron content in the 0-1400km altitude range.As envisat flies around 800km, the International Reference Ionosphere (IRI) model is uses to estimate the GIM correction at the altitude of Envisat:
$GIM_{[0-800]} = GIM_{[0-1400]} \times \frac{IRI_{[800]}}{IRI_{[1400]}}$

4 Missing and edited measurements

This section mainly intends to analyse the ability of the Envisat altimeter system to correctly sample ocean surfaces. This obviously includes the tracking capabilities, but also the frequency of unavailable data and the ratio of valid measurements likely to be used by applications after the editing process.

4.1 Missing measurements

From a theoretical ground track, a dedicated collocation tool allows determination of missing measurements relative to what is nominally expected. The cycle by cycle percentage of missing measurements over ocean has been plotted in figure 2. The measurement unavailability over the whole mission is about 6% in average. Thirteen cycles have more than 10% of unavailability, notably from cycle 13 to cycle 17, and cycle 47 to cycle 48. Passes 1 to 452 of cycle 15 have not been delivered because of a wrong setting of RA-2. Moreover, passes 1 to 790 of cycle 47 and passes 1 to 849 of cycle 48 have not been delivered due to RA2 RFSS configured to side B redundancy. This explains the high ratio of missing measurements for these cycles. Several long RA-2 events occurred during cycles 13, 14, 16, 17, 22, 34, 51, 53, 55, 56, 59, 62 which resulted in a significant number of missing passes. The 2007 average ratio of missing measurements over ocean is 5.6%. The significant missing data for cycle 51 is due to an interruption of the Envisat data transmission via the ESA Data Relay Satellite Artemis and a platform incident. The list of instrument and platform events is available in Part 11. Apart from instrumental and platform events, up to 3% of measurements can be missing because of data generation problems at ground segment level: LRAC or PDHS level1 data generation problems or ingestion problems on F-PAC side. The situation has been largely improved with a mean data availability of more than 95% from the beginning of 2004 (cycle 23 onwards). Notice that this ratio is slightly higher for several cycles of last year, due to several on-board anomalies. Figure 3 shows an example of missing measurements for cycle 60. The measurements which are missing over the Himalayan and Rocky montains region are due first to the IF Calibration Mode. Moreover, daily instrument switch-offs (Heater 2 mode) are performed over these regions to prevent the S-Band anomaly. Finally, it has been found that some pass segments were quasi-systematically missing. Figure 4 shows the pass segments missing more than 5 times over the 11 last cycles. Apart from that, the data retention rate is very good on every surface observed. This might be due to the tracker used by Envisat Ra-2, the Model Free Tracker (MFT).

4.2 Missing MWR data

The Envisat MWR exhibits nearly 100% (Dedieu et al., 2005) of availability since the beginning of the mission. However, MWR corrections can be missing in the GDRs due to data generation problems at ground segment level. When the Land/sea radiometer flag is set to land over ocean, it means that the radiometer data is missing. The percentage of missing MWR corrections over ocean has been plotted in figure 5. The mean value is around 1.8% but the radiometer unavailability is not constant. It is greater than 4% for cycles 14 to 19 but lower than 2% from cycle 21 onwards. From cycle 34 onwards the availability of the MWR correction is very good, except for cycles 58 and 60.

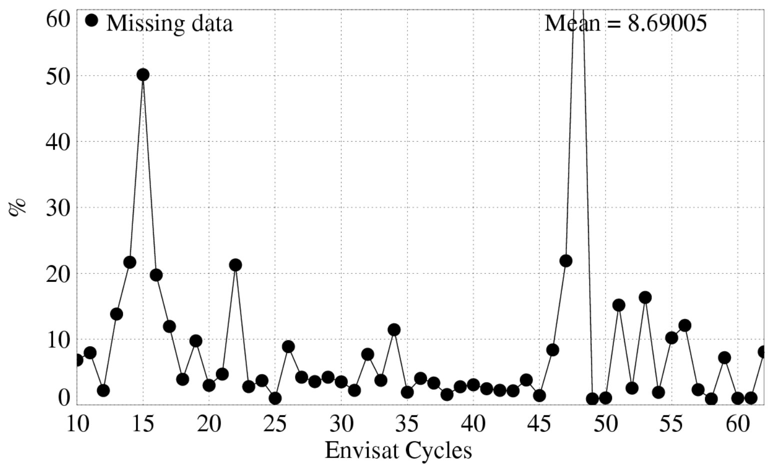

Figure 2: *Monitoring of the percentage of missing measurements relative to what is theoretically expected over ocean*

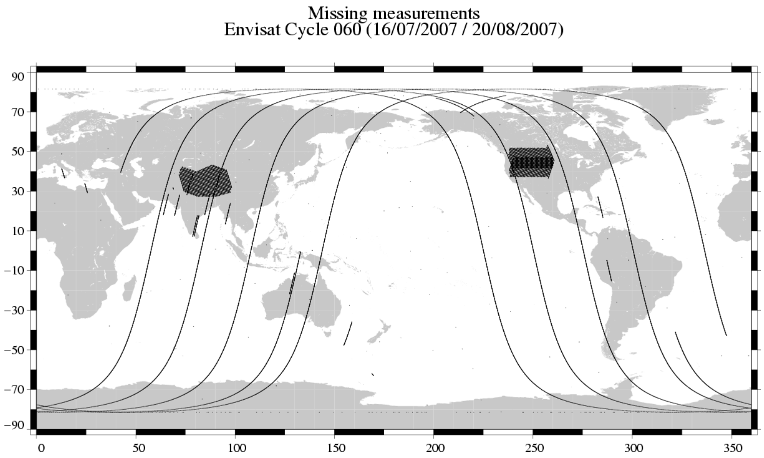

Figure 3: *Envisat missing measurements for cycle 60*

4.3 Edited measurements

Data editing is necessary to remove altimeter measurements having lower accuracy. There are 4 steps in the editing procedure. The first step of the editing procedure consists in removing data impacted by the S-Band anomaly or corrupted by sea ice. Then, measurements are edited using thresholds on several parameters. The third step uses cubic splines adjustments to the ENVISAT Sea Surface Height (SSH) to detect remaining spurious measurements. The last step consists in removing entire pass where SSH-MSS mean and standard deviation have unexpected value.

4.3.1 Measurements impacted by S-Band anomaly

During the Commissioning Phase, it has been discovered that the RA-2 data are affected by the so-called S-Band anomaly. The anomaly results in the accumulation of the S-Band echo waveforms (Laxon and Roca,

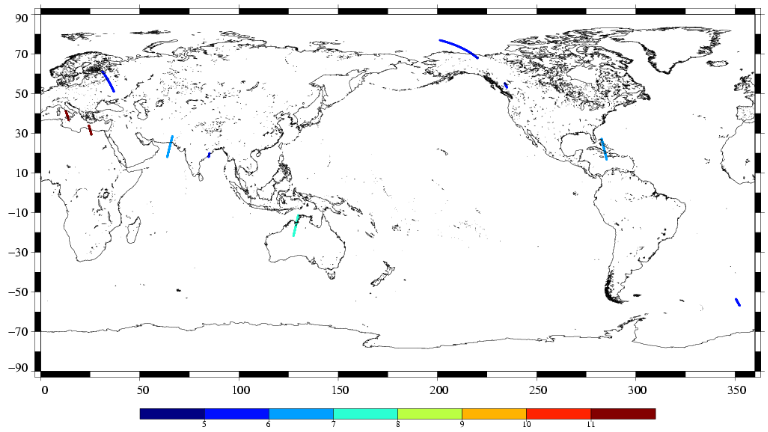

Figure 4: *Pass segments unavailable more than 5 times between cycles 52 and 62. The colour indicates the occurence of unavailability*

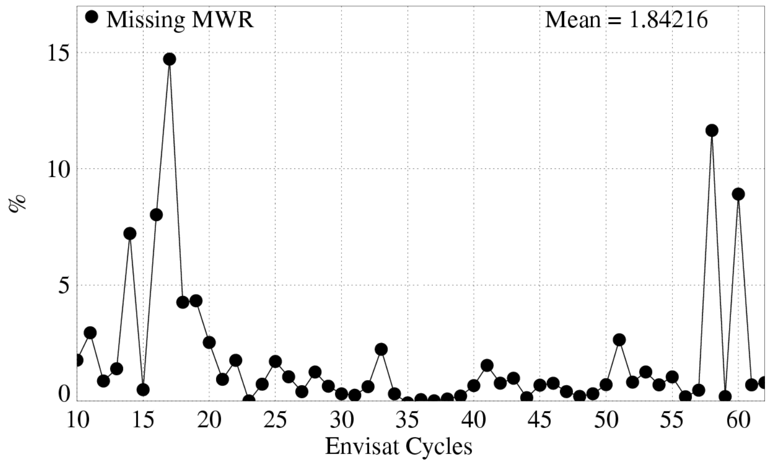

Figure 5: *Cycle per cycle percentages of missing MWR measurements*

2002 [36]). It happens randomly after an acquisition sequence and is only stopped by switching the Ra-2 in a Stand-By mode. When this anomaly occurs, the S-Band waveforms are not meaningful. Consequently, all the S-Band parameters and the Dual Frequency ionosphere correction are not reliable. Notably, the S-band Sigma0 is unrealistically high during these events. Thus applying a threshold of 5 dB on the (Ku-S) Sigma0 differences is very efficient for detecting the impacted data over ocean. The ratio of flagged measurements over ocean is plotted in figure 6. A method has been developed to flag the impacted data over all surfaces (Martini et al., 2005 [44]). This flag is available in the GDR product since cycle 51 and as been applied in our internal data base from cycle 54 onwards. A specific study is dedicated to the validation of this product flag over all the surfaces (see 8).

Between 0 and 8% of the data are impacted. From cycle 31 onwards, some modifications have been performed by ESA to decrease the duration of these events: instrument switch-offs (Heater 2 mode) are performed twice a day over the Himalayan and Rocky montain region. This prevents the S-Band anomaly from lasting more than half a day when it occurs. Thanks to this procedure the ratio of impacted data decreased from 4.2% (cycles 11 to 30) to 2.2% (cycles 31 to 38). On the 27th of June 2007 (cycle 60) an on-board patch solving the problem has been successfully uploaded. Since then no occurrences of the anomaly have been detected.

Finally, an algorithm for the S-Band waveform reconstruction has been developed which will enable recovery of data affected by the anomaly in the past. The correction will be achieved with the full mission reprocessing campaign scheduled for the second quarter of 2008.

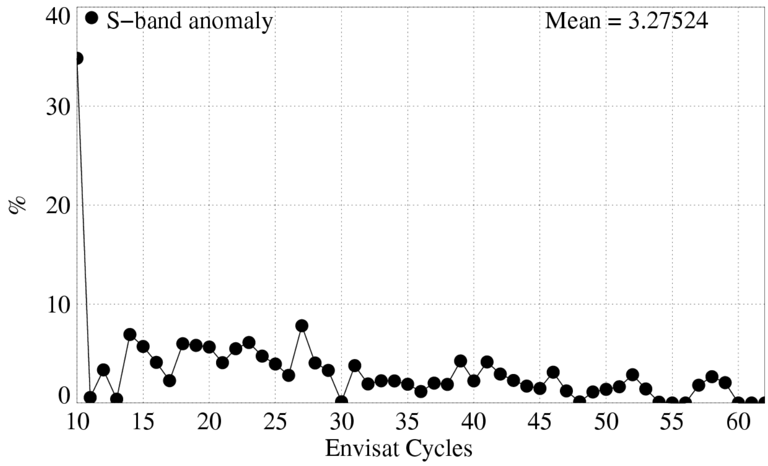

Figure 6: *Cycle per cycle percentages of data impacted by the S-Band anomaly*

4.3.2 Measurements impacted by Sea Ice

Since Envisat operates between 82N and 82S of latitude, sea ice detection is an important issue for oceanic applications. No ice flag is currently available in the Envisat products, therefore alternate sea ice detection techniques are employed in order to retain only open ocean data. A study performed during the validation phase showed that the combination of altimetric and radiometric criteria was particularly efficient to flag most of the data over ice. The method is described in detail in (Faugere et al, 2003 [20]). We employ the Peakiness parameter (Lillibridge et al, 2005 [40]) in conjunction with the MWR- ECMWF wet troposphere difference which appears to be a good means to complement the Peakiness parameter in all ice conditions. The ratio of flagged measurements over ocean is plotted on 7

4.3.3 Editing by thresholds

The second step of the editing procedure consists in using thresholds on several parameters. The minimum and maximum thresholds used in the routine quality assessment are given in table 4.

Parameter	Min thresholds	Max thresholds
Sea surface height (m)	−130	100
Variability relative to MSS (m)	−2	2
		.../...

Parameter	Min thresholds	Max thresholds
Number of 18Hz valid points	10	–
Std deviation of 18Hz range (m)	0	0.25
Off nadir angle from waveform (deg2)	−0.200	0.160
Dry troposphere correction (m)	−2.500	−1.900
Inverted barometer correction (m)	−2.000	2.000
MWR wet troposphere correction (m)	−0.500	0.001
Dual Ionosphere correction (m)	−0.200	−0.001
Significant waveheight (m)	0.0	11.0
Sea State Bias (m)	−0.5	0
Backscatter coefficient (dB)	7	30
Ocean tide height (m)	−5	5
Long period tide height (m)	−0.500	0.500
Earth tide (m)	−1.000	1.000
Pole tide (m)	−5.000	5.000
RA2 wind speed (m/s)	0.000	30.000

Table 4: *E*diting criteria

The thresholds are expected to remain constant throughout the ENVISAT mission, so that monitoring the number of edited measurements allows a survey of data quality. The percentage of edited measurements over ocean for the main altimeter and radiometer parameters has been plotted in figure 8. These ratios are very stable and surprisingly low over the period if compared to other altimeters. The RMS of elementary measurements has the strongest ratio among the altimeter parameters, more than 1% in average. On cycle 47, a special operation was executed to limit RA-2 Chirp Bandwidth to 80MHz. It has impacted this parameter as well as the dual frequency ratio. A slight seasonal signal is visible on the curve, mostly due to sea state seasonal variations. The number of elementary measurements has a surprisingly low ratio, except for cycles 14 and 20 when wrong configuration files were uploaded onboard after a RA-2 event. A slight increase is noticed from cycle 54 onwards dur to the use of the product S-Band anomaly flag instead of the criteria based on KU/S Sigma0 difference. The square of the off-nadir angle derived from waveforms leads to very stable editing ratio but with a drop on cycle 41, due to a change of the algorithm in CMA7.1. Variations of this parameter can reveal actual platform mispointing, if any, but can also reveal waveform contamination by rain or by sea-ice. It is indeed computed from the slope of trailing edge when fitting a typical ocean model to the waveforms. No seasonal signal is visible which may prove that the sea-ice detection method is efficient. The dual frequency ratio shows a slight increasing trend between cycles 15 and 28 which cannot be considered as significant, given the scatter of the curve. The Ku-band SWH, sigma0 and MWR ratios are very stable and low, less than 0.2% with no seasonal variations.

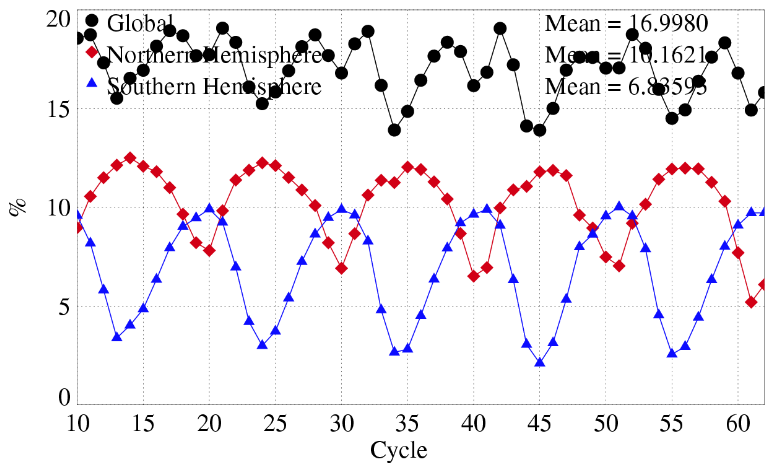

Figure 7: *% of edited points by sea ice flag over ocean*

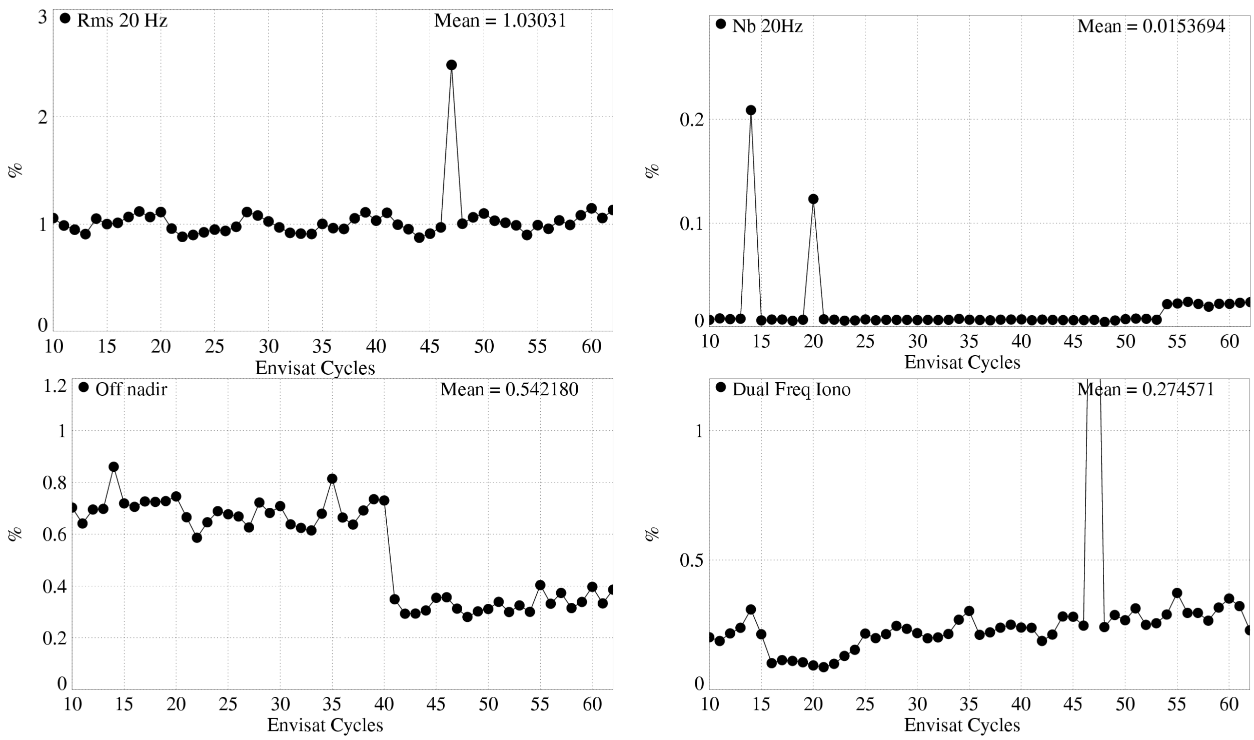

Figure 8: *Cycle per cycle percentages of edited measurements by the main Envisat altimeter and radiometer parameters: top-left) Standard deviation of 20 Hz range measurements > 25 cm, Number of 20-Hz range measurements < 10 top-right) Square of off-nadir angle (from waveforms) out of the [-0.2 deg2, 0.16 deg2] range, dual frequency ionosphere correction out of [-40 , 4 cm] bot-left) Ku-band Significant wave height outside > 11 m, Ku band backscatter coefficient out of the [7 dB, 30 dB] range bot-right) MWR wet troposphere correction out of the [-50 cm, -0.1 cm] range.*

4.3.4 Editing on SLA

It has been necessary to apply additional editing criteria on SSH-MSS differences in order to remove remaining spurious data. The first criterion consists in removing measurements with SSH-MSS greater than 2m. The strong value on cycle 30 is due to the first occurence of the USO anomaly. The second criterion was necessary to detect measurements impacted by maneuvers. Maneuvers are necessary to compensate the effect of gravitational forces but can have a strong impact on the orbit quality. Two types of maneuvers are operated to maintain the satellite ground track within the +/-1km deadband around the reference ground track: in-plane maneuvers, every 30-50 days, which only impact the altitude of the satellite and out-of-plane maneuvers, three times a year, to control the inclination of the satellite (Rudolph et al., 2005). The out-of-plane maneuvers are the most problematic for the orbit computation. The second criterion consists in testing the mean and standard deviation of the SSH-MSS over each entire pass. If one of the two values, computed on a selected dataset, is abnormally high, then the entire pass is edited.

A specific study has been performed to determine how to compute the statistics, and what threshold should be applied. The statistics have to be computed on very stable area. The criteria for selecting the area and the thresholds are detailed is:

- The latitude: the range value can be degraded near the ice, despite the use of the ice flag. Moreover, the MSS is less accurate over 66°, as it has been computed without Topex data.
- The oceanic variability: the standard deviation of SLA can be very high because of the mesoscale variability. Areas with high oceanic variability have to be removed to detect the abnormally high standard deviation.
- The bathymetry and distance from the coast: A lot of corrections (tides for example) are less accurate in low bathymetry areas and near the coast (Japan sea).
- The sample: The statistic have to be computed on a significant number of points

All those criteria have been tested and combined. The results are in Annex. The conclusion is that two criteria are needed: **1st criteria**: for small portion of pass (less than 200 points) the sample is not big enough to compute reliable statistic. The selection must not be severe: Selected areas: latitude>66°, variability<30cm, bathymetry>1000m, distance<100km Threshold: 30 cm on mean and standard deviation **2nd criteria**: for other passes Selected areas: latitude>66°, variability<10cm, bathymetry>1000m, distance<100km Threshold: 15 cm on mean and standard deviation

The percentage of edited measurements over ocean for the main altimeter and radiometer parameters has been plotted in figure 9. On cycles 11, 12, 21 and 26, several full passes have been edited because of bad orbit quality related to out-of-plane manoeuvre or lack of Doris data (cycle 11).The special operation on RA-2 Chirp Bandwidth mentioned previously impacted the SSH editing ratio on cycle 47. On cycle 56 an USO anomaly recovery, occured at the beginning of cycle and impacted the SSH statistic editing per pass.The behaviour of the Ultra Stable Oscillator (USO) clock frequency on this cycle is chaotic. The transitions between anomaly and normal mode has been very straight and the USO correction does not allow us to well correct some passes.

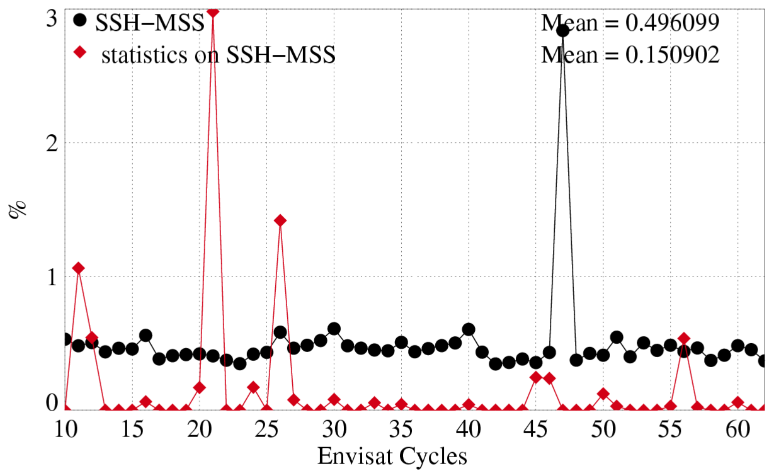

Figure 9: *SSH-MSS out of the [-2, 2m] and edited using thresholds on the mean and standard deviation of SSH-MSS on each pass*

5 Long term monitoring of altimeter and radiometer parameters

All GDR fields are systematically checked and carefully monitored as part of the Envisat routine calibration and validation tasks. However, only the main Ku-band parameters are presented here, as they are the most significant in terms of data quality and instrumental stability. Furthermore, all statistics are computed on valid ocean datasets after the editing procedure.

5.1 Number and standard deviation of 20Hz elementary Ku-band measurements

As part of the ground segment processing, a regression is performed to derive the 1 Hz range from 20 Hz data. Through an iterative regression process, elementary ranges too far from the regression line are discarded until convergence is reached. The mean number and RMS of Ku 20Hz elementary data used to compute the 1Hz average are plotted in figure 10. These two parameters are nearly constant, which provides an indication of the RA-2 altimeter stability. The mean number of Ku 20Hz values over one cycle is about 19.97. This value is very high compared to other altimeters. It is almost not disturbed in wet areas or near the coast. The two drops on the Ku-band on cycles 14 and 20 are due to wrong setting of the RA-2 just after recovery. A slight seasonal signal is visible on the mean RMS of Ku 20Hz. Higher values correspond to higher waves occurring during the austral winter. The mean value is about 9.0 cm. This value represents a rough estimation of the 20 Hz altimeter noise (Zanifé et al. 2003, Vincent et al. 2003a). Assuming that the 20Hz measurements have uncorrelated noise, it corresponds to a noise of about 2 cm at 1Hz. It is consistent with the expected noise values.
The corresponding S-band parameters have a less stable behaviour (see figure 11). The S-band mean number and RMS of 20Hz measurements have respectively an increasing and decreasing trend. Moreover jumps are noticed on the two plots on cycle 41. Moreover, from this cycle, the ascending and descending values are slightly different on the S-band mean RMS of 20Hz measurements.

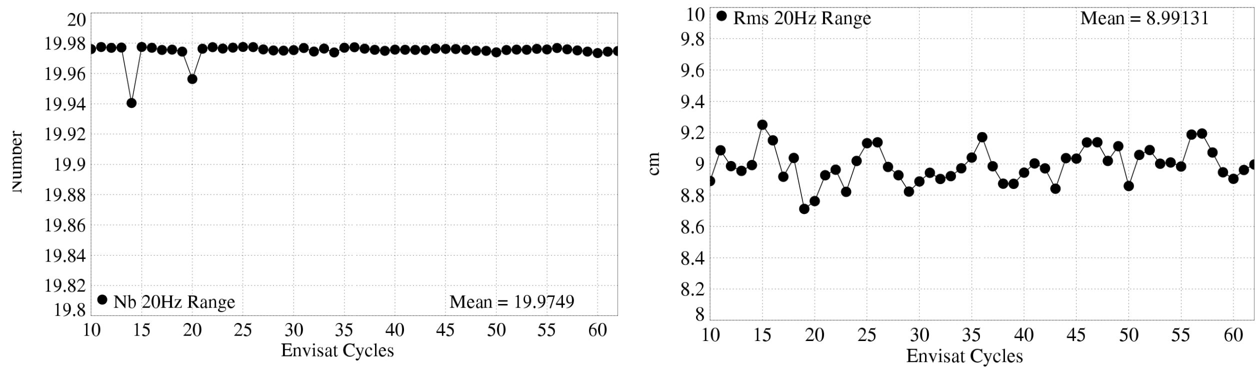

Figure 10: *left) Mean per cycle of the number of 20 Hz elementary range measurements used to compute 1 Hz range. right) Mean per cycle of the standard deviation of 20 Hz measurements.*

Histograms of RMS of Ku and S-band Range on cycle 51 are plotted in figure 12.

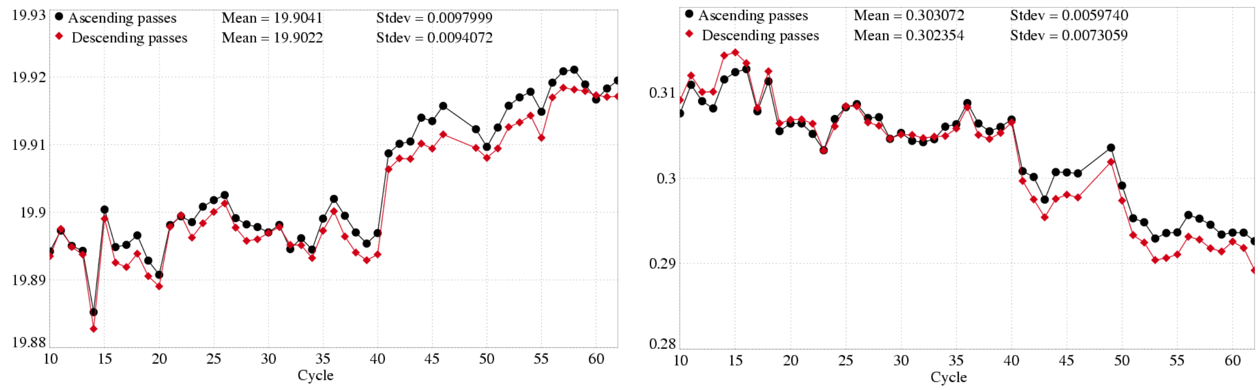

Figure 11: *Mean per cycle of the S-band standard deviation of 20 Hz measurements separating ascending and descending passes (cm)*

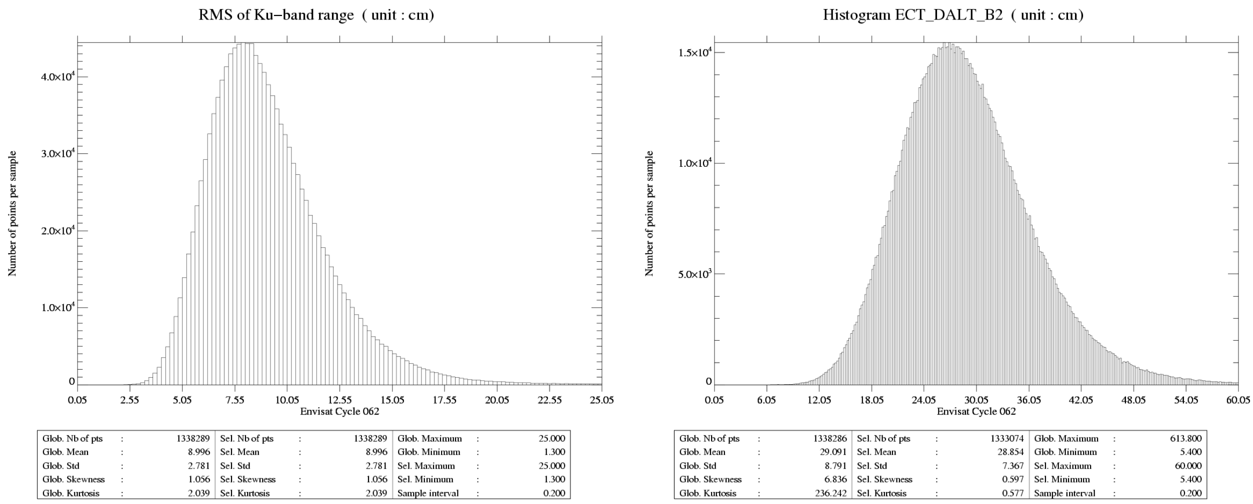

Figure 12: *Histogram of RMS ofKu and S range (cm)*

5.2 Off-nadir angle from waveforms

The off-nadir angle is estimated from the waveform shape during the altimeter processing. The square of the off-nadir angle is plotted in figure 13. The mean value is between 0.02 deg2 and 0.03deg2 before cycle 41. There is a slight rising trend over this period and a 0.005 deg2 jump between cycles 21 and 22 which is due to the upgrade of the IF mask filter auxiliary data file. The mean value observed during this period is not significant in terms of actual platform mispointing. This is due to the way the slope of the waveform trailing edge is computed. On cycle 41, a 0.02 deg2 drop occurs, due to an improvement of the mispointing estimation in IPF 5.02. The mispointing was estimated through the waveform trailing edge slope using an adaptative window that defines the beginning and the end of the slope. To avoid the filter bump effect that leads to high value of the mispointing, an optimum and fixed gate was estimated and implemented. Note that the rising trend observed previously desappeared. This is probably an effect of the regular update of the IF filter since cycle 41.

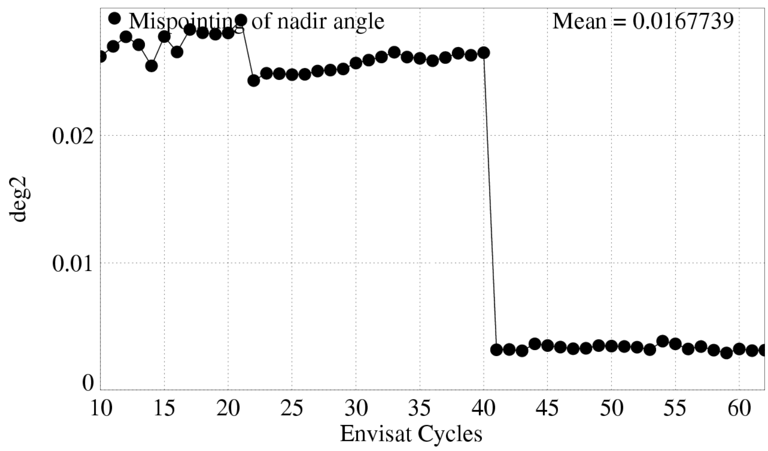

Figure 13: *Mean per cycle of the square of the off-nadir angle deduced from waveforms (deg2).*

The histogram of the squared mispointing is plotted in figure 14.

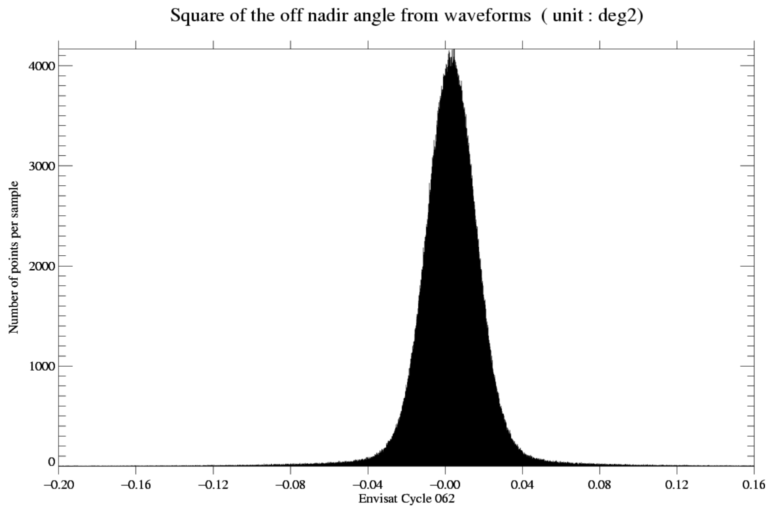

Glob. Nb of pts	:	1338289	Sel. Nb of pts	:	1338284	Glob. Maximum	:	0.160
Glob. Mean	:	0.003	Sel. Mean	:	0.003	Glob. Minimum	:	−0.200
Glob. Std	:	0.019	Sel. Std	:	0.019	Sel. Maximum	:	0.160
Glob. Skewness	:	−0.489	Sel. Skewness	:	−0.492	Sel. Minimum	:	−0.200
Glob. Kurtosis	:	14.313	Sel. Kurtosis	:	14.302	Sample interval	:	0.000

Figure 14: *Histogram of off-nadir angle from waveforms (deg2)*

5.3 Significant Wave Height

The cycle by cycle mean and standard deviation of Ku and S-band SWH are plotted in figure 15. The curve reflects sea state variations. The mean value of Ku SWH is 2.66 m. The S-band mean SWH is very close, less than 10 cm apart. The cycle by cycle mean of Envisat-Jason-1 differences and ERS-2-Envisat differences are plotted in figure 15. These differences are quite stable. Envisat SWH is respectively 14 cm and 22 cm higher than Jason-1 and ERS-2 SWH. It is also noticed, as for range parameters, some strange behaviours on S-band SWH (see 16): jumps in the S-band time series (cycle 41, 54), and inconsistencies between ascending and descending passes.

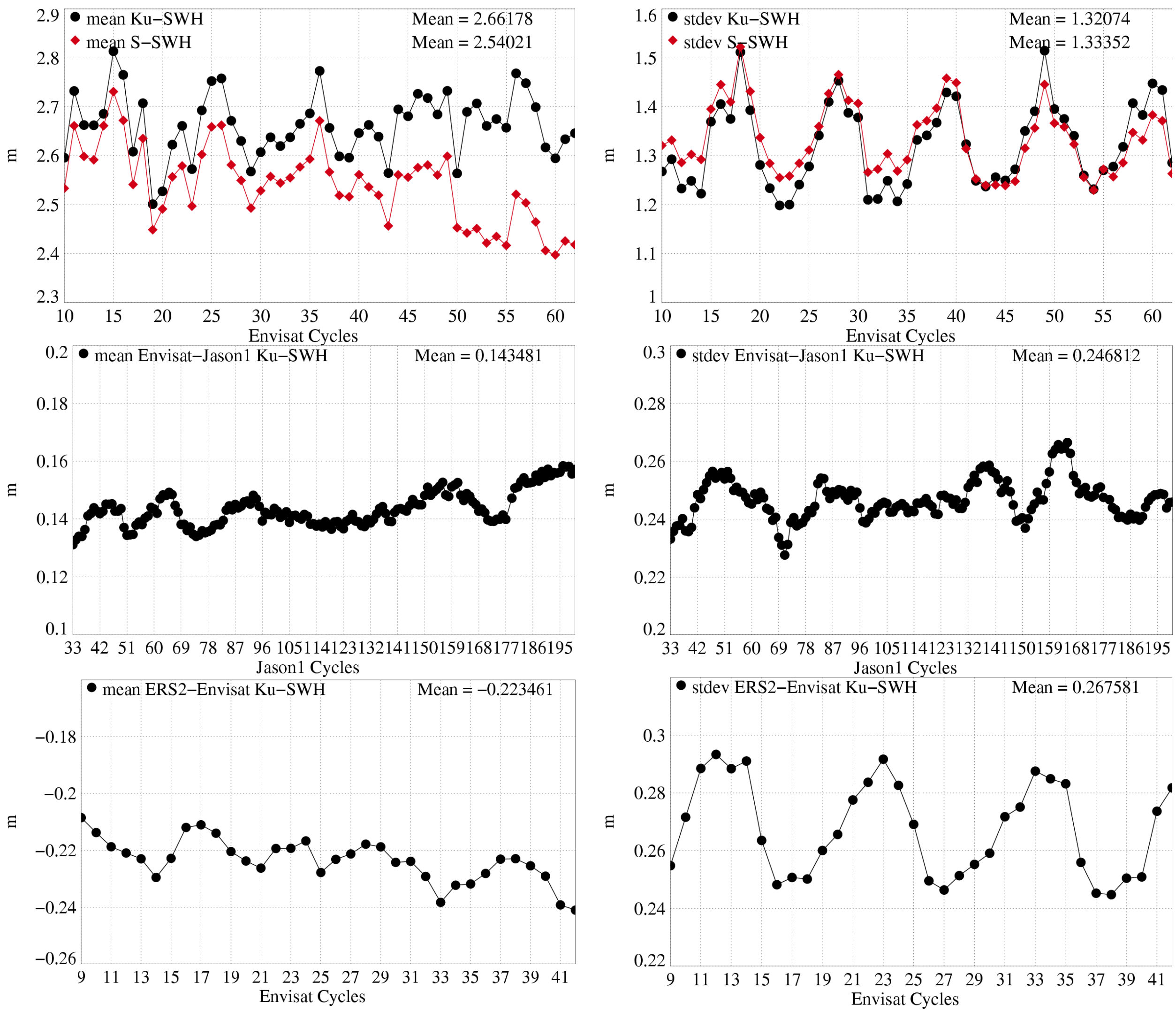

Figure 15: *Global statistics (m) of Envisat Ku and S SWH top-right) Mean and top-left) Standard deviation. bot-right) Mean Envisat-Jason-1 Ku SWH differences at 3h EN/J1 crossovers computed with 120 days running means. bot-left) Mean. ERS-2-Envisat Ku SWH collinear differences over the Atlantic Ocean.*

Histograms of Ku and S-band SWH are plotted in figure 17. The Ku SWH histogram has a good shape.

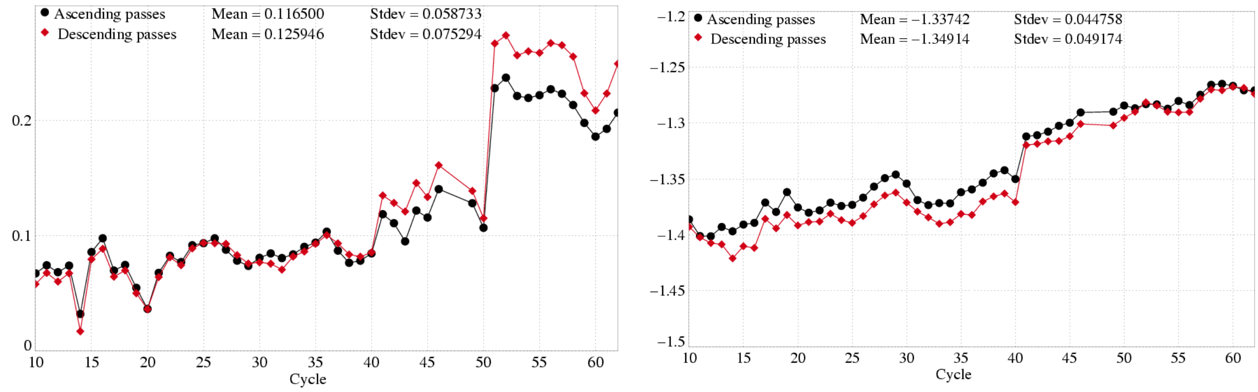

Figure 16: *left) Mean per cycle of SWH(Ku)-SWH(S). right) Mean per cycle of RMS20Hz[SWH(Ku)]-RMS20Hz[SWH(S)].*

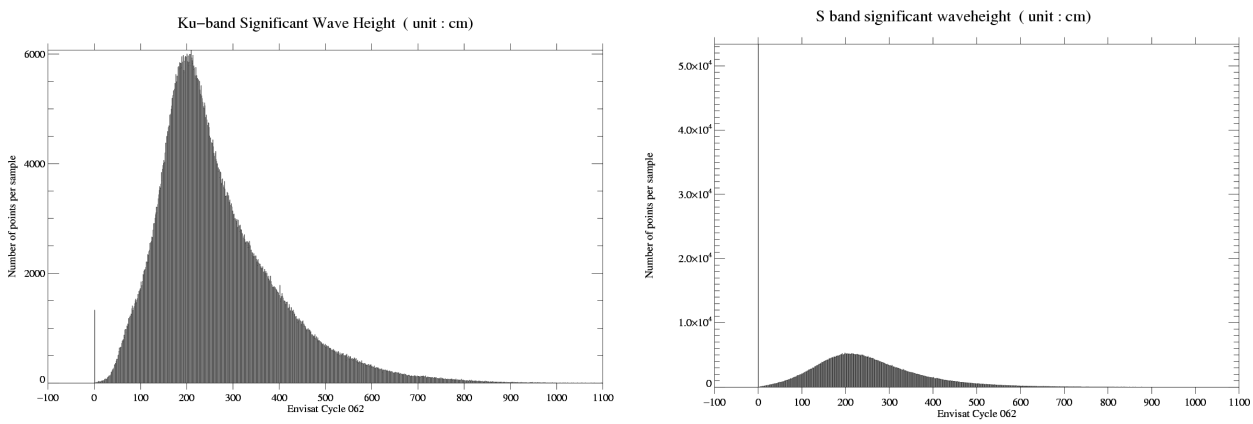

Glob. Nb of pts	:	1338289	Sel. Nb of pts	:	1338289	Glob. Maximum	:	1099.500
Glob. Mean	:	264.596	Sel. Mean	:	264.596	Glob. Minimum	:	0.000
Glob. Std	:	128.558	Sel. Std	:	128.558	Sel. Maximum	:	1099.500
Glob. Skewness	:	1.193	Sel. Skewness	:	1.193	Sel. Minimum	:	0.000
Glob. Kurtosis	:	1.967	Sel. Kurtosis	:	1.967	Sample interval	:	1.000

Glob. Nb of pts	:	1338289	Sel. Nb of pts	:	1338055	Glob. Maximum	:	2839.600
Glob. Mean	:	241.778	Sel. Mean	:	241.571	Glob. Minimum	:	0.000
Glob. Std	:	126.313	Sel. Std	:	125.290	Sel. Maximum	:	1100.000
Glob. Skewness	:	0.832	Sel. Skewness	:	0.678	Sel. Minimum	:	0.000
Glob. Kurtosis	:	3.213	Sel. Kurtosis	:	1.302	Sample interval	:	1.000

Figure 17: *Histogram of Ku and S SWH (m)*

5.4 Backscatter coefficient

The cycle by cycle mean and standard deviation Ku and S-band Sigma0 are plotted in figure 18. Note that a -3.5 dB bias has been applied (Roca et al., 2003 [51]) on the Ku-band Sigma0 in order to be compliant with the wind speed model (Witter and Chelton, 1991 [63]). The mean values in Ku band are stable, around 11.1 dB. Two 0.66 dB jumps are visible on the S-Band on cycles 14 and 22. They are due to a correction of the AGC evaluation. This modification has been included in IPF version 4.56, used from cycle 22 onwards for the current processing and for all the reprocessed cycles. The cycle by cycle mean of Envisat-Jason-1 differences and ERS-2-Envisat differences are plotted in figure 18. The mean difference between Envisat and Jason-1 Ku-band Sigma0 is -2.9 dB. This high value is explained by the fact that, Envisat Sigma0 value has been biased and not Jason-1. This mean difference has increased by 0.1dB between cycles 48 and 140 Jason-1. The mean trend of the difference is approximately -0.02dB/year over the whole period. These sigma0 differences obviously impact the wind consistency between the two satellites. Note that the wind from the ECMWF model, which does not assimilate Jason-1 data, shows a very good agreement with the Jason-1 wind with a slope close to 6 cm/s/yr whereas Envisat wind trend is much lower, 1.3cm/s/year (see [4]. This trend difference could mean that the Envisat slightly drifts. This potential trend, though slight, has to be closely monitored. In particular the impact the atmospheric attenuation, once recomputed using a reprocessed set of brightness temperature, has to be checked.

The mean ERS-2-Envisat Ku-band Sigma0 difference is 0.05 dB. However, this mean value accounts for the calibration correction applied in the ground processing to be compliant with the wind speed algorithm (Witter and Chelton, 1991 [63]). The monitoring of (ERS-2 - Envisat) Sigma0 differences exhibits a 0.1 dB jump between cycles 38 and 39. This jump occurs at the end of cycle 38, on the 4th July 2005 11:29 UTC. Since no jump is observed on the Envisat/Jason-1 differences, it may be attributed to ERS-2. This jump is still under investigation.

Histograms of Ku and S-band Sigma0 are plotted in figure 19. The Ku Sigma0 histogram has a good shape.

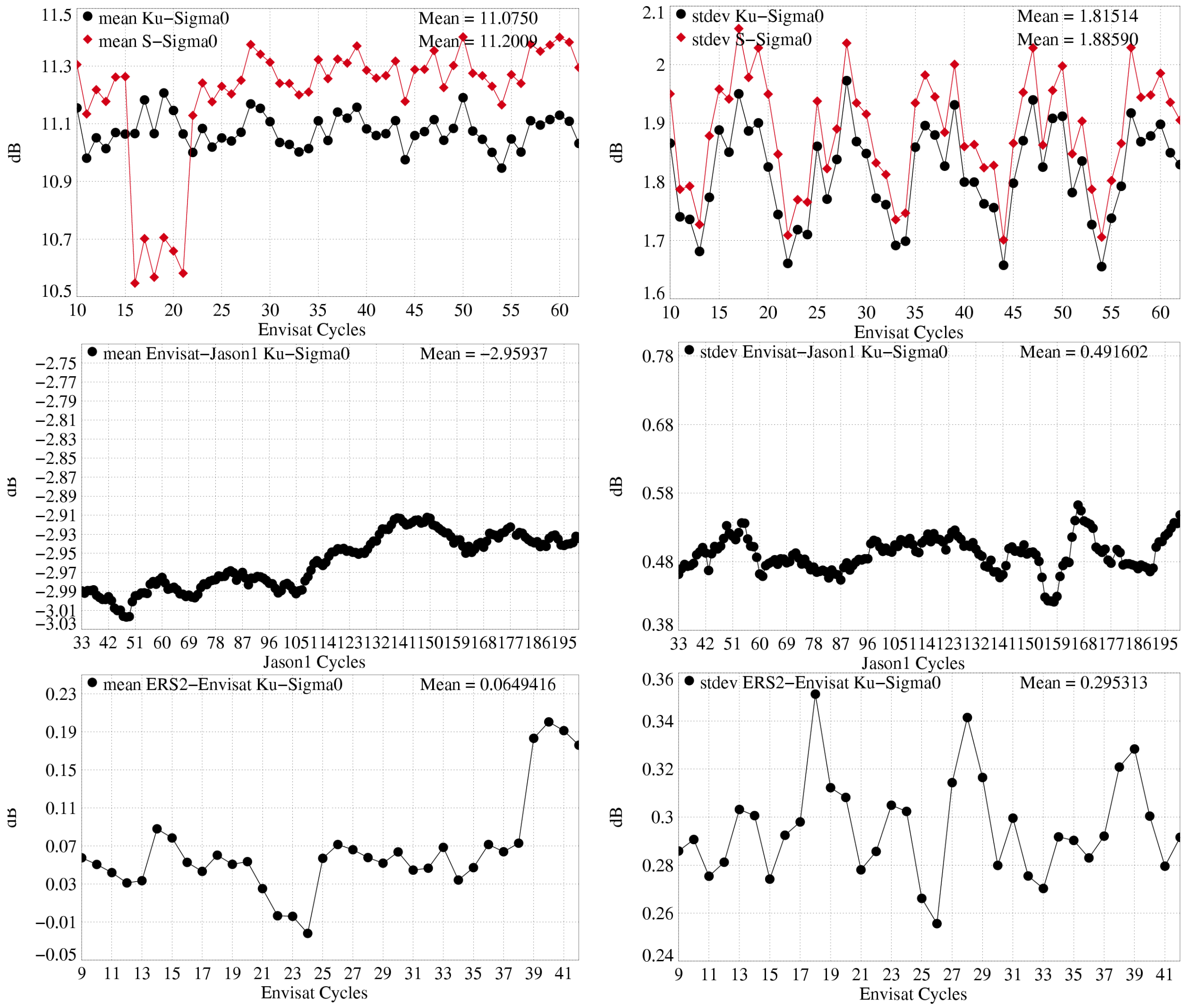

Figure 18: *Global statistics (dB) of top) Envisat Ku and S Sigma0 Mean and Standard deviation. middle) Mean Envisat-Jason-1 Ku Sigma0 differences at 3h EN/J1 crossovers computed with 120 days running means. bottom) Mean and Standard of ERS-2-Envisat Ku Sigma0 collinear differences over the Atlantic Ocean.*

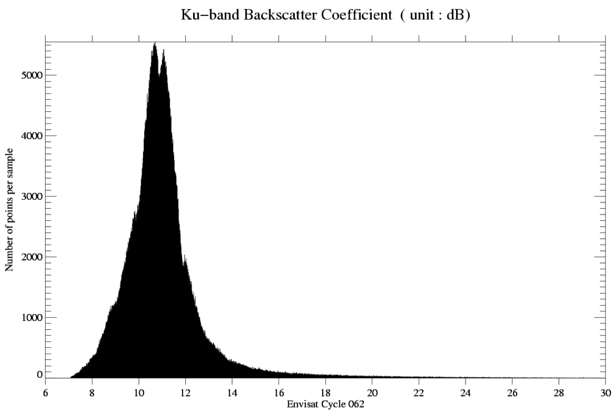

Glob. Nb of pts	:	1338289	Sel. Nb of pts	:	1338288	Glob. Maximum	:	30.000
Glob. Mean	:	11.032	Sel. Mean	:	11.032	Glob. Minimum	:	7.080
Glob. Std	:	1.829	Sel. Std	:	1.829	Sel. Maximum	:	29.980
Glob. Skewness	:	2.896	Sel. Skewness	:	2.896	Sel. Minimum	:	7.080
Glob. Kurtosis	:	16.046	Sel. Kurtosis	:	16.040	Sample interval	:	0.010

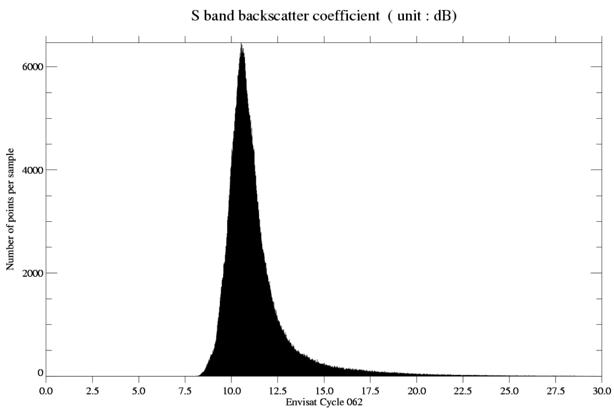

Glob. Nb of pts	:	1338289	Sel. Nb of pts	:	1338271	Glob. Maximum	:	32.050
Glob. Mean	:	11.295	Sel. Mean	:	11.295	Glob. Minimum	:	7.460
Glob. Std	:	1.905	Sel. Std	:	1.904	Sel. Maximum	:	29.970
Glob. Skewness	:	3.071	Sel. Skewness	:	3.064	Sel. Minimum	:	7.460
Glob. Kurtosis	:	14.022	Sel. Kurtosis	:	13.930	Sample interval	:	0.010

Figure 19: *Histogram of Ku and S Sigma0 (dB)*

5.5 Dual frequency ionosphere correction

As performed on TOPEX (Le Traon et al. 1994 [37]) and Jason-1 (Chambers et al. 2002 [9]) it is recommended to filter dual frequency ionosphere correction on each altimeter dataset to reduce noise. A 300-km low pass filter is thus applied along track on the dual frequency ionosphere correction. As previously mentioned, the JPL GIM ionosphere corrections are computed to assess the dual frequency altimeter based ionosphere correction. The cycle by cycle mean of dual frequency and JPL GIM ionosphere correction are plotted in figure 20. The mean value of the two corrections is clearly decreasing since the beginning of Envisat mission due to inter-annual reduction of the solar activity. The mean differences (GIM-Dual frequency), plotted in figure 20, is stable around -0.7 cm. It is stronger in absolute value for high ionosphere corrections, for descending passes (in the daytime). The standard deviation of the difference is plotted in figure 20. Low values, less than 2 cm, indicate a good correlation between dual-frequency and GIM corrections. Notice that, in this analysis, the same sea state bias (SSB) has been used to correct the Ku and S-Band Ranges for cycles 9-40, as it is done so far in the GDR processing. Since cycle 41, a suitable Ku and S-band SSB correction is used on the two bands before computing the dual frequency ionosphere correction from Ku and S-band ranges (Labroue (2004 [33])). The differences with the GDR correction are very small with no impact on the global statistics and only small geographic variations between -1 mm and +1.5 mm (Labroue 2004 [33]).

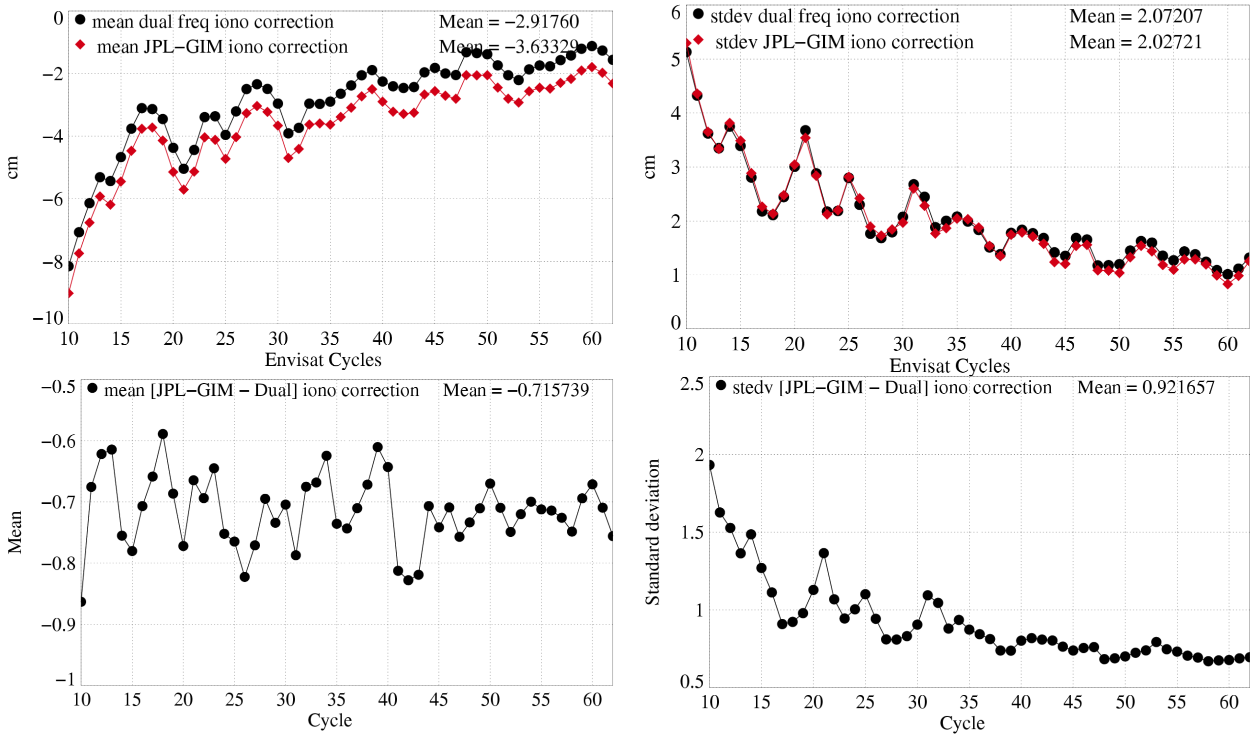

Figure 20: *Comparison of global statistics of Envisat dual-frequency and JPL-GIM ionosphere corrections (cm). top) Mean and standard deviation per cycle of Dual Frequency and GIM correction. bot) Mean and standard deviation of the differences*

5.6 MWR wet troposphere correction

A neural network formulation has been used in the inversion algorithm retrieving the wet troposphere correction from the measured brightness temperatures (Obligis et al., 2005 [49]). As an example, the scatter plot of MWR correction according to ECMWF model for cycle 62 is given in figure 21.

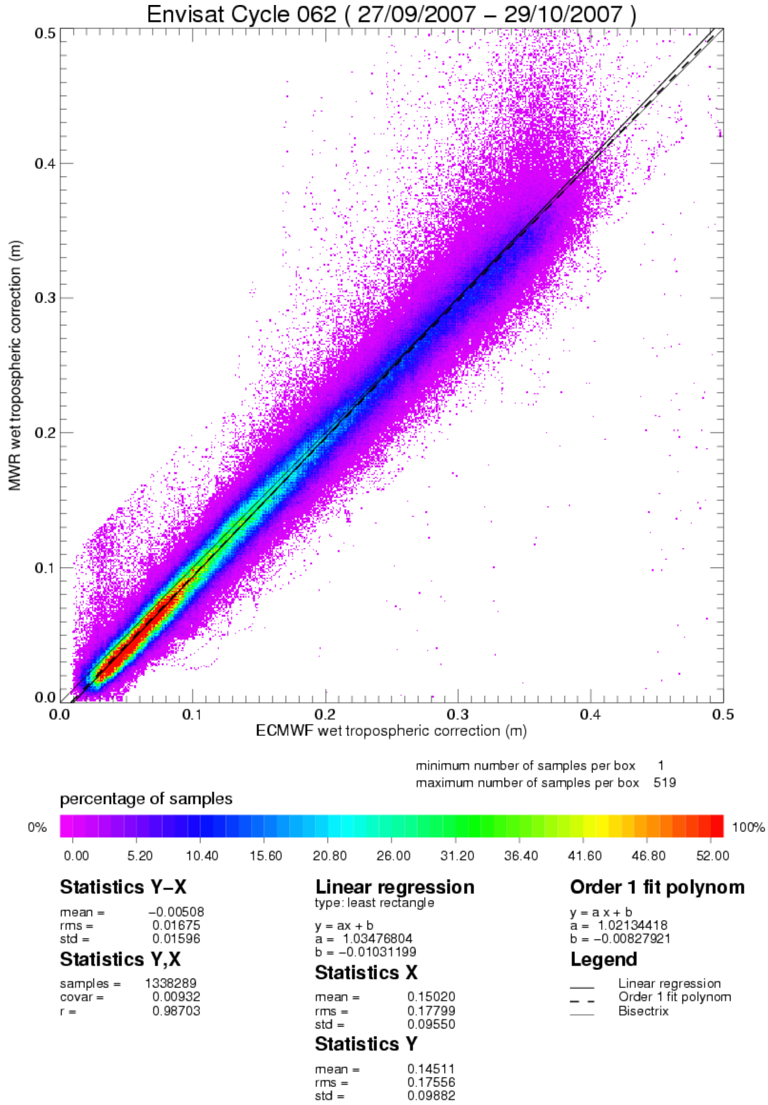

Figure 21: *Scatter plot of MWR correction according to ECMWF model (m)*

Since the beginning of the mission, the instrumental parameters at 36.5 GHz have been drifting and investigations are in progress to identify the source for these drifts. A correction of the TB36.8 GHz has been proposed in Tran et al., 2006 [61] (not applied here). In particular, different behavior is observed depending on the brightness temperature values. Mean and standard deviation of (MWR-ECMWF model) differences are plotted in figure 22. The difference is not really stable, though the global mean remains small. It rises by 3mm between cycles 11 and 27, which corresponds to 1.8 mm/year. Then, it decreases by 2mm between cycle 27 and 46. Finally, an annual signal of about 1.5mm of amplitude seems to appear on cycle 47. The

standard deviation drops down by 2 mm from cycle 13. This is due to a change in the ECMWF model on the 14th of January 2003 [15]. The impact of these changes has been found to be meteorologically positive, and it is confirmed by the improved consistency with the MWR. Note that this change did not impact the MWR-ECMWF mean differences. Similar results are visible on Jason-1 mission.
From cycle 46 onwards, a 1.5 of amplitude annual signal seems to appear on the mean MWR-ECMWF time series. Moreover this annual signal has not the same amplitude on ascending (night) and descending (day) passes (figure 23). A specific analysis of this signal is proposed in 8.3. Moreover, a complete monitoring of all the radiometer parameters is available in the cyclic Envisat Microwave Radiometer Assessment (Dedieu et al., 2005 [10]).

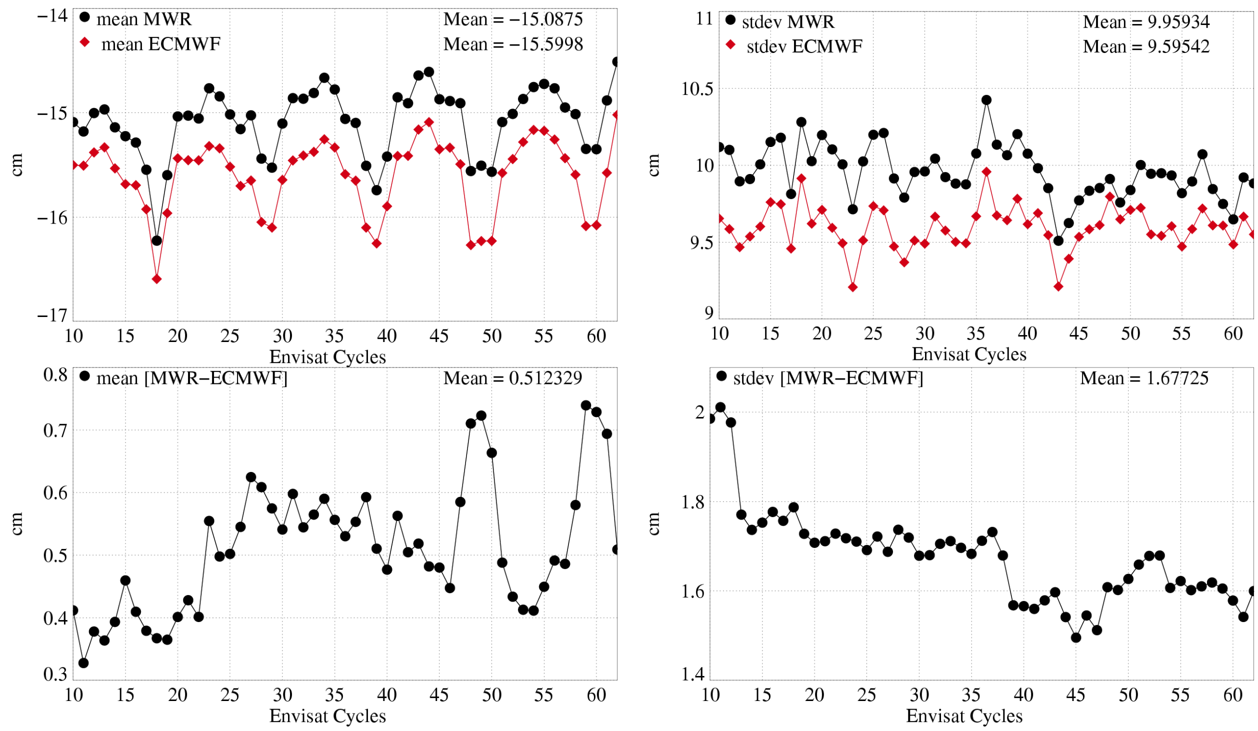

Figure 22: *Comparison of global statistics of Envisat MWR and ECMWF wet troposphere corrections (cm). top) Mean and standard deviation per cycle of MWR and ECMWF corrections bot) Mean and standard deviation of the differences.*

The (ERS-2 -Envisat) cyclic 23.8 GHz brightess temperatures differences over the Atlantic area are plotted on figure 24. The ERS-2 drift proposed by Eymard et al., 2003 [18] is applied. The correction of the drift proposed by Scharroo et al., 2004 [56], should decrease the mean difference by 0.8K as described in Mertz et al., 2004 [46]. Nevertheless, the mean difference variations are more steady for the period after cycle 21. The (ERS-2 -Envisat) TB36.5 GHz values are also reported in figure 24. The differences before and after cycle 18 have a different behaviour: one observes a great decrease from -2 to -4 K between cycles 13 and 17 whereas the curve seems to be steadier after cycle 18. This is not an impact of the coverage of the data since in the restricted area, the statistics reveals the same features. Tran et al., 2006 [61], propose a correction for the drift of the 36.5 GHz TB on Envisat (not used here). They also show an unusual behaviour of the TB values during that period. Note that this behaviour is not visible on hottest or coldest values but mainly on the mean values. The impact of the drift of the TB36.5 on (ERS-2 -Envisat) wet troposphere correction differences is visible in figure 25.

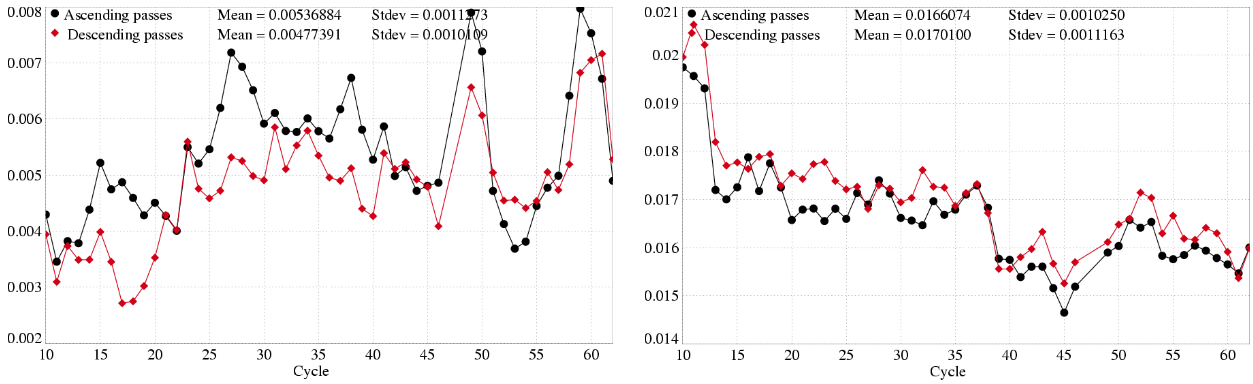

Figure 23: *Comparison of global statistics of Envisat MWR and ECMWF wet troposphere corrections separatin ascending and descending passes (cm). Mean (left) and standard deviation (right) per cycle of MWR and ECMWF corrections.*

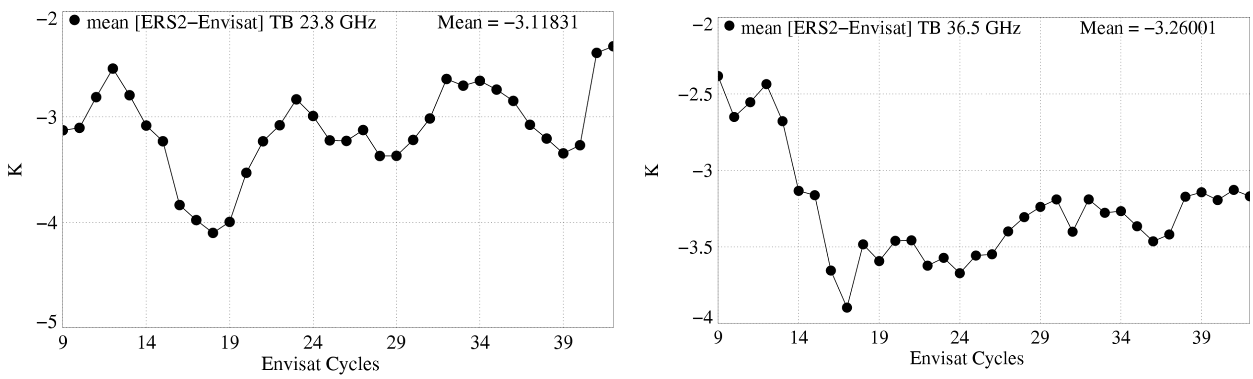

Figure 24: *Monitoring of the (ERS-2 - Envisat) brightness temperatures*

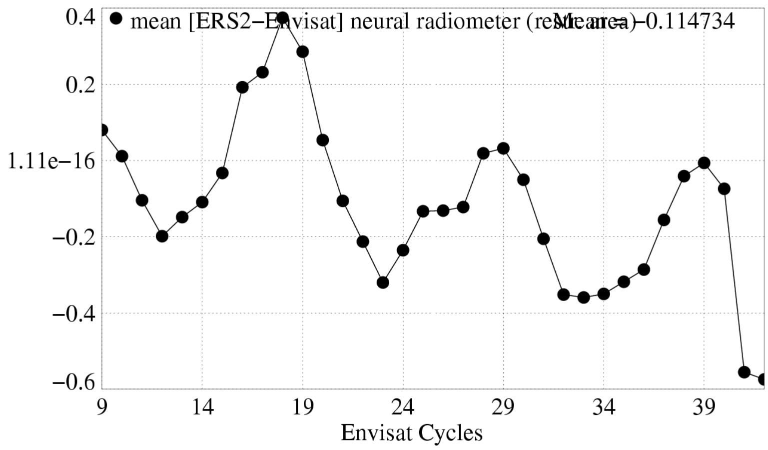

Figure 25: *Monitoring of the (ERS-2 - Envisat) wet troposphere correction*

6 Sea Surface Height performance assessment

One of the main objectives of the Calibration and Validation activities is to assess the performance of the whole altimeter system. This means that the quality of each parameter of the product is evaluated, in particular if it is likely to be used in the Sea Surface Height (SSH) computations. Conventional tools like crossover differences and repeat-track analyses are systematically used in order to monitor the quality of the system.

6.1 SSH definition

The standard SSH calculation for Envisat is defined below.

$$SSH = Orbit - Altimeter\ Range - \sum_{i=1}^{n} Correction_i$$

$$\begin{aligned}
\sum_{i=1}^{n} Correction_i \quad = \quad & Dry\ troposphere\ correction : new\ S1\ and S2\ atmospheric\ tides\ applied \\
+ \quad & Combined\ atmospheric\ correction :\ MOG2D\ and\ inverse\ barometer \\
+ \quad & Radiometer\ wet\ troposphere\ correction \\
+ \quad & Filtered\ dual\ frequency\ ionospheric\ correction \\
+ \quad & Non\ parametric\ sea\ state\ bias\ correction \\
+ \quad & Geocentric\ ocean\ tide\ height,\ GOT\ 2000 :\ S1\ atmospheric\ tide\ is\ applied \\
+ \quad & Solid\ earth\ tide\ height \\
+ \quad & Geocentric\ pole\ tide\ height
\end{aligned}$$

As said in 3.2, the new geophysical correction associated with version CMA7 have been updated on the whole data-set in order to have the most homogeneous time series. For Envisat, the only discontinuities existing in our dataset are between cycle 40 and 41 due to:

- Envisat orbit is computed using GRIM5 gravity model for cycles 9 to 40 and EIGEN-CG03C from cycle 41 onwards.
- The retracking (IF monthly estimations from cycle 41 onwards).

The USO auxiliary correction distributed by ESA are used in Envisat SSH computation.

6.2 Single crossover mean

SSH crossover differences are computed on a one-cycle basis, with a maximum time lag of 10 days, in order to reduce the impact of ocean variability which is a source of error in the performance estimation. The mean of crossover differences represents the average of SSH differences between ascending and descending passes. This difference can reflect orbit errors or errors in geophysical corrections. The fact that Envisat is

Sun-synchronous can play a role since the ascending passes and descending passes respectively cross the equator at 10pm local time and 10am local time. Thus all the parameters with a daily cycle can induce errors resulting in ascending/descending differences. The error observed at crossovers can be split into two types: the time invariant errors and the time varying errors.

To analyse the time invariant errors, we have computed local averages of crossover differences over cycles 10 to 40 and 41 to 62. The maps of the mean differences at crossovers are shown in figure 26. On the 10-40 map, systematic differences between ascending and descending passes are observed in some areas. Mean ascending/descending differences are locally higher than 4 cm (Southern Pacific and Southern Atlantic). These patterns, called geographically correlated radial orbit errors, are induced by errors in the gravity models currently used in the orbit computation. Notice that the signal visible around the equator on ERS-2 (Scharroo, 2002 [54]), related to poor quality of the ionosphere correction, is not present for Envisat thanks to a good correction of the dual frequency correction. On the 41-62 map the geographically correlated orbit errors are almost fully removed thanks to the use of EIGEN-CG03C gravity model. Small signals remain in Indian and Pacific Oceans.

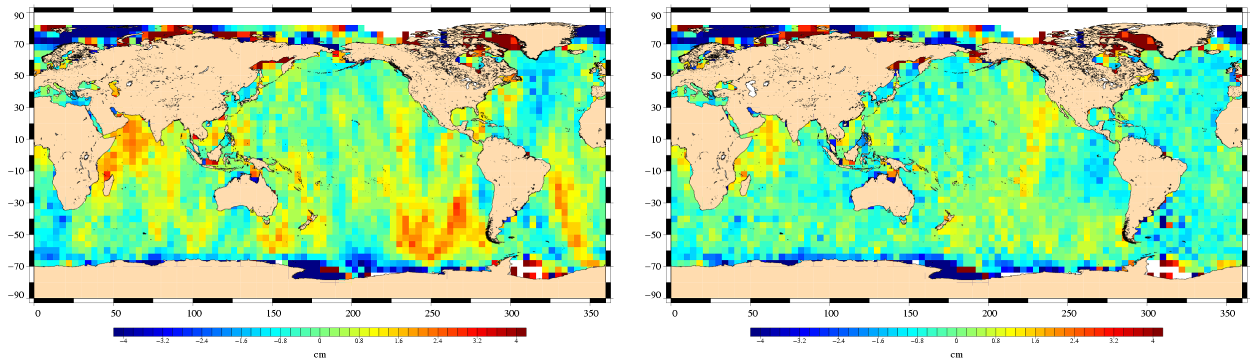

Figure 26: *Maps of the time invariant 35-day crossover mean differences (cm) for Envisat averaged in (3° x 3°) geographical bins over cycles 10 to 40 (left) and over cycles 41 to 62 using the new POE orbit using a new gravity model (right).*

Besides the systematic ascending-descending errors, a time varying error can also be observed at crossovers. The cyclic mean ascending-descending SSH differences at crossovers shows this error in figure 27. The cyclic mean crossover differences have been plotted in three different configurations: full data set, deep ocean data, and deep ocean data with low variability, and excluding high latitudes. A strong annual signal is evidenced on the 3 curves. Its amplitude is approximately 1 cm.

A specific study has been carried out in order to analyse deeply this signal. The results of this study are available in [25]. The main results of this study is first that the amplitude is geographically dependent, and then that the geographical patterns depend on the oceanic tide model used in the SSH.

6.3 Variance at crossovers

The variance of crossover differences conventionally gives an estimate of the overall altimeter system performance. Indeed, it gathers error sources coming from orbit, geophysical corrections, instrumental noise, and part of the ocean variability. The standard deviation of the Envisat SSH crossover differences has been plotted in figure 28, depending on three data selection criteria. Without any selection, a seasonal signal is observed because variations in sea ice coverage induce changes in ocean sampling by altimeter

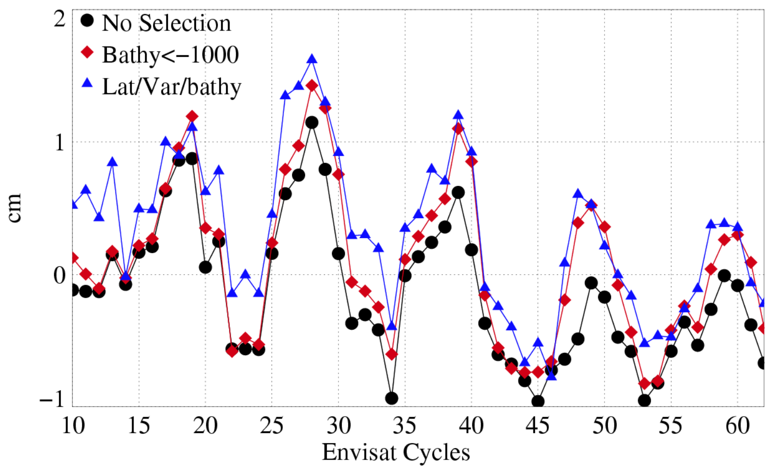

Figure 27: *Time varying 35-day crossover mean differences (cm). Cycle per cycle Envisat crossover mean differences. An annual cycle is clearly visible. Diamonds: shallow waters (1000 m) are excluded. Triangles: shallow waters excluded, latitude within [-50S, +50N], high ocean variability areas excluded*

measurements. When only retaining deep ocean areas, excluding high latitudes (higher than 50 deg.) and high ocean variability areas, the standard deviation then gives reliable estimate of the altimeter system performances. In that case most of the cycles have a standard deviation between 7.5 and 7.7 cm. But there are some exceptions that can be explained. Cycles 15 and 48 are strongly different because of the low number of crossover points. There are less than 10000 crossovers whereas other cycles lead to more than 20000. Cycles 21 and 26 have higher values because of bad orbit quality over a few passes related to out-of-plane maneuvers. Cycle 21 has a strong value (8.5 cm) because of the combined effect of 2 maneuvers, intense solar activity between these 2 maneuvers, and lack of laser measurements between these two maneuvers. Cycle 11 has a relative high value because of missing Doris data. No degradation of the performances have been noticed since the beginning of the USO anomaly on cycle 46. This shows that the correction provided by ESA allows Envisat Ra2 data to maintain the same level of quality.
In order to compare Envisat and Jason-1 performances at crossovers, Envisat and Jason-1 crossovers have been computed on the same area excluding latitude higher than 50 degree, shallow waters and using exactly the same interpolation scheme to compute SSH values at crossover locations. Performances at crossovers are compared, for the two satellites on figure 29. The standard deviation of Envisat/Envisat and Jason-1/Jason-1 SSH crossover differences are respectively 6 cm and 5.7 cm. The use of MLE4 retracking on Jason-1 leads to slightly lower than Envisat standard deviation at crossovers. A slight decrease is visible on Envisat plot at cycle 41, thanks to the new standards used for the POE orbit. From cycle 41 onwards, the performances of the two missions are very close.

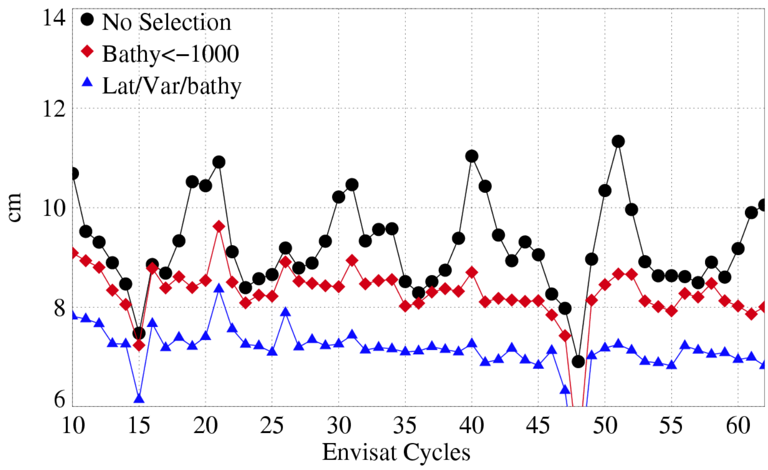

Figure 28: *Standard deviation (cm) of Envisat 35-day SSH crossover differences depending on data selection. Dots: without any selection. Diamonds: shallow waters (1000 m) are excluded. Triangles: shallow waters excluded, latitude within [-50S, +50N], high ocean variability areas excluded.*

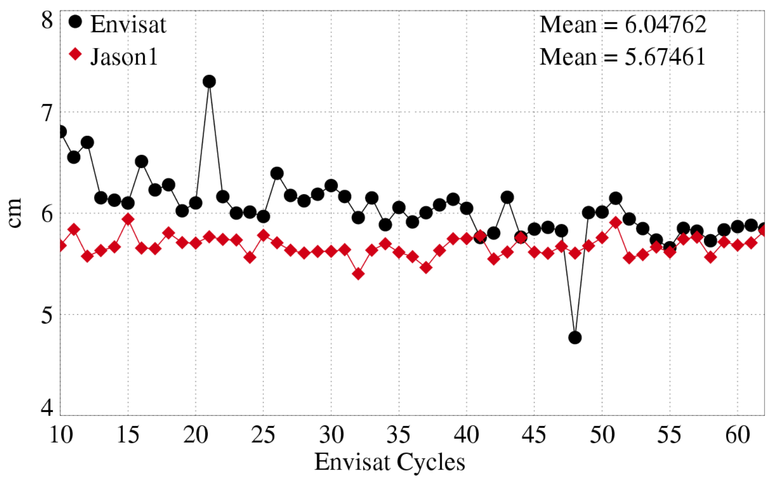

Figure 29: *Comparison of the Standard deviation (cm) of Envisat (dot) and Jason-1 (diamond) 10-day SSH crossover differences*

7 Envisat SSH bias and Mean Sea Level trends

7.1 SSH definition

As previously mentioned, a drift is suspected on the MWR correction. Consequently, the ECMWF wet troposphere correction is used, as no major change in the model has impacted the data since the beginning of the Envisat mission (ECMWF web page). Apart from that, the same SSH as for 6.1 is used.

7.2 Envisat Bias

Envisat Mean Sea Level (MSL) estimations are plotted in figure 30 for three different editing criteria in order to estimate the impact of shallow waters and high latitudes. The mean SSH bias relative to the CLS01 MSS is about 49.5 cm over this period. Seasonal signals are observed on the three curves, though the annual cycle is more pronounced on the full data-set.

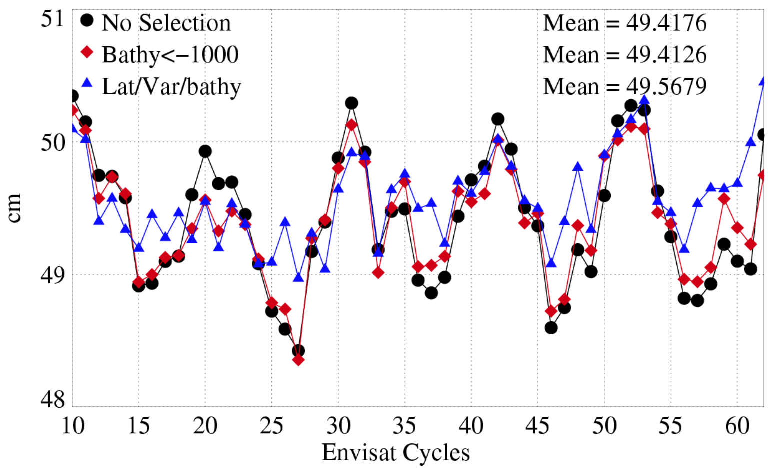

Figure 30: *Mean of Envisat Sea Level depending on data selection. Dots: without any selection. Diamonds: shallow waters (1000 m) are excluded. Triangles: shallow waters excluded, latitude within [-50S, +50N], high ocean variability areas excluded.*

In order to compare Envisat and Jason-1 SSH estimations, 10-day dual crossovers have been computed for each Envisat cycle. The same ECMWF correction has been used for both Jason-1 and Envisat to avoid potential radiometer errors. Figure 31 shows the mean Envisat-Jason-1 differences at global and hemispheric scales. The global mean is about 33.6 cm over the period. There is a decreasing trend on the difference between cycles 10 and 20 then the differences seem to stabilize. This behavior remains unexplained. The hemispheric differences seem consistent from one cycle to another. From cycles 10 to 16, no hemispheric difference is observed, while after Cycle 16, high hemispheric biases are evidenced. The differences are periodically strongly reduced with a period of 6-8 Envisat cycles (200-300 days). The same kind of observation had been made on Jason-1 T/P differences (Dorandeu, 2004b). These differences might be attributed to residual orbit errors on at least one of the satellites. Particular investigations have been performed this year to know the geographical structure of the Envisat/Jason-1 bias (see 8).

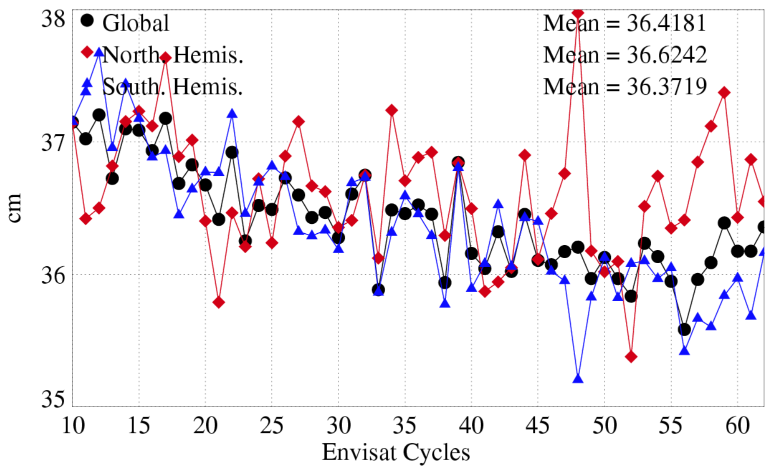

Figure 31: *Mean of Envisat -Jason-1 differences at 10-day dual crossovers. Dots: Global. Diamonds: Northern Hemisphere. Triangle: Southern Hemisphere.*

7.3 MSL trends

Finally MSL estimations from Envisat and Jason-1 have been compared. The results are obtained after area weighting (Dorandeu and Le Traon 1999). The same corrections are used for the 2 satellites. Annual have been removed. An additional 60-day period sinusoid has been fitted and removed on Jason to remove residual orbit errors (Luthcke et al. 2003). Biases relative to MSS have been removed for each mission to ease the comparison. Figure 32 shows the global MSL trend for the two satellites on the whole Envisat period (2002-2007). The Envisat curve shows 0.5mm/year trend while Jason-1 leads to an increasing trend of about 2.2 mm/year. This difference is partly due to the unexplained behavior of Envisat MSL estimations before mid 2003. Indeed the MSL has a decreasing trend until the last months of 2003, around cycle 20. This is consistent with the Envisat-Jason-1 trend observed at dual crossovers. Figure 33 shows the global MSL trend for the period 2004-2007 and Figure 34 shows the global MSL trend for the last two years (2005-2007) where both missions show a flat trend. This last observation is very positive: on the two last years, Envisat and Jason-1 have the same MSL trend. Deep investigations have been performed in order to understand this behaviour. A summary of this investigation is available in part 8 of this document. A complete study on the MSL seen by all the operational altimeter missions and its comparison to the Reynolds SST is also available in Ref [4].

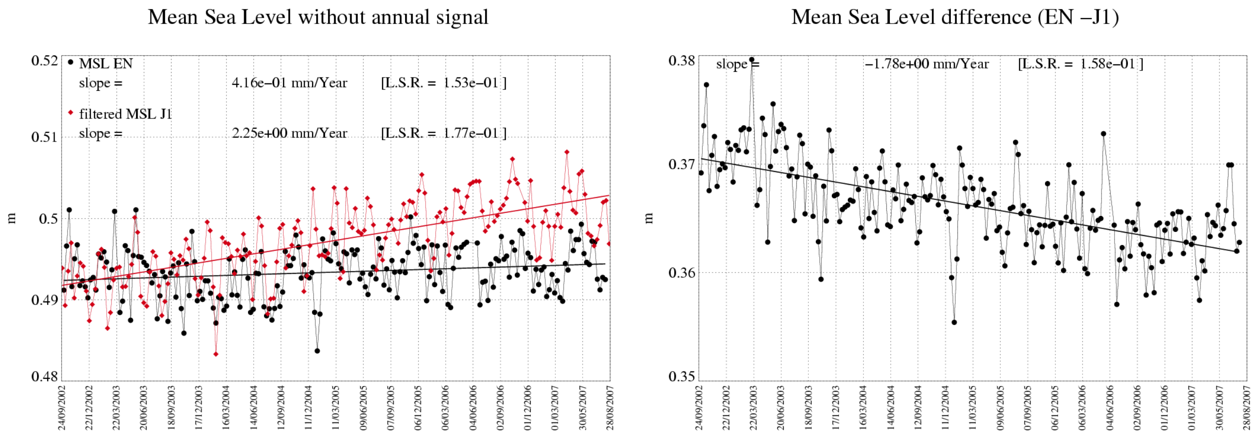

Figure 32: *Envisat and Jason-1 MSL trend over the period 2003-2007 (cycles Envisat 9 to 62) (left), Envisat - Jason-1 MSL trend (right)*

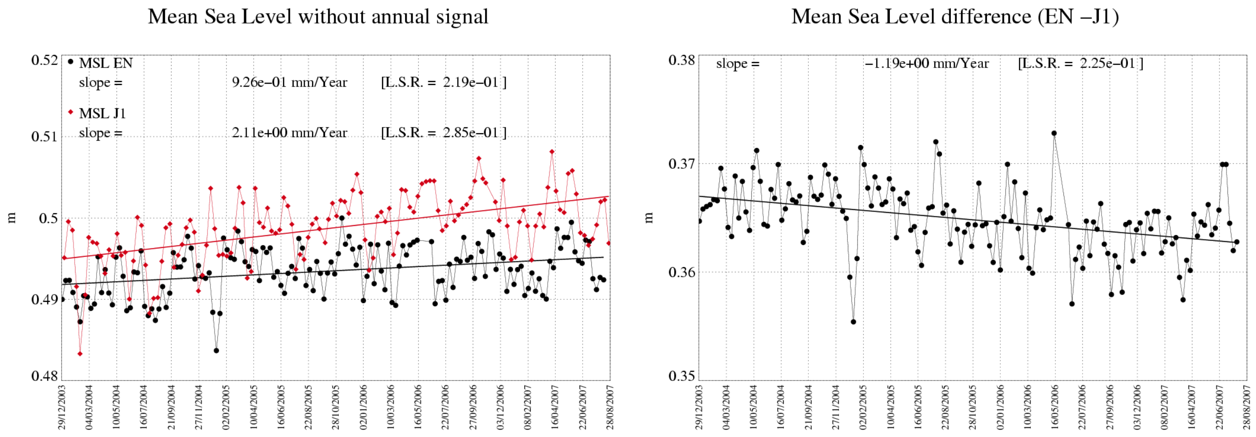

Figure 33: *Envisat and Jason-1 MSL trend over the period 2004-2007 (cycles Envisat 23 to 62) (left), Envisat - Jason-1 MSL trend (right)*

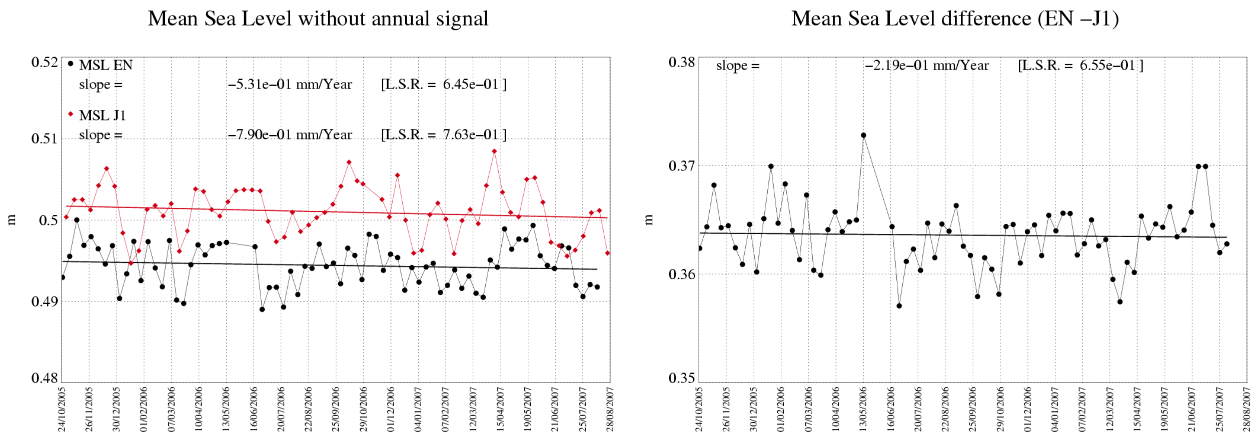

Figure 34: *Envisat and Jason-1 MSL trend over the period 2006-2007 (cycles Envisat 42 to 62) (left), Envisat - Jason-1 MSL trend (right)*

8 Particular investigation

8.1 Quality assessement of the product' S-Band Anomaly Flag over all surfaces

8.1.1 Introduction

Before cycle 60, an anomaly occured regularly on S-Band ENVISAT RA-2 data, provoking a degradation of altimetric S-Band range. Because S-Band Range is an input of the dual frequency ionospheric correction. This anomaly is a major issue for the RA2 data.
To remove spoiled data, two types of editings were used:

- an editing based on a threshold applied on the Sigma 0 difference in S and Ku Band. This method is applied since the Beginning of the Mission.
- an editing computed in the product (detailled in [44]). This method is in the product since Cycle 54.

On the 27th of June 2007, (Cycle 59, pass 433) an on board patch was installed to solve S-Band Anomalies. From that date, the anomaly no longer exists.

The aim of this document is to check the efficiency of the product flag on all (ocean, ice and lands) surfaces.

The validation of this flag consists in checking that after Cycle 54:

- All flagged data do correspond to S Band Anomalies periods : to bring out the so called Over-Editing
- All S Band Anomalies are flagged : to bring out the so called Under-Editing

8.1.2 After the on board patch installation: check of Over-Edited points

After the on board patch was installed to solve S-Band Anomalies, the anomaly no longer exists. In order to check the existence of over-edited points, the edited points are plotted for both flags for such a patched cycle.
The example of Cycle 61 is shown on Figure 35. The data edited on Sigma 0 criteria flag are plotted on the top left map and the data edited on the product flag are plotted on the top right map. Data edited with the Sigma 0 criteria flag and NOT edited with the product flag appear in red on the bottom map. Data edited with the product flag and NOT edited with the Sigma 0 criteria would appear in blue on the same map (no points are concerned).

On ocean surfaces, these figures show that isolated points are over-edited by the Sigma 0 criteria flag whereas the product flag is never activated. No over editing can be noticed with the product flag on ocean.

On non ocean surfaces, it is seen on Figure 35 (top left) that Sigma 0 criteria is almost systematically set to default on lands and ice. Contrarily, the product flag seems reliable, however, high altitudes area (The Andes Cordillera, Rocky mountains, Himalaya mountains) as well as some icy zones are still edited where they should not.

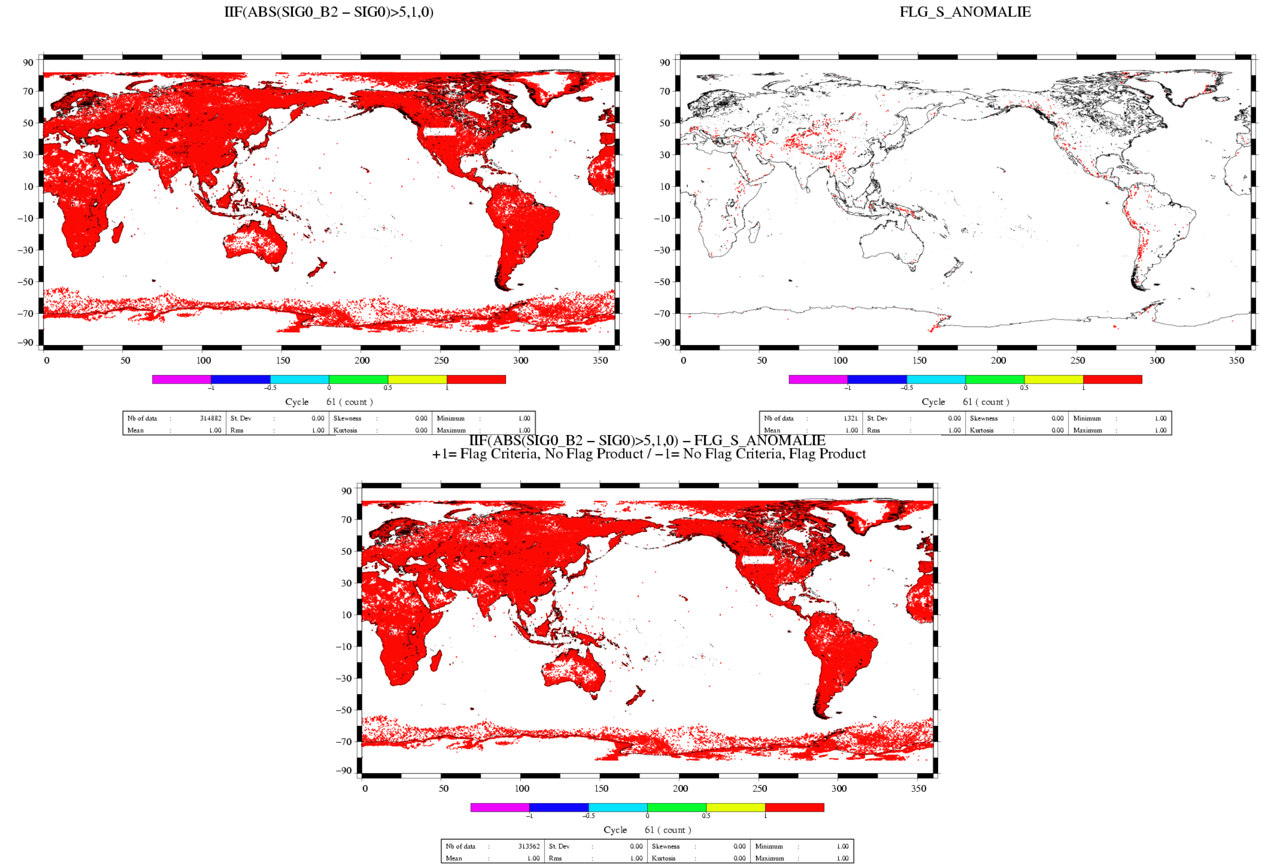

Figure 35: *Map of the data edited on Sigma 0 criteria flag (top left). Map of the data edited on the product flag (Top right). Difference of data edited with both flags (bottom). CYCLE 61: No more Anomaly.*

This study showed similar conclusions on these zones when performed on other cycles before and after the correcting patch.

Conclusion: The on board product flag is efficient over ocean. On lands, points are regularly over-edited on high altitudes area as well as on some icy zones.

8.1.3 Before the on board patch installation: check of Under-Edited points

On ice and lands, the Sigma 0 criteria flag is unusable because almost systematically set to default as seen on Figure 35 (top left). This part therefore focuses on the product flag.
In order to check the existence of under-edited points, the S Band anomaly flag's value was plotted for a S Band anomaly period. The example of passes 183 to 193 of Cycle 59 (see Figure 36 top left) is taken. Red points correspond to edited points (flag=1) whereas green points correspond to not edited points (flag=0).

Figure 36 top right shows that some points are actually "forgotten" on land during the anomaly. Those points are isolated and not located in a particular area.

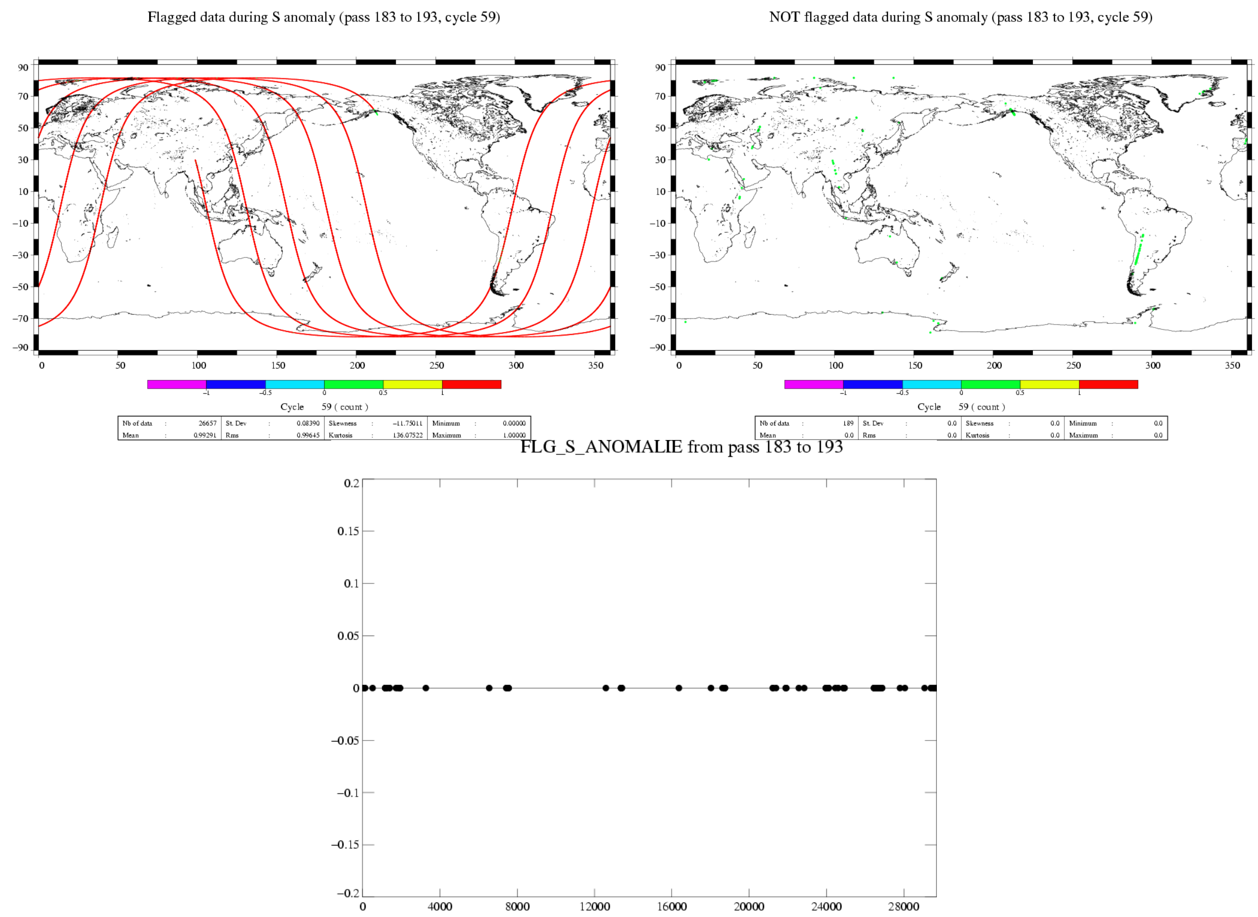

Figure 36: *Values of the product FLAG during an anomaly period (top left). Map of data NOT edited by the product FLAG on this period (Top right). Values of the product FLAG during an anomaly period (bottom). Cycle 59 pass 183 to 193: S-Band Anomaly noticed.*

Conclusion: Some points can be punctually "forgotten" by the product flag on lands.

8.1.4 Conclusion

The product flag was assessed on all surfaces. The on board product flag is efficient over ocean. However, on lands, points are regularly over-edited on high altitudes area as well as on some icy zones.

Similarly, few isolated points are not flagged when the Anomaly occurs.

8.2 Study on High frequency content

8.2.1 Introduction

This year, a study was performed to analyse and compare the high frequency content of data observed by Envisat and Jason-1 altimeters. Spectral analysis were performed, with 20Hz and 1Hz data. This study folows preliminary studies ([22] and [29]) which had shown that the high frequency content was different on Jason-1 and Envisat missions. Concerning Jason-1, differences were also noticed when comparing GdrA and GdrB. This new study enables to precise the questions raised by these analysis.

The full study is available at [28]. This part synthetises its main results.

8.2.2 Data and methods

The different estimation algorithms, data used, as well as the method of HF extraction are presented hereafter.

8.2.2.1 Data used

The parameters estimation is based on a Least Square fitting of the measured echo by a model with 3 or 4 parameters. This mean square fitting is derived from a Maximum Likelihood Estimator [Ref 2].
- **MLE3** is an acronym to define the Least Square fitting of the measured echo by a model with 3 parameters: Sigma 0, Range and Significant Wave Height (SWH).
- **MLE4** is an acronym to define the Least Square fitting of the measured echo by a model with 4 parameters, the additional parameter being the mispointing of the waveform.

Envisat Gdr (MLE3), Jason-1 GdrA (MLE3) and GdrB (MLE4) are used for this study. Both missions are analysed on 1Hz and 20Hz data.
- 1Hz Envisat GdrB/Jason-1 GdrB comparison is performed over the periods 7 to 26 September 2006.
- 1Hz Envisat GdrB/Jason-1 GdrA comparison is performed over the periods 5 to 14 September 2005.
- 20Hz Envisat GdrB/Jason-1 GdrB comparison is performed over the periods 7 to 8 September 2006.
- 20Hz Envisat GdrB/Jason-1 GdrA comparison is performed over the periods 5 to 6 September 2005.

8.2.2.2 Spectral analysis method

The spectral analysis enables to identify the location of the energy contained in a given bandwidth.
If the spectrum is modelled as a signal added to noise, the spectrum can be seen (cf. Figure 37) as a decreasing spectrum added to a white noise spectrum that is a uniform plateau (energy equally distributed on all frequencies).
The high frequency plateau can therefore be interpreted as the noise level of the data.

The method used to plot spectra is based on the spectrogram method which consists in averaging N Fast Fourier Transform, calculated on samples constituted of M points along track. The length of the samples is 300 points or 15 seconds for 20Hz data and 160 seconds for the 1Hz data.

The bandwidth analysed with this method concerns frequencies between the inverse of the spectrogram window's size and Shannon frequency (inverse of the sampling period). These frequencies can also

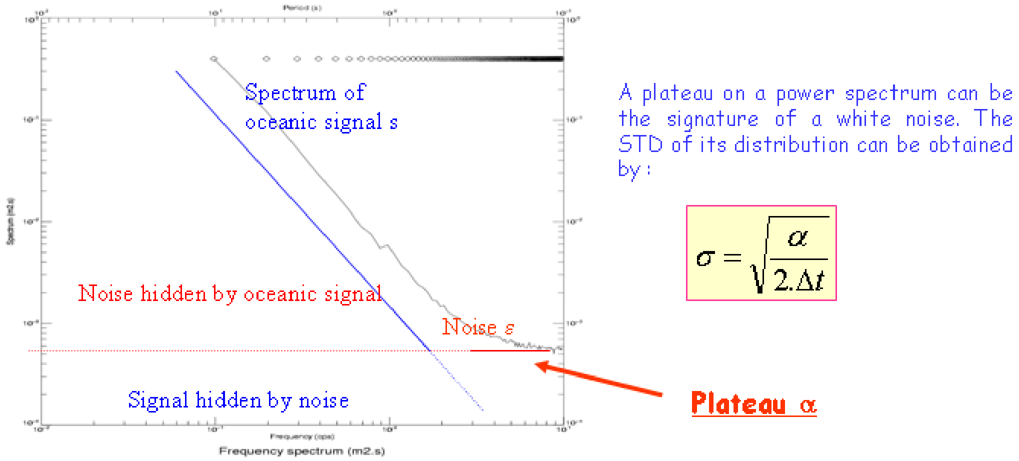

Figure 37: *The spectral method.*

be converted into distances with the relation: Distance = Ground_Satellite_Speed * Frequency, where Ground_Satellite_Speed = 7km/s.

For **1hz data**, analysed frequencies are:
- between 2 and 160 seconds.
- between 0.006 Hz (1/160 seconds) and 0.5 Hz (1Hz/2).
- between 14 km and 1120 km.

For **20hz data**, frequencies analysed are:
- between 0.1 and 15 seconds.
- between 0.07 Hz (1/15 seconds) and 10 Hz (20Hz/2).
- between 700 m and 105 km.

Because the Fourier Transform needs continuous samplings, managing gaps of data is a major issue in this method. Here, holes are filled up by an average value in order to have continuous samples. The number of missing data as well as the amount of consecutive missing data can be chosen. For this study, we allowed 10% missing points and 7 consecutive missing points.

8.2.2.3 SLA frequency content

SLA is a difference of Orbit, Range, Corrections and Mean Sea Surface (MSS) :

$$SLA = Orbit - Range - MSS - Corrections \quad (1)$$

Where the sum of correction is:

$$Corrections = ssb.cls + iono.smooth + dry\_tropo.ecmwf + wet\_tropo.ecmwf\_G + inv\_baro.mog2d + ocean\_tide.got00V2\_S1\_S2 + solid\_tide + pole\_tide \quad (2)$$

All SLA components are available at 1Hz. Orbit and Range are also available at 20Hz. Corrections are supposed to sign at low frequencies. Thus, the 20Hz corrections are a duplication of 1Hz correction, only the MSS which contains strong gradient in several part of the globe is interpolated using a spline technique at 20Hz. Spectra are performed using uncorrected SLA.

8.2.3 Difference of High Frequency content using MLE4 instead of MLE3

Thanks to Jason-1 reprocessing from GdrA to GdrB, differences of behaviour could be analysed between a SLA using a Range estimated with MLE3 or MLE4. In term of high frequency content, big differences were observed.

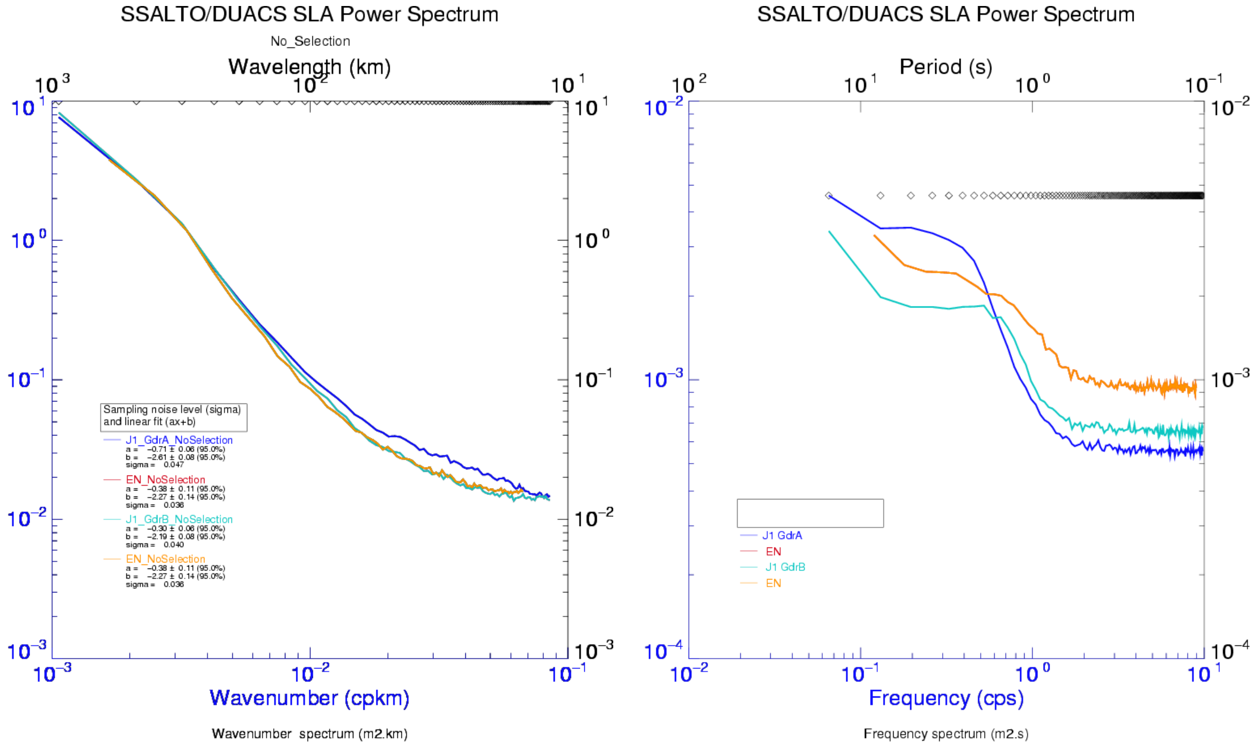

Figure 38: *1Hz versus km (left) and 20Hz versus seconds (right) Spectrums using MLE3 (GdrA) or MLE4 (GdrB). No selection.*

Figure 38 shows the impact of changing the estimation algorithm on Jason-1 with GdrA, GdrB and on Envisat.

Figure 38 (left) shows that Jason-1 GdrB 1Hz data are more consistent with Envisat data although the estimating algorithm is different. Unlike with Jason-1 GdrA, GdrB spectrum is almost super-imposed to Envisat's and it now presents a flat part corresponding to the so called 1Hz noise which is slighly higher for Envisat than for Jason-1.

For frequencies greater than 1Hz, Figure 38 (right) also shows a better consistency between Jason-1 GdrB and Envisat than between GdrA and Envisat. The noise level is increased on GdrB compared to GdrA because the estimation of a 4th parameter in a MLE increases noise. However, the difference between MLE3 and MLE4 is that the mispointing is estimated in the latter, in addition to the three others (range, waves and sigma0). Therefore, those spectra show that estimating the apparent mispointing more precisely reduces the bump observed for the frequencies between 0.1-0.4Hz (between 20km and 70km).

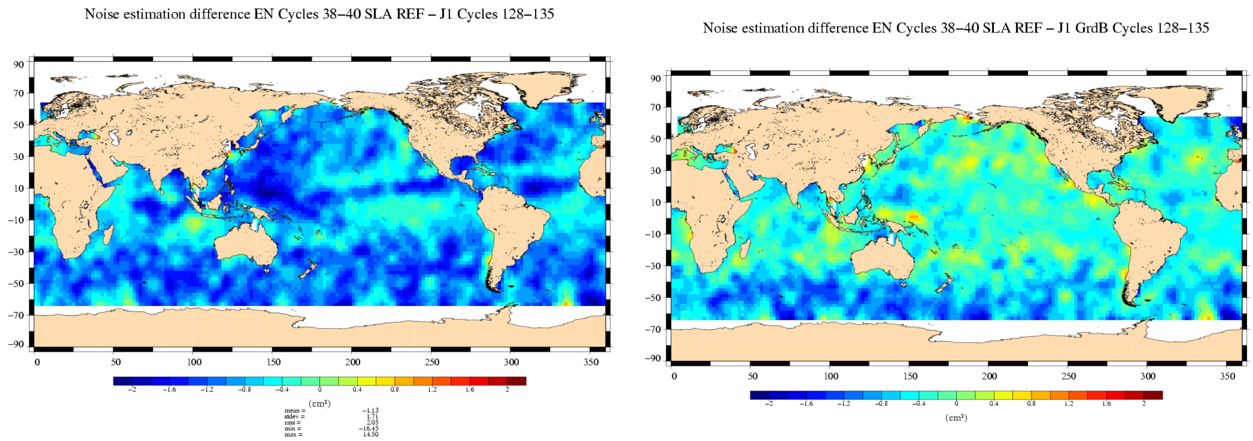

Figure 39: *Difference of Variance Envisat - Jason-1 GdrA (left) and Envisat - Jason-1 GdrB (right).*

The MLE4 seems to decorrelate the high frequency signal (increase of high frequency 20Hz plateau) and to correlate a signal signing in a frequency bandwidth of 20km to 70km.

In order to localise the geographical zones where Envisat and Jason-1 are consistent in term of noise, the SLA was high pass filtered with a 20km cut off distance. The difference of variance calculated per 2deg/2deg boxes is plotted on Figure 39. It shows that Envisat and Jason-1 are more consistent in term of noise at low latitudes and mainly in wet areas (from 5cm^2 to 0.5cm^2 in western pacific and altantic basins) but the difference remains rather high in the circumpolar zone (still around 2cm^2).

On Figure 40, 1Hz and 20Hz spectra are plotted on the same graph. This underlines that the 1Hz frequency of the 20Hz spectrum is not totally superimposed to the 1Hz frequency of the 1Hz spectrum.

Four points are therefore raised:

1. Contrarily to the theoretical ocean spectrum which is mostly a low frequency signal + high frequency noise, Envisat and Jason spectrum present a bump in a frequency bandwidth of 20km to 70km. What causes this unexpected energy?

2. The bump on Jason-1 spectrum is smaller when the apparent mispointing is estimated (GdrB) than when it is not (GdrA).

3. At 1Hz and 20Hz, Envisat MLE3 spectrum is more consistent with Jason-1 MLE4 (GdrB) spectrum than with Jason-1 MLE3's (GdrA). Can this be explained?

4. Plotting both 1Hz and 20Hz spectra on the same Figure 40 underlines that the 1Hz frequency of the 20Hz spectrum is not totally superimposed to the 1Hz frequency of the 1Hz spectra. Does it reveal a problem of compression in the 1Hz data?

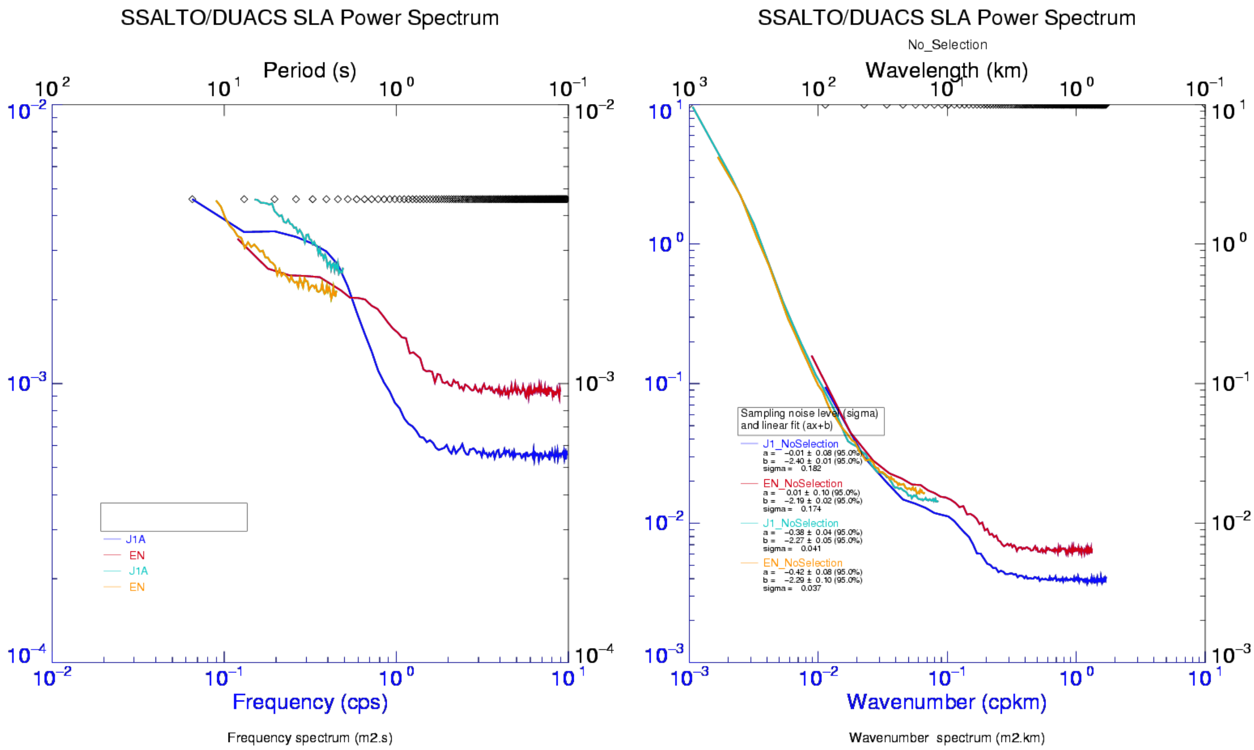

Figure 40: *1Hz and 20Hz Spectrums using MLE3 (GdrA) versus seconds (left) or MLE4 (GdrB) versus km (right). No selection.*

8.2.4 Energy bump in the bandwidth 20km - 70km

8.2.4.1 Impact of selection on mispointing value

Contrarily to the theoretical ocean spectrum which is mostly a low frequency signal + high frequency noise, Envisat and Jason spectrum present a bump in a frequency bandwidth of 20km to 70km (or 0.1-0.4Hz or 2.5-10s) which is likely to be due to a signal appearing or disappearing with this frequency. It is shown that Envisat and Jason-1 are more consistent when apparent mispointing is estimated on Jason-1. Furthermore, the energy bump disappears when high apparent mispointing zones are excluded and increases when small apparent mispointing zones are excluded (Figure 41 shows the results for Jason which are similar to Envisat's (Figure 42)).

The associated zone edited by the threshold on the absolute value of apparent mispointing are plotted on Figure 41 and 42, for low apparent mispointing (top left) and for high apparent mispointing (top right). Those maps represent the percentage of data used, averaged on 2° by 2° boxes relatively to a reference grid of valid ocean points, with bathymetry greater than 1000m.
Purple boxes represent the zones were less than 40% of the data are selected for the spectral analysis. Red boxes represent the zones were 100% of the data are selected for the spectral analysis. These maps show that high mispointing are mostly placed in humid zones but also randomly spread on all oceans.

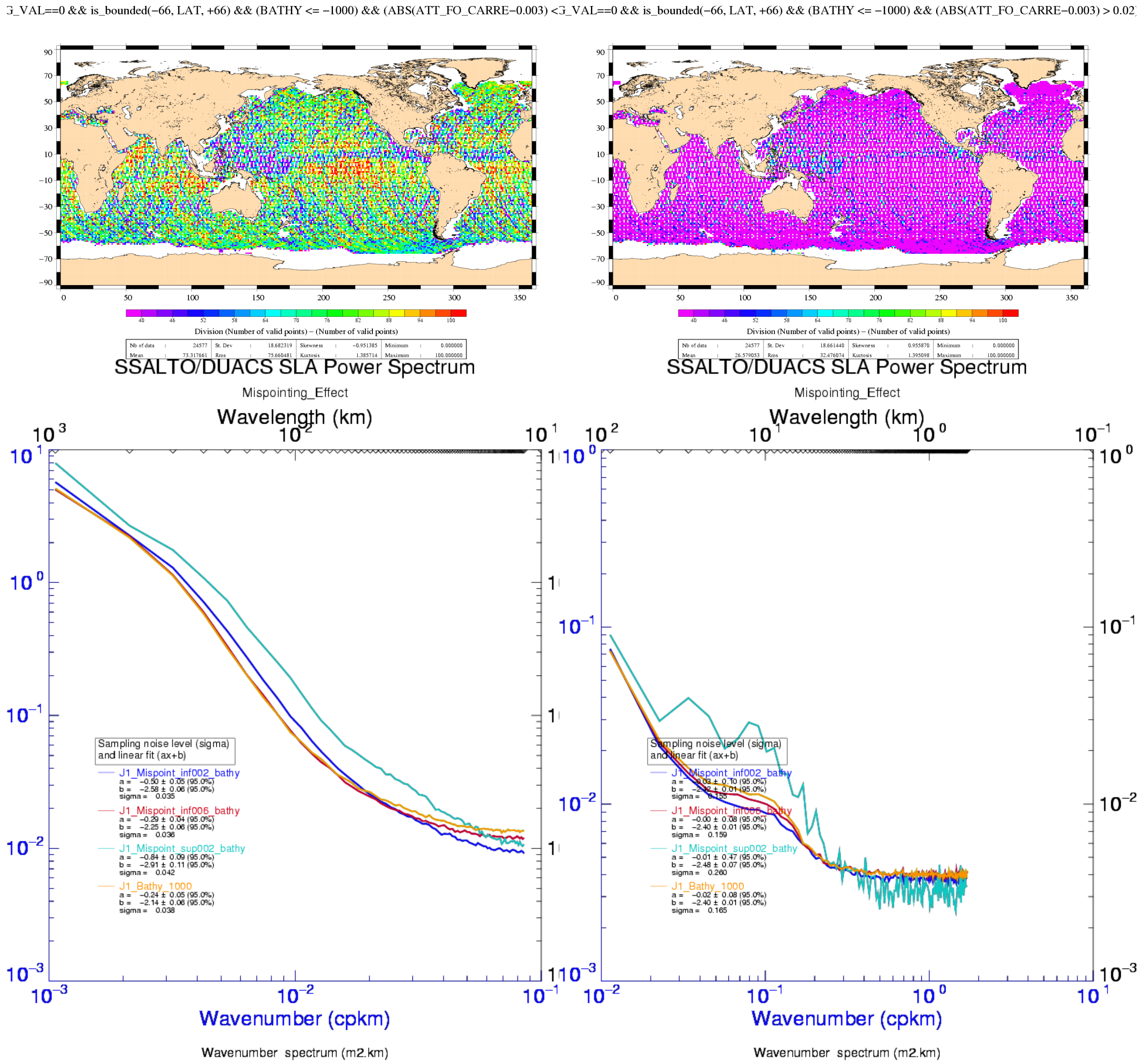

Figure 41: *Centred apparent mispointing smaller than 0.02deg² (top left), greater than 0.02deg² (top right). Percentage of points used for the analysis on Jason-1 for low mispoointing:* ***73%*** *and low mispoointing:* ***26%****. Jason-1 impact of mispointing selection on 1Hz spectrum (bottom left), and on 20Hz spectrum (bottom right).*

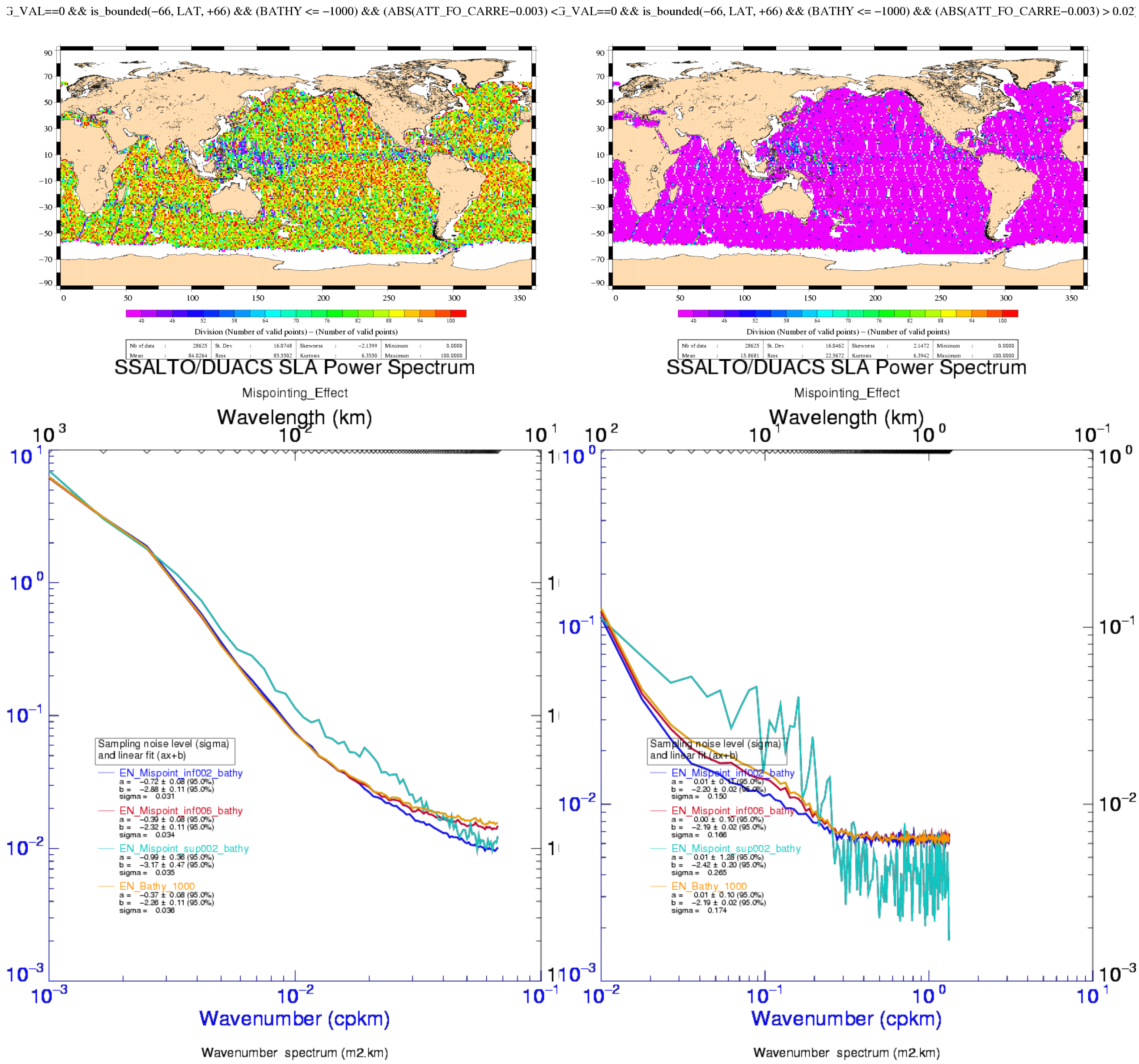

Figure 42: *Centred apparent mispointing smaller than 0.02deg² (top left), greater than 0.02deg² (top right). Percentage of points used for the analysis on Envisat for low mispoointing:* ***84%*** *and low mispoointing:* ***16%****. Envisat impact of mispointing selection on 1Hz spectrum (bottom left), and on 20Hz spectrum (bottom right).*

8.2.4.2 Physical meaning of high mispointing values

High apparent mispointing zones seem to coincide with wet areas (between tropics) which are also zones of high Sigma 0, high liquid water content, but when high mispointing is compared to those parameters, the link is less direct than expected.

Figure 43 (left and right) shows that a high apparent mispointing does not correspond systematically to an active rain flag.

Figure 44 (left and right) shows that on the points of high apparent mispointing, a high variability is observed on the range parameter.

And figure 45 (left and right) shows that high apparent mispointing points correspond to high values of liquid content and high sigma zero values.

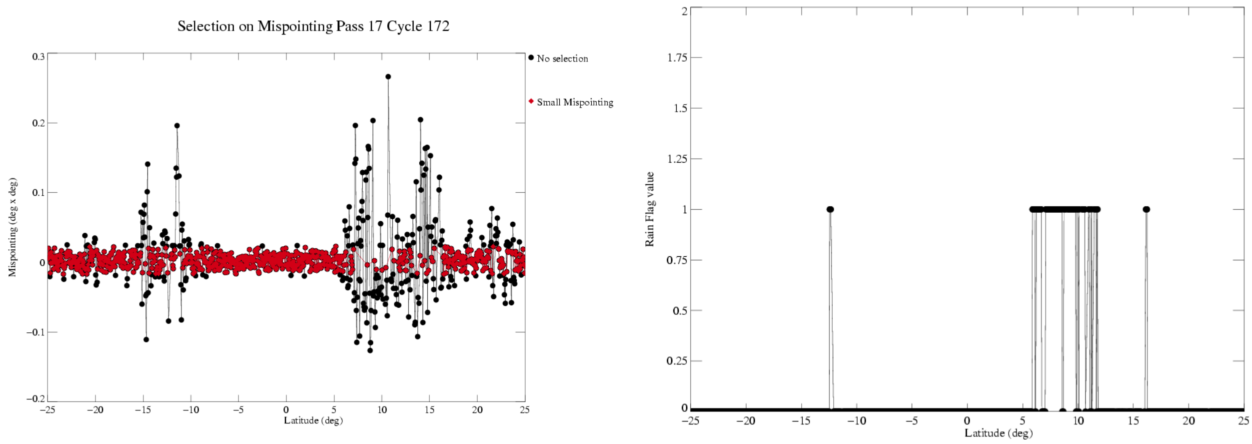

Figure 43: *Selection on apparent mispointing (left) small apparent mispointing red, high apparent mispointing black compared to the Rain flag value (right).*

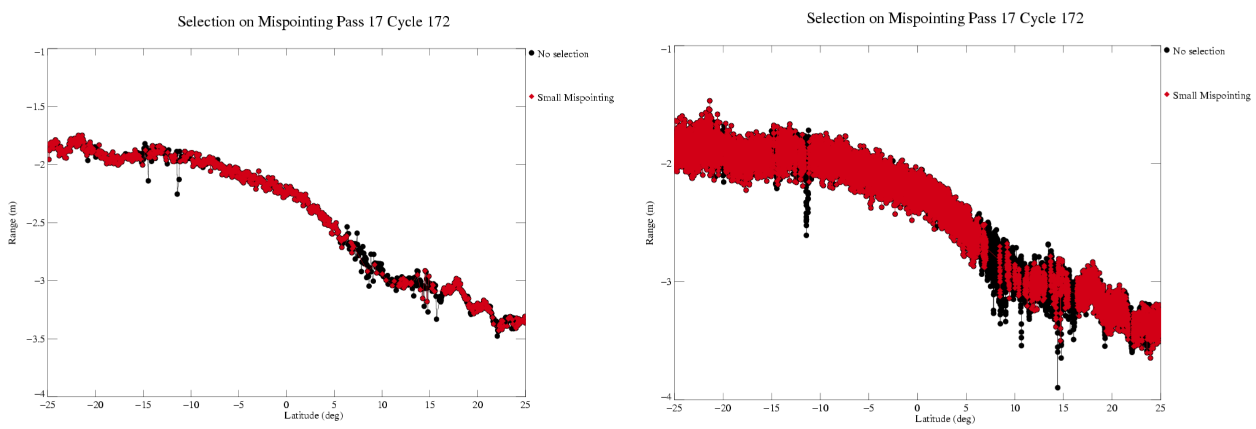

Figure 44: *Selection on apparent mispointing: on Range 1Hz (left), Range 20Hz (right).*

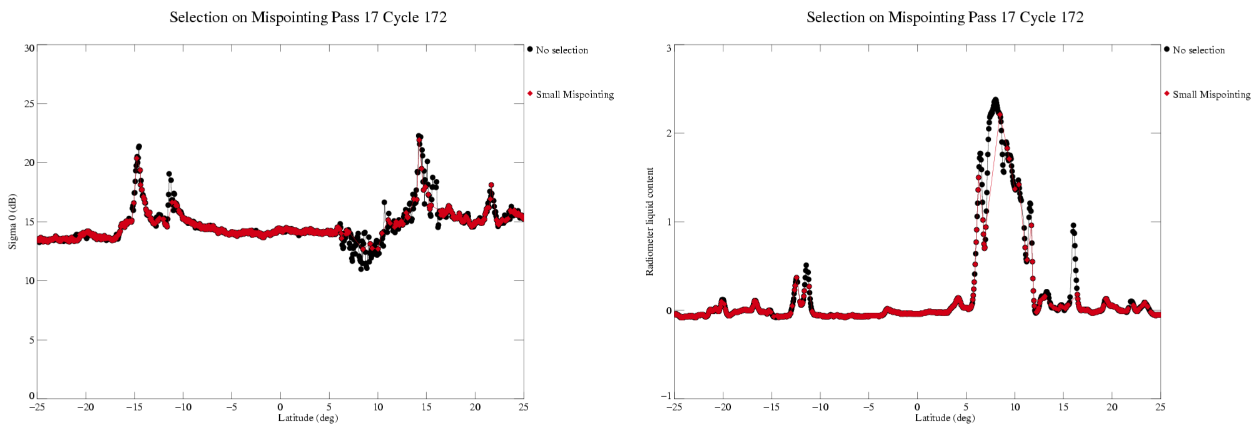

Figure 45: *Selection on apparent mispointing: on Sigma 0 (left), on Radiometer liquid content (right).*

The variability of those different parameters compared to the high apparent mispointing zones enables to conclude that in the high apparent mispointing zones, the waveforms seem to be polluted by a particular sea surface state (sigma bloom or rainy zone) which are not entirely identified by the current rain flag.

Figure 46 shows the corresponding spectrum. The two first editings enable to keep more than 90% of the data and do not change much the spectrum. But the third one enables to see that throughout the percentage (14% for Envisat and 26% for Jason-1) of data with a apparent mispointing higher than 0.02deg^2, less than 20% are situated in rainy zones, the rest being spread on all oceans ($\frac{(16-14)}{14}$=14% for Envisat and $\frac{(26-21)}{26}$=20% for Jason-1.

This test enables to show that the selection on these parameters is not equivalent to an editing on high mispointing because the 1Hz spectrum is unchanged with this selection unlike with the apparent mispointing threshold of 0.02deg^2.

Editing small wave height (which is another way of avoiding humid zones) does not give either the same results as editing high mispointing. Selection on low wave heigh shows interesting result as seen in the next part.

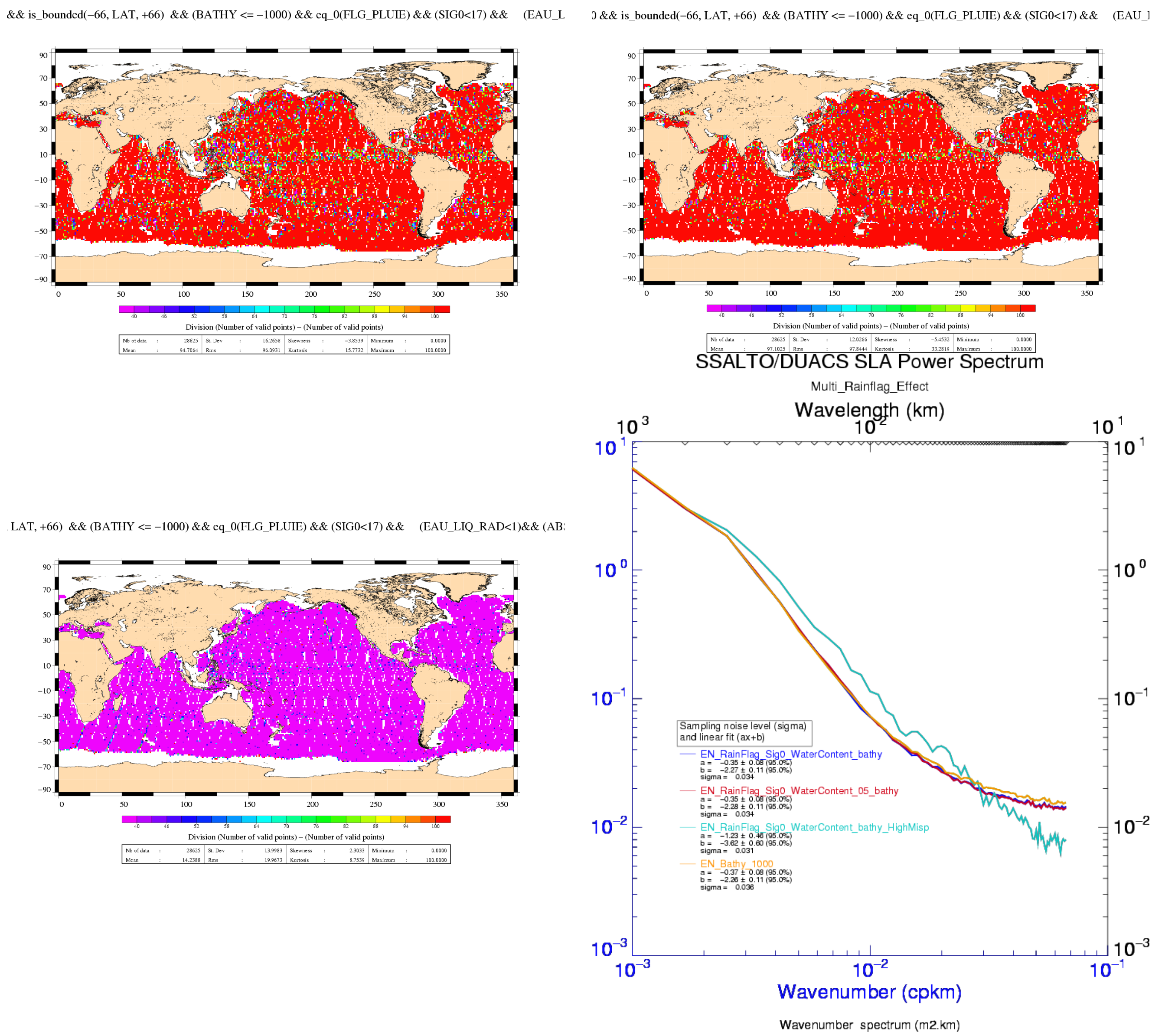

Figure 46: *On Envisat, Rain flag off, Water content lower than 1, Sigma0 greater than 17 effect compared to the low mispointing selection effect.*

8.2.4.3 Impact of selection on waves

Selection on wave heigh on Jason-1 20Hz data is seen Figure 47.

Without any surprise, and similarly on Envisat data, the spectrum shows that the higher the waves the higher the noise. But it is also seen that for both missions, small waves are more correlated at 20-70km frequency than high waves. The remark must be taken cautiously because of the small amount of data concerned (10%) but the pic at 20-70km frequency would worth beeing investigated.

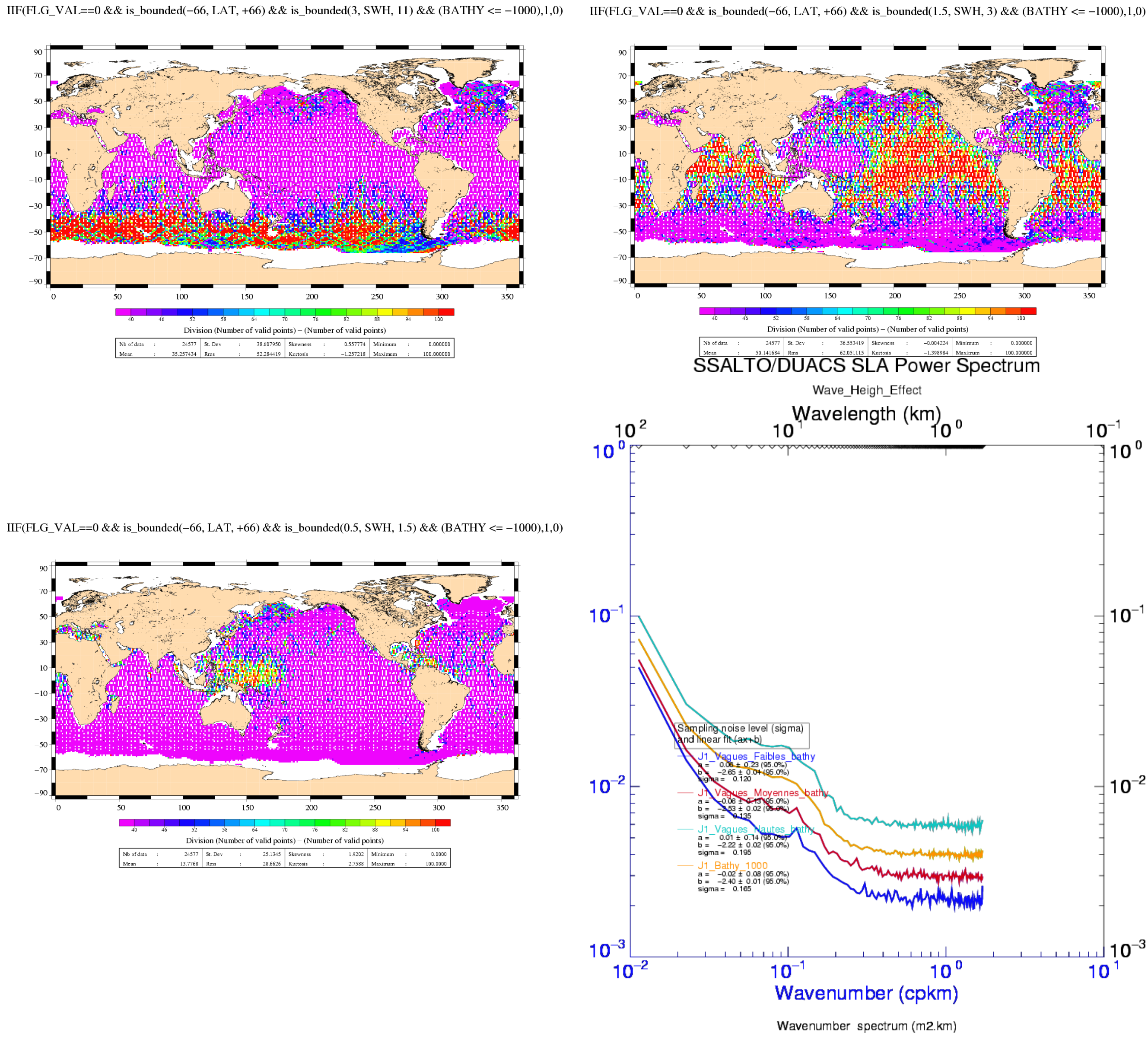

Figure 47: *A: High waves (between 3 and 11m). Percentage of points used for the analysis on Jason-1 35% (top left). B: Average waves (between 1.5 and 3m). Percentage of points used for the analysis on Jason-1 50% (top right). C: Small waves (between 50cm and 1.5m). Percentage of points used for the analysis on Jason-1 14% (bottom left). D: Impact of selection on Wave height on spectra for Jason-1 20Hz (bottom right).*

8.2.4.4 Impact of valid points per seconds

The bump seems to be due to data localised on zones where waveforms differ from the ocean model. Indeed, the map of valid data per second greater than 19 (Figure 48) is seen to be different from Envisat (global coverage) and Jason-1 (data missing in the same zones as high mispoining zones). Furthermore, applying a selection of 20 valid values per seconds for Jason-1 enables to obtain a 1Hz spectrum similar to the one obtained with mispointing higher than $0.02deg^2$.

This means that unlike Jason-1, editing Envisat valid values per seconds does not enable to edit atypical waveforms.
The difference of valid values per seconds for both data raise two questions:
- Why is the number of data lower on Jason-1 than on Envisat? Do Jason-1 aquire fewer data? or does its processing edit more data?
- For the points where few data are kept: is the 1Hz average less robust because there is less data? or are the remaining waveform still degraded which unvalidates the retracking?

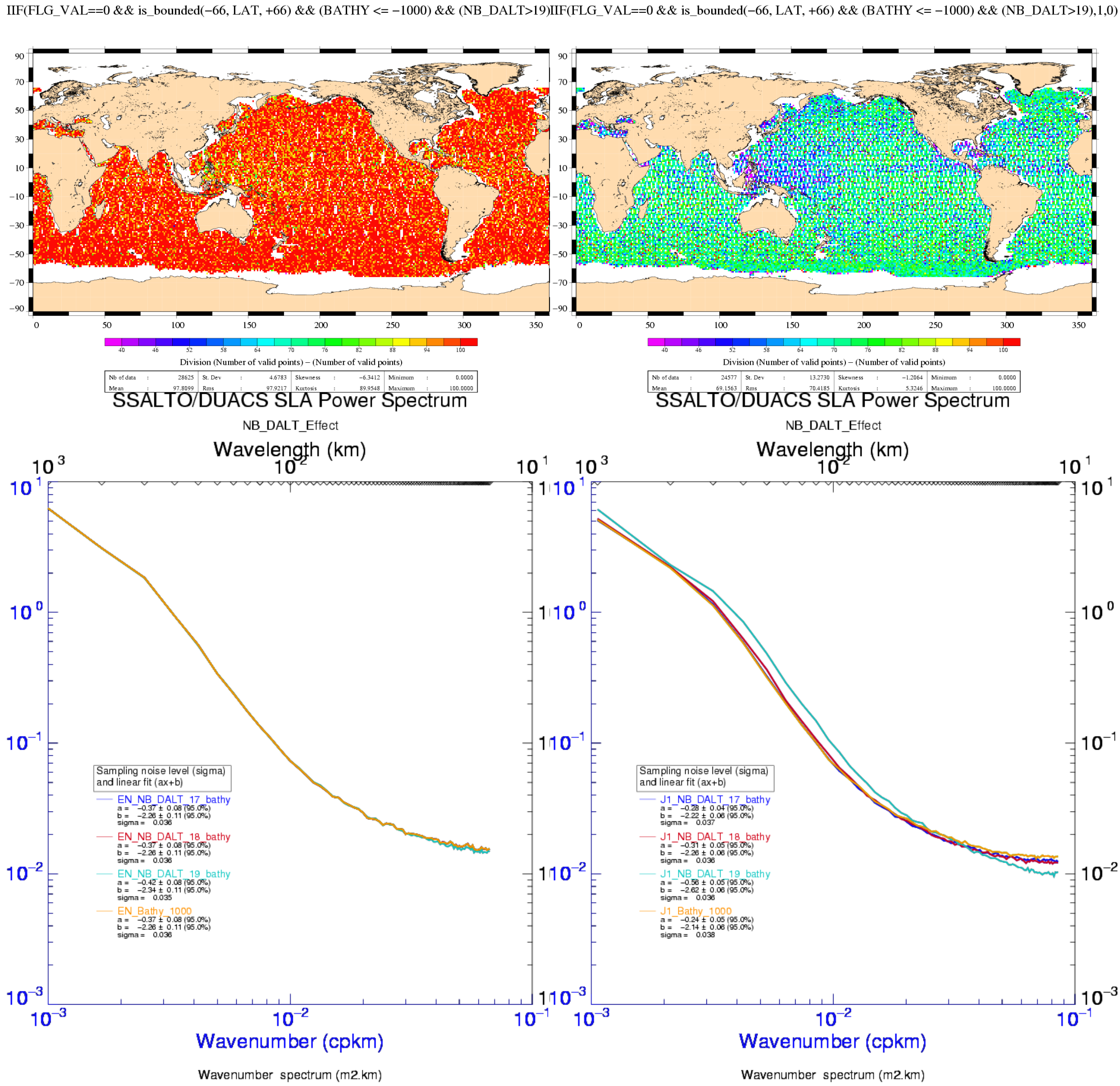

Figure 48: *Number of valid data per second greater than 19. Percentage of points used for the analysis on Envisat: 98% (top left) and Jason-1: 69% (top right). Impact of selection on valid number per second on 1Hz spectra for Envisat (bottom left) and Jason-1 (bottom right).*

8.2.5 Conclusion

This document shows that a bump on Envisat and Jason-1 spectra can be seen in the 20-70km band. This bump seems to be due to data localised on zones where waveforms differ from the ocean model. For the moment, no physical editing of atypical waveforms could be identified although the apparent mispointing or the number of valid values per seconds (for Jason-1) are seen to have a significant impact.

Further analysis would be needed to understand the processing of atypical waveforms:
- the differences of editing on both missions must be analysed in order to understand why more data are edited on Jason-1 than Envisat.
- the waveforms situated on zones where the mispointing is high and where the number of valid data per second is low must be looked at more precisely in order to identify the causes of the range instability which seems to cause the bump.
- the results of geometric classifications would be an interesting way of selecting data in order to caracterize better this bump and the associate signal it reveals.

8.3 Wet Troposphere Range Correction: Difference Radiometer / Model

8.3.1 Introduction

There are two wet troposheric correction in the GDR products :

- A correction estimated along track by a microwave radiometer (MWR) on board
- A model correction estimated from ECMWF center (1 field every 6 hours).

The first one is known to be more accurate but noisier than the second one.

When looking at the monitoring per cycle of the mean per cycle of the difference between the MWR and the model Wet Tropospheric Correction, a sinusoidal annual signal seems to appear at the end of the serie(from 21/04/2006).
The aim of this study is to analyse this signal.

When plotted as a function of the latitude (blue and red plots on 49), this sinusoidal annual signal appears to be stronger (5mm amplitude) at high latitudes (between 30 and 66 degrees, red plot) than at low latitudes (sub tropical zone, for latitudes lower than 30 degrees, blue plot) (1 to 2mm of amplitude).

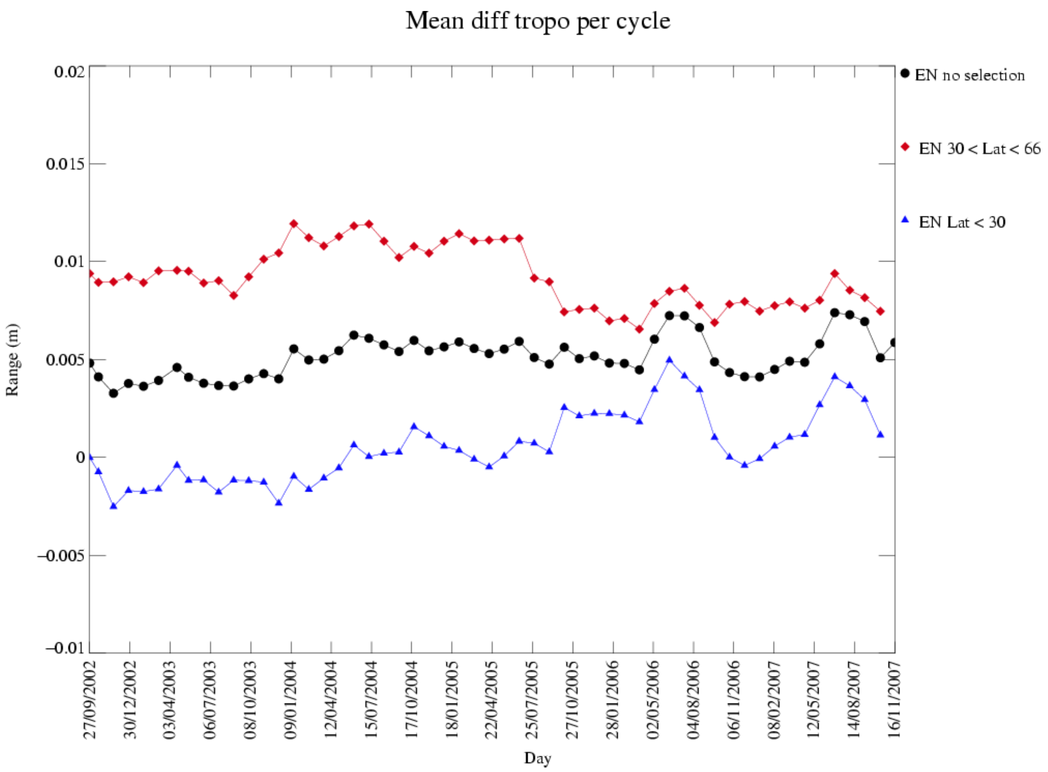

Figure 49: *Monitoring of the average difference MWR - ECMWF wet tropospheric corrections per cycle.*

Furthermore, at high latitudes, the signal is not the same if the monitoring is computed separatly on Ascending and Descending tracks (cf. Figure 50).

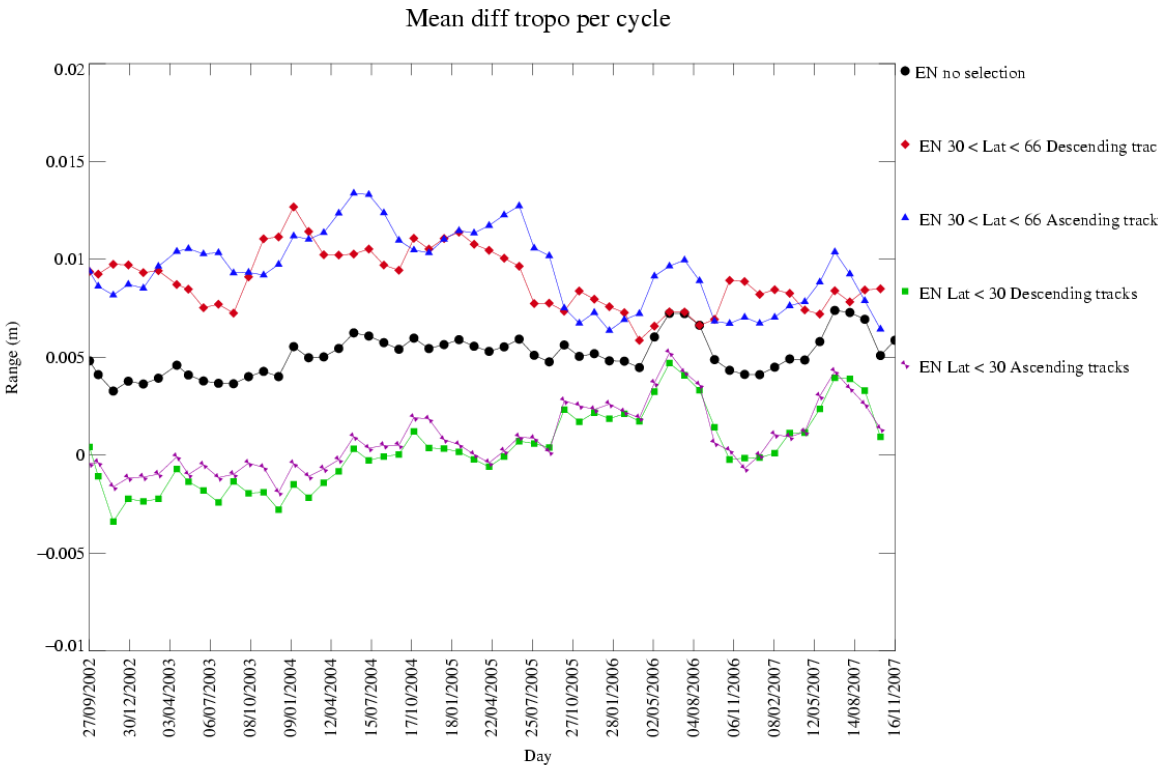

Figure 50: *Monitoring of the average difference MWR - ECMWF wet tropospheric corrections per cycle. Ascending and Descending tracks do not have the same behaviour at high latitudes*

8.3.2 Annual signal on Ascending and Descending difference

Concerning high latitudes, the Ascending and Descending difference MWR - ECMWF wet tropospheric corrections vary in opposition of phase.
Let's analyse the asymetry of estimation between modele and radiometer through the difference:
Descending (MWR - ECMWF) - Ascending (MWR - ECMWF)
For high latitudes, this difference is traduced by a clear annual signal of about 3mm (cf. Figure 51).
A regression is performed on the monitorings with a function of the type:

$$A1 \cos(\omega\, t + \phi) + K1\, t + K0$$

Where the parameters A1 (Amplitude), ϕ (Phase), K1 (slope) and K0 (Bias) are estimated through a Least Square fit.

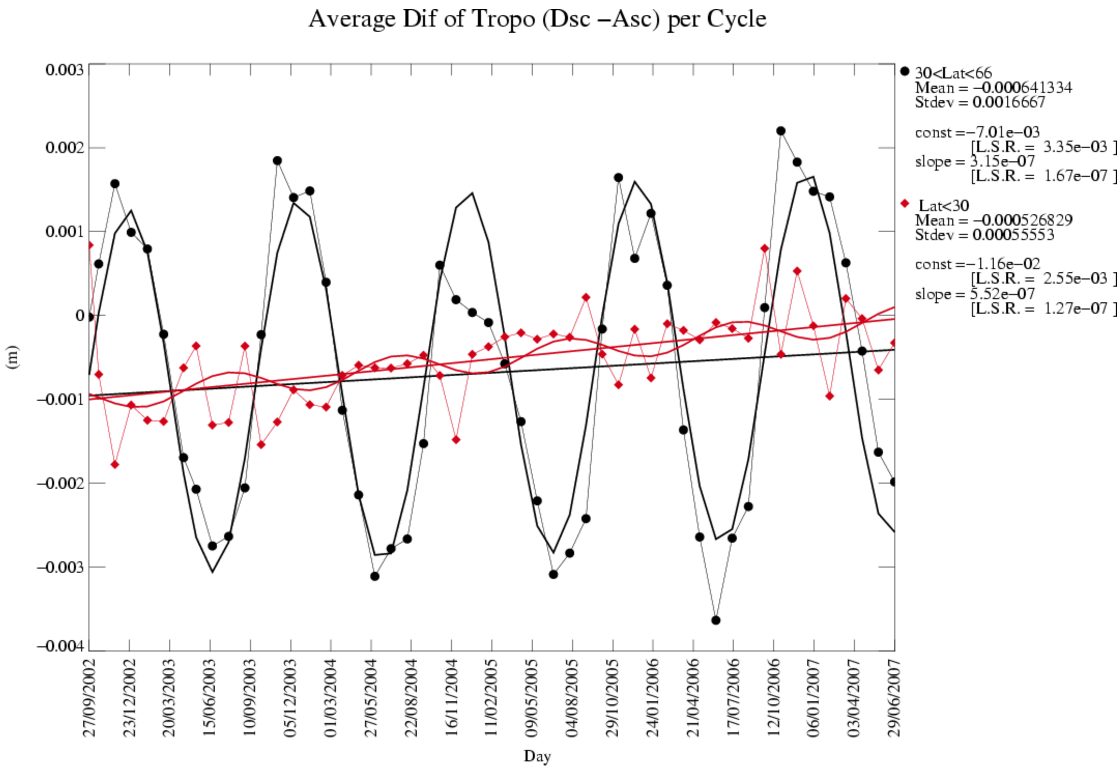

Figure 51: *Monitoring of the average difference [Descending (MWR - ECMWF) - Ascending (MWR - ECMWF)] wet tropospheric corrections per cycle.*

In order to specify the zones where the annual signal is the strongest, the regression seen on Figure 51 is performed by boxe of 2 degres by 2 degrees on all the ocean. The resulting parameters of every regression per boxe are then plotted. The more revelant parameters are shown hereafter: A1 (Amplitude) is plotted on Figure 52). ϕ (Phase) is plotted on Figure 53).

Those plots show that the zone affected by the annual signal of error between modele and radiometer is rather homogeneous with a mean amplitude of of 3mm except for Est Pacific and Atlantic basins where it reaches only 1.5mm and in the circumpolar current zone, in the southern hemisphere where it is maximum (around 5mm).
The amplitude of the annual signal is maximal in this zone and the signal seems to be in opposition of phase with the northern signal. Thus, this phase is consistent with what can be seen on Figure 51 as well (red and black plots are in oposition of phase).

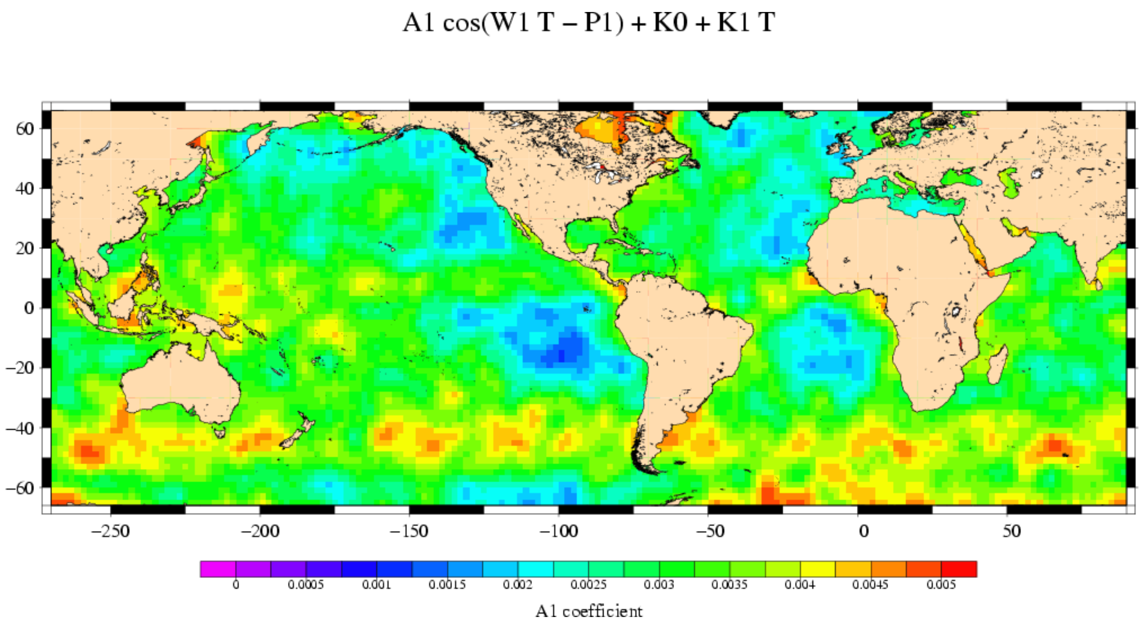

Figure 52: *Amplitude of the linear sinusoidal regression.*

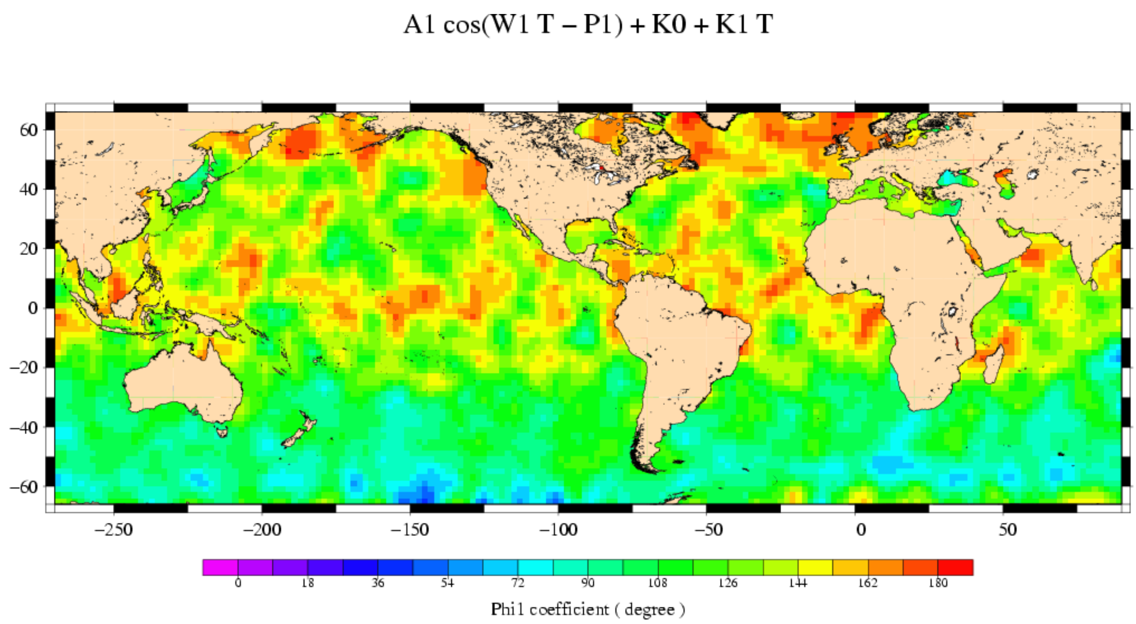

Figure 53: *Phase of the linear sinusoidal regression.*

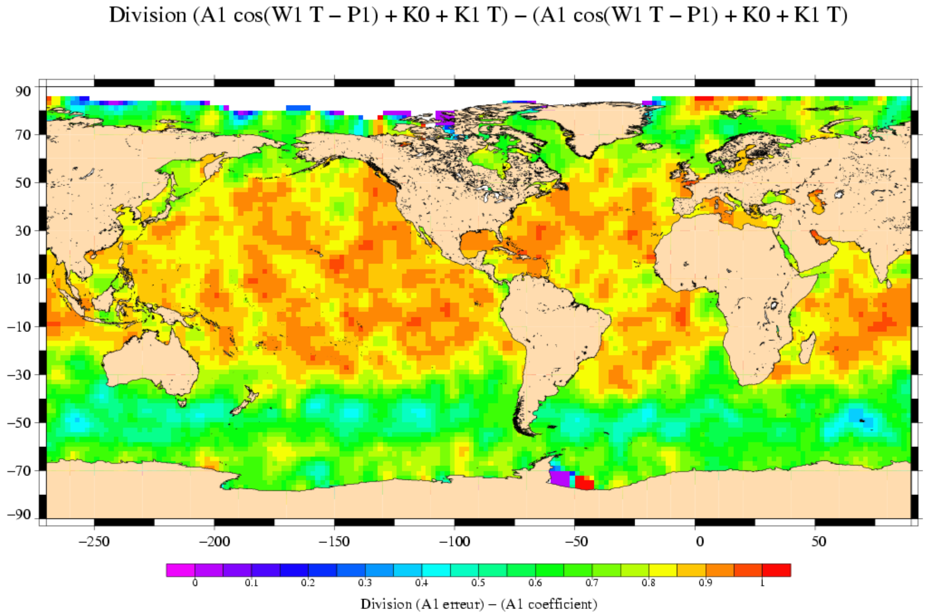

Figure 54: *Normed Error on Amplitude of the linear sinusoidal regression (in meters).*

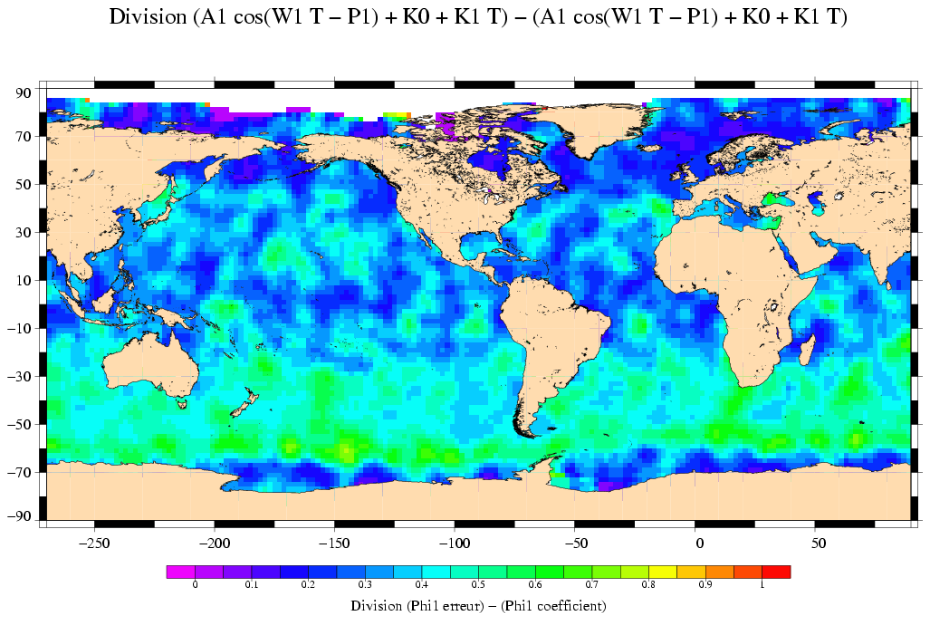

Figure 55: *Normed Error on Phase of the linear sinusoidal regression (in degres).*

8.3.3 Conclusion

An annual signal is observed when looking at the consistency of radiometric and model wet tropospheric correction.
- The monitoring per cycle of the mean per cycle of the difference between the MWR and the model Wet Tropospheric Correction is a signal of 1 to 2 mm amplitude reaching 5mm at low latitudes only.
- The differences between ascending and descending tracks on the two estimations (model or measure) is also sinusoidal of about 3mm in average, reaching 5mm in the circumpolar zone.

The cause of this bad consistency between ascending and descending tracks is likely to be due to a bad consitency of the diurnal (day/night) cycle of the tropospheric humidity content estimations. Actually, descending tracks are on the sunny side of the Earth whereas the ascending tracks are on the dark side.
By now, however, the cause of this difference between measure and model could not be attributed to one or the other of the estimations.

8.4 Orbit comparison analysis

8.4.1 Introduction

The aim of this study is to compare the orbit included in the product (CNES POE) to two other existing solutions developed in the European Space Operations Centre (ESOC POE) and the Department of Earth Observation and Space Systems of the Delft University of technology (Delft POE). These two solutions use recent standards, and are available over a long period, cycles 10-60. This allows us, first, to assess the quality of the GDR orbit through a cross comparison study over the GDR-B period (41 to 60). This also allows us to produce homogeneous SLA time series over the whole Envisat period, which is of interest for the analysis of MSL trend for exemple.

8.4.2 Orbit configuration

8.4.2.1 Envisat CNES POE (after cycle 41)

Reference systems:
- polar motion and UT1: IERS bulletin D with IERS 1996 daily and sub-daily corrections
- stations coordinates: DPOD2000 reference for Doris Stations, ITRF 2000 with minor corrections for a few SLR
- satellite reference: Post-Launch value of Mass + variations generated by Control Center, attitude model: Nominal Yaw Steering Law

Force models:
- EIGEN-CG03C gravity field model
- IERS 2003 Solid Earth tides
- FES 2004 (all principal constituents, with admittance) ocean tides
- Haurwitz and Cowley atmospheric tides
- Sun, Moon, Venus, Mars and Jupiter third bodies
- thermo-optical coefficient from pre-launch box and wing model for solar radiation with smoothed Earth shadow model
- MSIS86 model (ENVISAT), DTM 94(Jason), best available solar activity (unchanged), physical box and wing model for atmospheric drag with 1 Cd adjustment per 2Rev with a priori constraint
- Knocke-Ries albedo and IR model for Earth radiation
- 1/rev along-track and cross-track constant per 24 hours for empiricals

Tracking data:
DORIS:
- Troposphere correction: CNET1 model, vertical bias adjusted
- Frequency: Bias per pass adjusted
- Weight: 1.5 mm/s (for Jason : underweighting of the SAA stations)
- 6.5 microseconds datation bias on ENVISAT in order to cope with a 4.5 cm along-track bias with Laser orbits (6 microseconds on Jason).

LASER
- Troposphere correction: Marini-Murray following IERS 2000
- Retroreflector correction: Constant radial correction of 5.0 cm (Jason) and cm (ENVISAT) for all stations
- Bias/Pass: Solved-for for a few stations
- Weight: Globally 10 cm

- Ocean loading correction (FES99)
GPS (Jason) - Constellation ephemeris and clocks (5 min): precise JPL solution - Measurements sampling in orbit determination: 5 min - JPL Antenna diagram phase correction (Jason receiver) - phase windup correction - Receiver clock adjusted at every epoch - phase ambiguity per pass - Weight: 10 cm on phase, 1 m on code

8.4.2.2 Envisat ESOC POE

Configuration used for the solution generated November 2007 for CLS.
Reference systems:
- polar motion and UT1: IERS bulletin A with IERS 2003 daily and sub-daily corrections
- stations coordinates: ITRF-2005 reference for Doris Stations, ITRF 2005 rescaled append with ITRF-2000 for station not in ITRF-2005 - satellite reference: Post-Launch value of Mass + variations generated by Control Center, attitude model: Nominal Yaw Steering Law
Force models:
- EIGEN-GL04C gravity field model
- IERS 2003 Solid Earth tides
- FES-2004, 99 major constituents to order and degree 30
- Sun, Moon, and all Planets
- ANGARA model for drag, solar, infrared and albedo radiation
- MSIS-90 model for atmospheric density
Parameters
- 7-Day arcs, estimated Satellite State Vector, Solar radiation pressure per arc (constrained)
- ten drag coefficient and two 1/rev along-track and cross-track constant per 24 hours.
Tracking data:
- All station displaced corrections according to IERS 2003
- DORIS:
- Frequency: Bias per pass adjusted
- Weight: 0.5 mm/s
- Laser
- Troposphere correction: Mendes-Pavlis following IERS 2003 update
- Retroreflector correction: Constant radial correction of 5.12 cm for all stations
- Weight: Globally 4 cm

8.4.2.3 Envisat Delft POE

The orbits are available at http://www.deos.tudelft.nl/ers/precorbs/orbits/
Software:
- GEODYN-II (GSFC)
Force models:
- EIGEN-GRACE03C gravity field model
- Tides: PGS7751E (GSFC)
- Non-gravitational forces: or cycles up to cycle 52, the CNES box-wing panel model was used, and from cycle 53 onwards, the ANGARA models were used.
- Thermospheric density: MSIS-86
- for cycles up to cycle 52, the CNES box-wing panel model was used for surface forces
Reference systems:
- Earth-orientation parameters: from IERS EOP-C04
Parameters:

- Arc length: 5.5 days, new arc every 3.5 days, 2 days overlap
- Drag estimation sub-arc length: 1/4 orbit (25.1496 minutes)
- 1-cpr along/cross-track sub-arc length: 12 hours

Tracking data:

- DORIS data sigma: 0.50 mm/s
- SLR data sigma: 4 cm + 1-20 cm depending on station

8.4.3 Processing

The reprocessed CNES, ESOC and Delft orbits have been updated in the Envisat database for cycles 10-60. Before using these orbits the editing used for CNES orbit has been applied to the ESOC and Delft orbit in order to remove wrong measurements, mainly around maneuvers. A criteria base on differences between CNES and orbits studied has also been applied.

Criteria	Min	Max
SSH	-130m	100m
SLA	-2m	2m

Table 5: *E*diting based on threshold on SSH

Criteria	Maximum autho-rized $\|Mean/pa$	Maximum autho-rized Stdev/pass
Differences between CNES and orbits studied	5cm	5cm
SLA ($Bathy < -1000m$,$Var < 30cm$)	30cm	30cm
SLA ($Bathy < -1000m$,$Var < 10cm$, Nbr of points>200)	15cm	15cm

Table 6: *E*diting based on statistics per pass

8.4.4 Orbit differences

Figure 56 shows the mean and variance of orbit differences over cycles 41 to 60. The differences are quite small in both cases, lower than 1 cm.

- Delft/CNES: The global bias is about 0. A South/North pattern is clearly visible. Delft is higher than CNES orbit in Southern Pacific Ocean and at high latitudes in the Southern Hemisphere whereas CNES is higher in the Northern Hemisphere. Separating ascending and descending passes (figure 57), the same South/North pattern is visible. We can notice two areas with a strong variance of difference, between longitudes 100° and 175°, and between longitudes 275° to 360°.

- ESOC/CNES: The global bias is about 0 as well. Moreover the two orbits are quite homogeneous geographically . In spite of the editing applied on ESOC SSH, high variance of difference is noticed on some passes, which is probably due to specific passes around maneuvers.

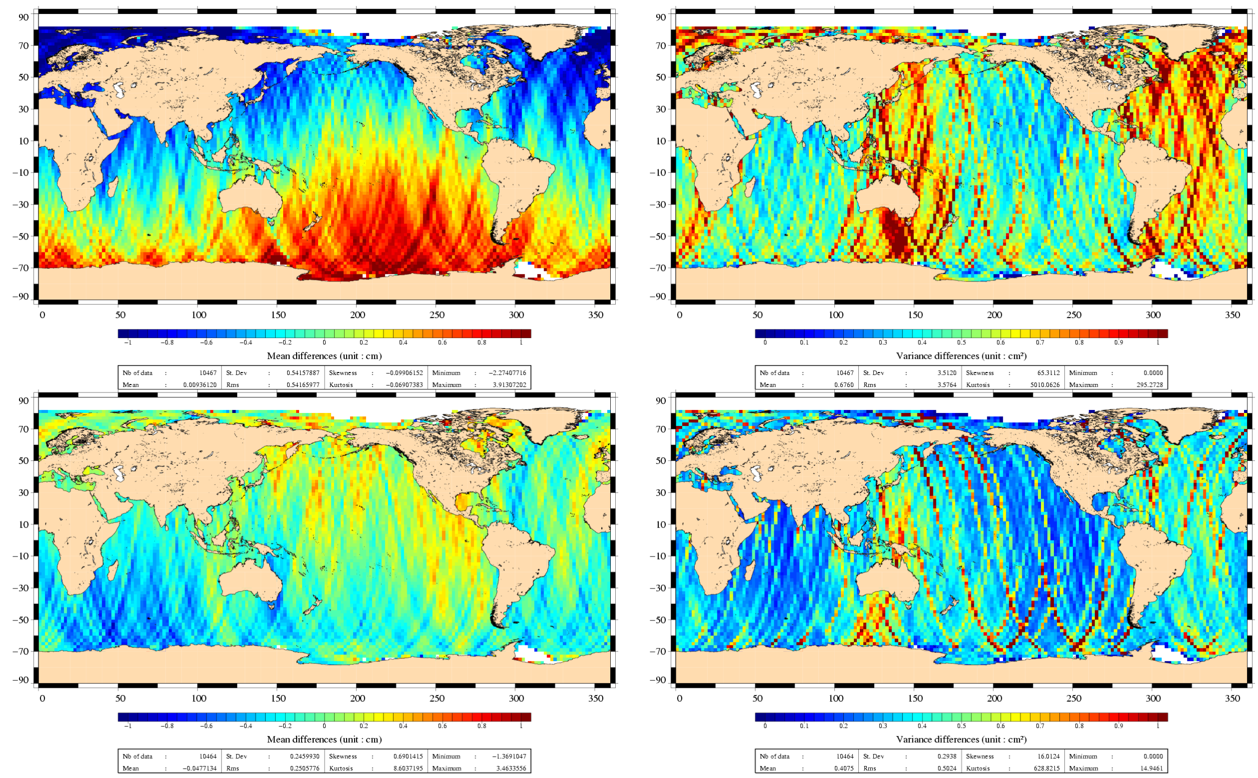

Figure 56: *[Delft-CNES (top) and ESOC-CNES (bottom)] mean of differences cycles 41 to 60 (left) and variance of differences (right)*

Figure 58 shows the mean and variance of differences per cycle. The mean difference is very stable, between -2 and 2mm in both cases. An annual signal seems to appear on the Delft/CNES difference from cycle 30 onward. The high differences of variance in the two cases before cycle 41 are due to the use of the GRIM5 Gravity model in the CNES POE. After cycle 41, the variance is lower than 1cm2.

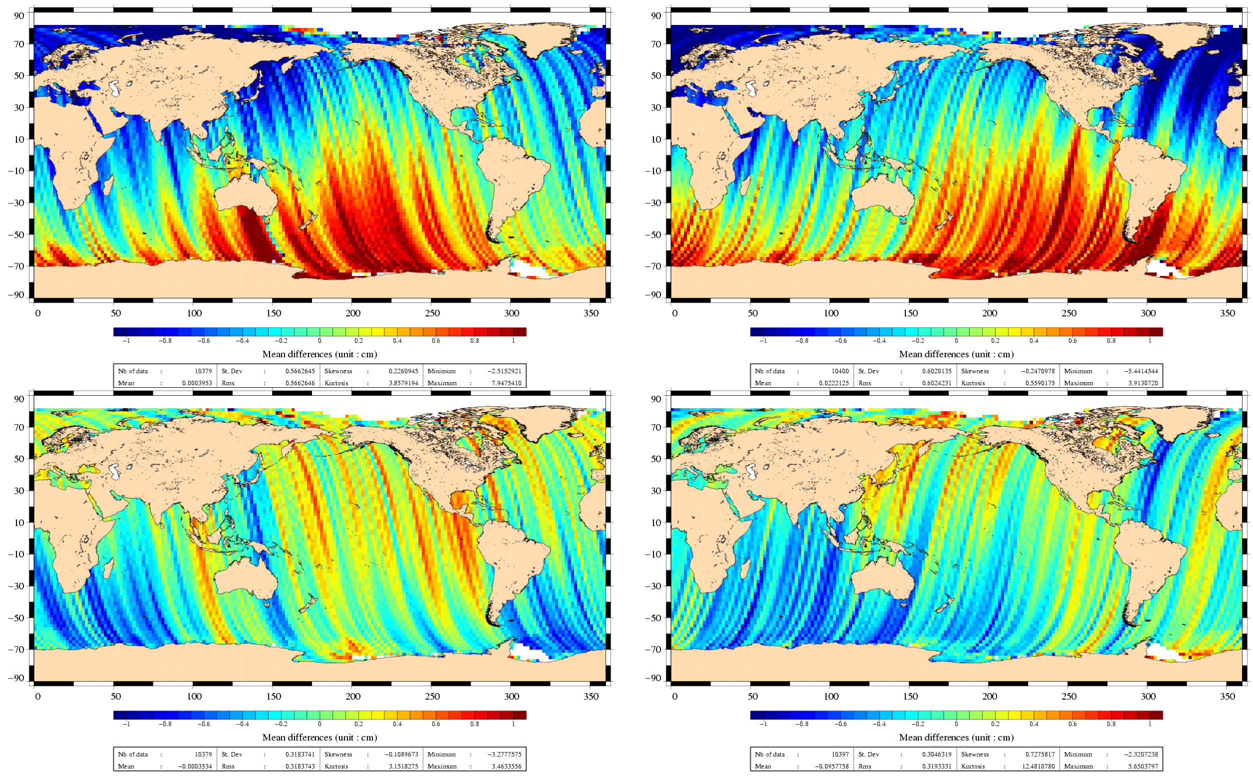

Figure 57: *[Delft-CNES (top) and ESOC-CNES (bottom)]] mean differences cycles 41 to 60 on ascending passes (left) and descending passes (right)*

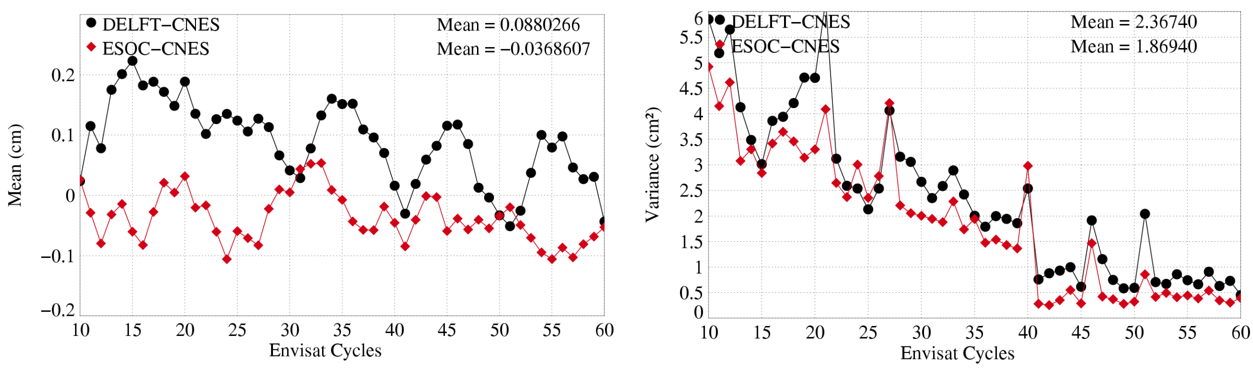

Figure 58: *Mean and Variance of differences*

8.4.5 Performances at crossovers

In figure 59 the mean ascending/descending differences are small and very similar using the three orbits. Some geographically correlated biases are slightly stronger using the Delft orbit, notably in East Pacific and West Indian Ocean.

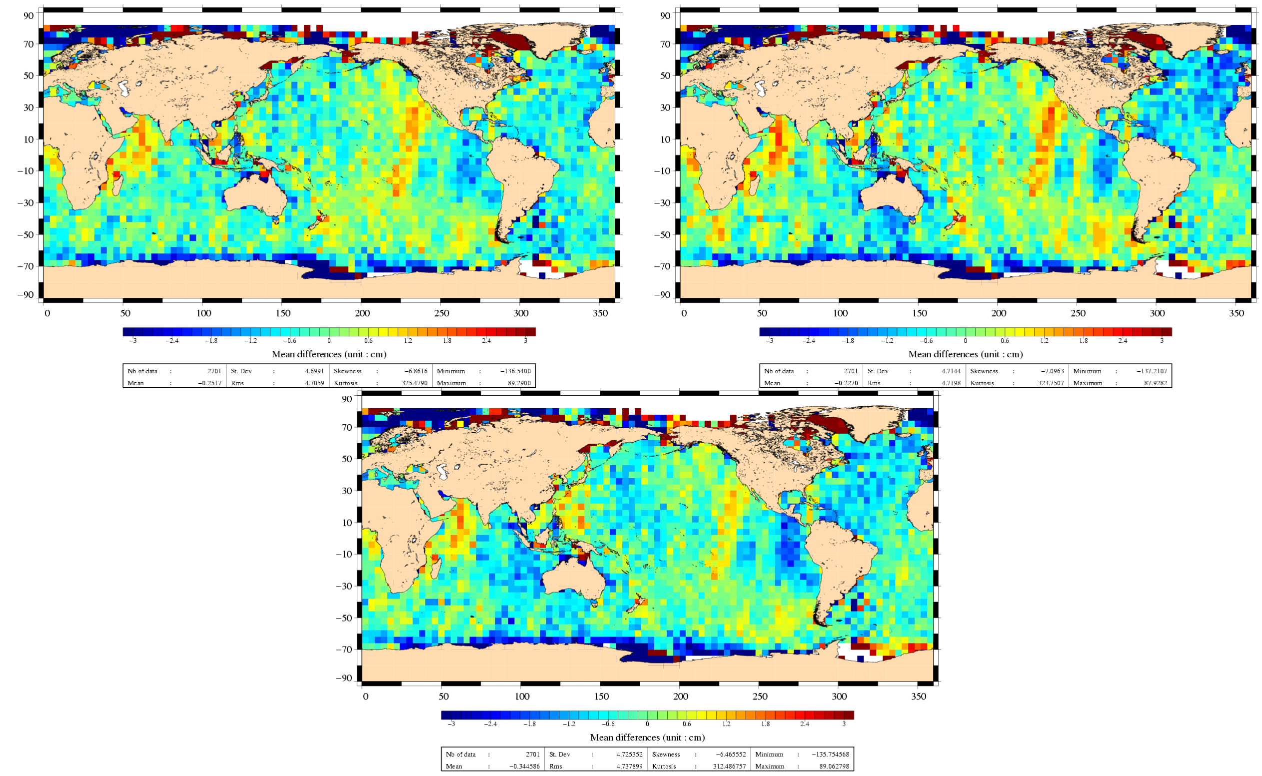

Figure 59: *Crossover mean differences over cycles 41 to 60. SSH using CNES orbit (left), Delft orbit (right) and ESOC orbit (bottom)*

Figure 60 shows the mean SSH differences at crossovers for the 3 orbits. The 3 curves are very similar, dominated by a decreasing 0.5-1cm of amplitude annual signal. Removing this annual signal highlight a decreasing trend on the 3 curves, meaning that the sea level on ascending passes is increasing relatively to on descending passes. The CNES and ESOC ascending/descending trend is about 2mm/year. The Delft orbit seems to have the best stability.

Figure 61 shows the differences between the variance of SSH with the two studied orbits and the CNES SSH. Before cycle 40, the differences are negative which means that the performances of Delft and ESOC are better than the CNES SSH. From cycle 41 onwards, it seems that the GDR orbit has slightly higher performances than the two others.

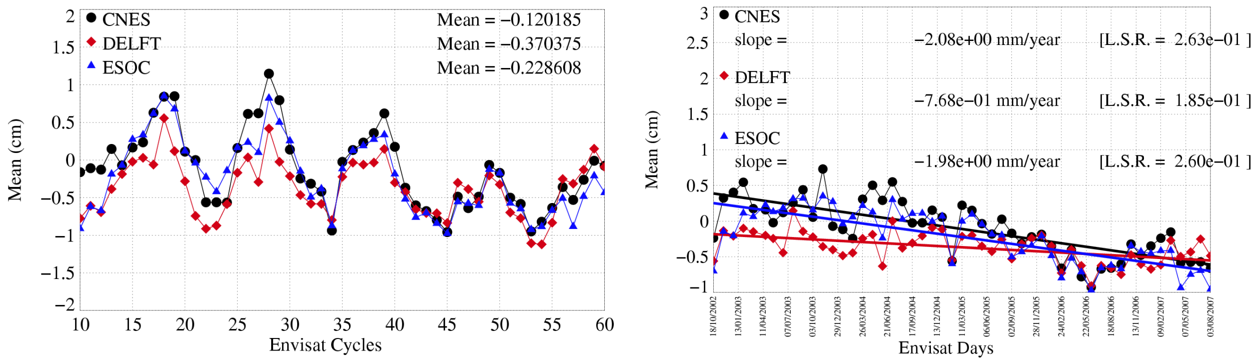

Figure 60: *Mean SSH differences at crossovers without (left) and with annual signal removed (right) (cm)*

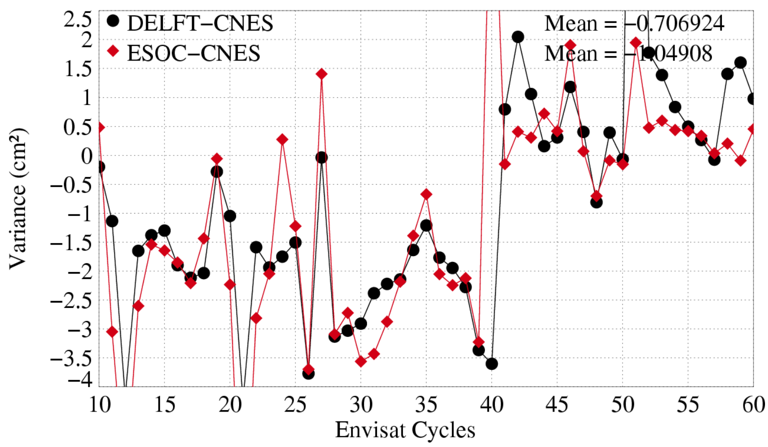

Figure 61: *Differences of variance [Var(SSH(Studied orbit))-Var(SSH(POE CNES))] (cm2)*

8.4.6 Long term trends

The analysis of the long term trend is interesting because it impacts directly Mean Sea Level trends estimation. In this parts, the statistics are estimated over a quarter of a cycle, and a area weighting procedure is applied in order to gave the same weight to all parts of the Globe. Figure 62 shows the trend of the orbit differences. The main observation is the CNES trend is greater than ESOC and Delft trend respectively by 0.2 and 0.4mm/year. A source of trend differences is the difference of reference system used for each solution, (i.e. ITRF2005 for ESOC and ITRF2000 for CNES). Taking only the two last years, where the CNES orbit is homogeneous, does not change sentitively the results.
The same result separating the ascending and descending passes is given in figure 63. The difference of trend between DELFT/CNES ascending and DELFT/CNES descending is noticeable. This inconsistency is mainly due to two jumps of opposite sign on cycle 41 which are approximately canceled at global level. These jumps are probably caused by the change of version of the CNES POE configuration. No jump is however noticed on the ESOC/CNES differences. Finally, on the two last years, the ESOC-CNES ascending and ESOC-CNES descending are respectively -0.4mm/year and 0.7mm/year.

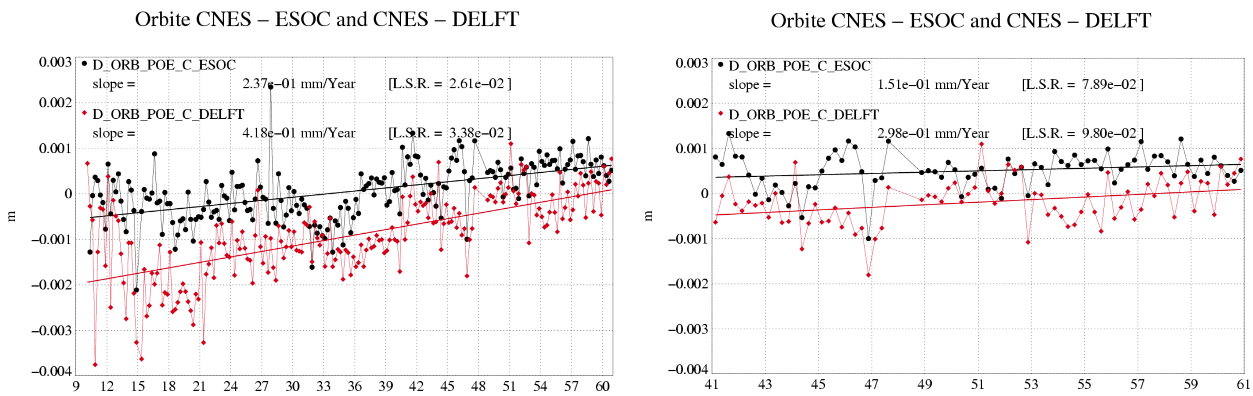

Figure 62: *Trend of orbit differences over the whole mission (left) and over the two las years (right)*

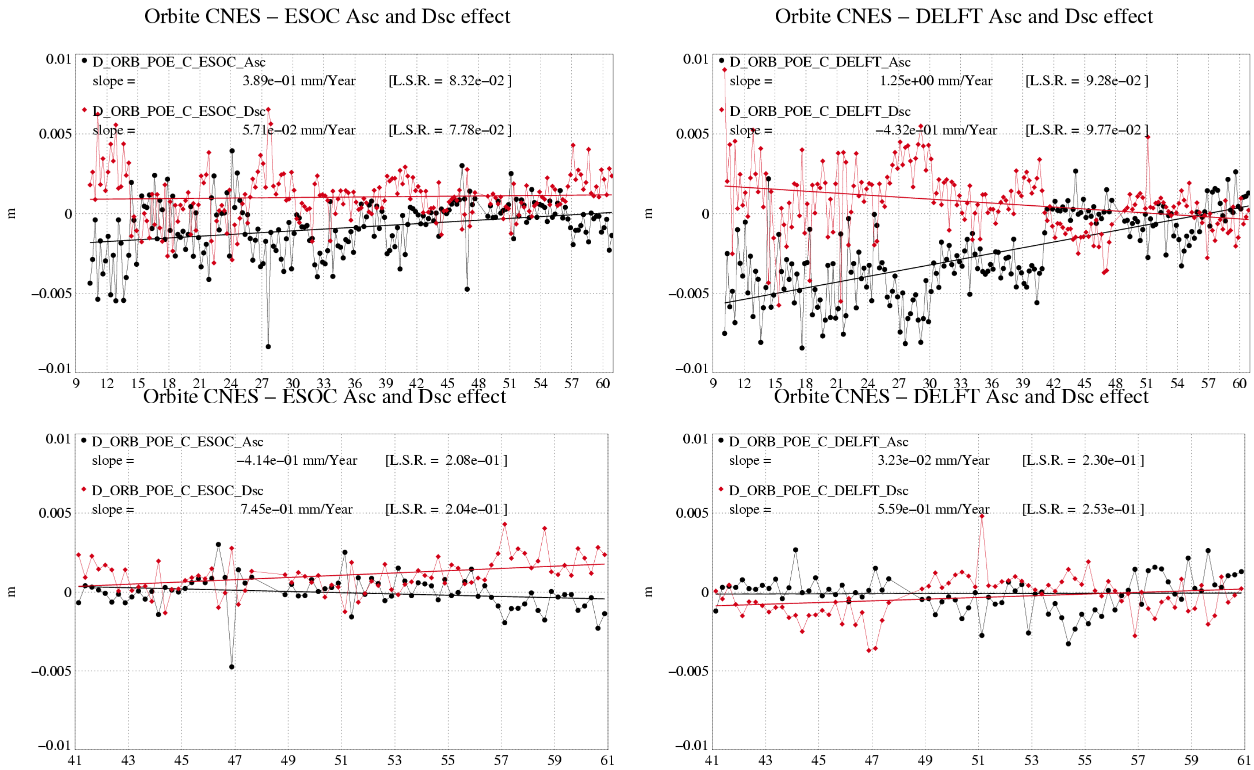

Figure 63: *Trend over the whole mission (top) and over the two las years (bottom) of orbit differences CNES-ESOC (left) and CNES-DELFT (right)*

8.4.7 Conclusion

This cross comparison study of the GDR, ESOC and Delft orbit shows that the 3 orbits are very similar in terms of global bias and performances. However, up to 1cm geographically correlated differences are observed between CNES and Delft. Moreover the mean per cycle of ascending/descending SSH differences has an unexplained trend, particularly on CNES and ESOC POE.

8.5 Study on ENVISAT Mean Sea Level Trend

8.5.1 Introduction

This year, a fine analysis of the Envisat Mean Sea Level trend has been performed in order to understand the particular behaviour of the CLS estimation compared to other missions (Jason-1) or other experts (Altimetrics). A first study consists in a detailed comparison with Altimetrics estimations in order to evaluate the contribution of each component of the Mean Sea Level in the difference. Then the impact of two SSH components, the orbit and the ionosphere correction, are detailed. Additionally some strange ascending/descending behaviours are analysed.

8.5.2 ENVISAT's Mean Sea Level trend computed at CLS and Altimetrics

8.5.2.1 Introduction

This part describes the results of the investigation on the differences between the CLS and Altimetrics Envisat Mean Sea Level trend. Comparisons were performed for latitudes [-66˚,66˚] and analysed in order to understand the causes of the differences.

8.5.2.2 Mean Sea Level Anomaly recipe

The Altimetrics time series are supplied with a 8.75 day periodicity. In order to ease the comparison, the CLS time series are computed with the same periodicity. Both time series are then smoothed with a 10 points (87.5 days) sliding window excluding the high latitudes (>66˚). This smoothing enables to smooth the noise and to reduce the Signal to Noise Ratio on the slope computation. The Altimetrics and CLS Sea Level Anomaly (SLA) recipe is given below.

SLA(Altimetrics) = [alt.eiggc03c - range - mss.cls01] - ssb.cls - iono.smooth - wet_tropo.rad - dry_tropo.ecmwf - inv_baro.mog2d - ocean_tide.fes2004 - load_tide.fes2004 - solid_tide - pole_tide

SLA(CLS) = [alt.cnes - range - mss.cls01] - ssb.cls - iono.smooth - wet_tropo.ecmwf - dry_tropo.ecmwf - inv_baro.mog2d - ocean_tide.got00 - solid_tide - pole_tide

There are many differences between the two recipes:
- The orbit used (alt.cnes/alt.eiggc03c)
- The inputs (wind and waves) of Sea State Bias algorithm (ssb.cls)
- The wet tropospheric correction (from the radiometer at Altimetrics, from ECMWF model at CLS)
- The tidal correction (GOT00 ocean tide at CLS including the load effect, FES 2004 ocean and load tide at altimetrics).
- ...

A comparison of each component has been performed and is detailed in ([27]). Here, only a summary of the results is shown.

8.5.2.3 Comparison of Mean Sea Level Anomaly trends

The comparison of the two MSL is shown in figure 64. The corresponding difference is plotted (without smoothing and no annual cycle removed) on figure 65. The Altimetrics MSL is higher than the CLS MSL by 0.9mm on the whole period, and even by 1.5mm/year without the first year. The table 7 sums-up the trends of [CLS-Altimetrics] difference on each SLA component.

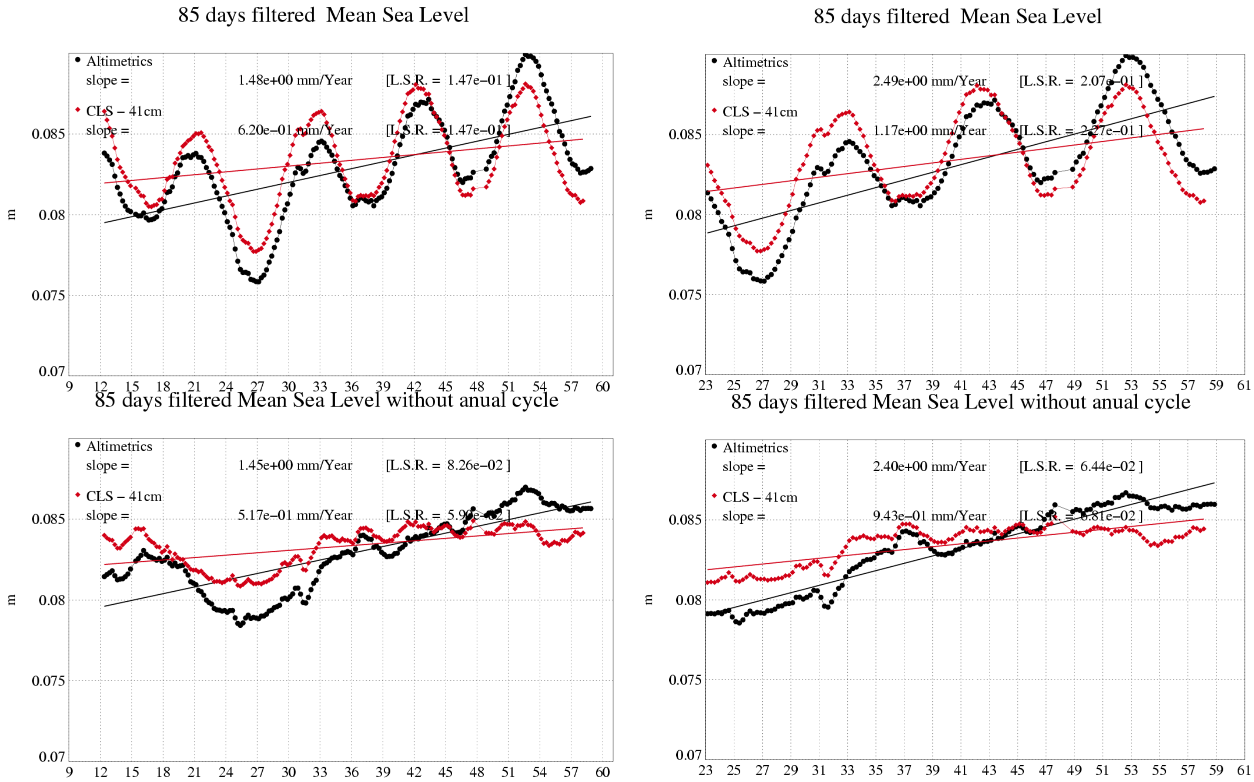

Figure 64: *85-day low pass filtered MSL trend at CLS and Altimetrics (A,top-left), A + without the first cycles (B,top-right), A + a removal of the annual signals (C,bottom-left), C + without the first cycles (bottom-right)*

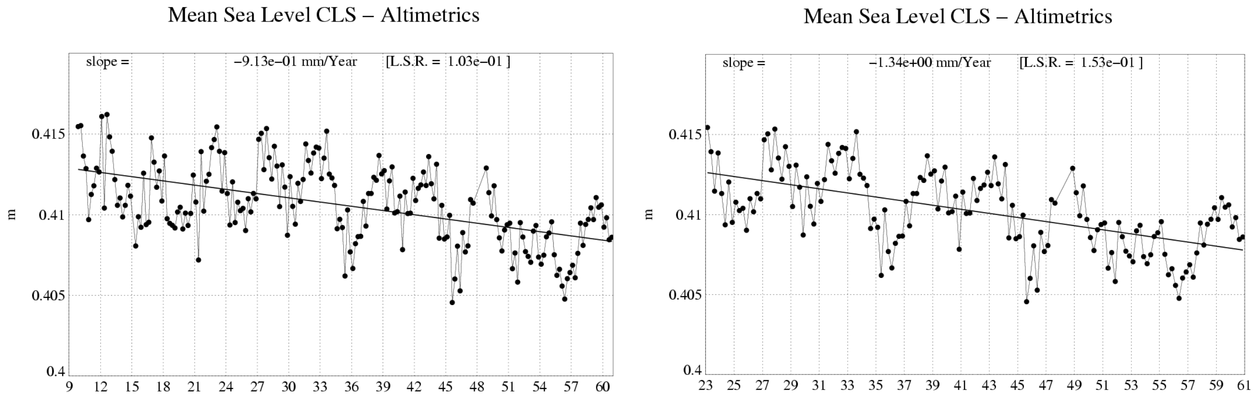

Figure 65: *Difference of MSL: CLS - Altimetrics (A, left), A + without the first cycles (B, right)*

CLS-Altimetrics Contribution of SSH Component	Cycles 9 to 61	Cycles 23 to 61
SLA	**-0.913**	**-1.34**
Explained SLA (Uncorrected SLA - Sum of corrections)	**-0.941**	**-1.310**
Uncorrected SLA	**+0.536**	**+0.861**
- SSB correction	-0.681	-0.737
- Ionospheric correction	-0.093	-0.348
- Wet Troposphere correction	-0.373	-0.690
- Dry Troposphere correction	-0.236	-0.383
- MOG2D Inverse barometer	+0.089	-0.057
- Ocean Tide correction	-0.199	-0.135
- Solid Earth Tide correction	-0.008	+0.159
- Polar Tide correction	+0.001	+0.006
- Sum of corrections	**-1.50**	**-2.185**

Table 7: *D*ifference of trends estimated from CLS and Altimetrics MSL and associated components. (mm/year)

This table show that our MSL trend difference has several causes, which makes the problem quite complex. To simplify the problem we consider here only the data excluding the first year and the high latitudes. The differences are identified and explained below:

1) [alt-range-mss]

The trend of [CLS-Altimetrics] +0.9mm/year.

When using the CNES orbit on both time series the difference becomes +0.3mm/year. Thus, most of this difference is explained by the orbit used. This can be due to the fact that the CNES orbit is not homogeneous on the whole data set. The remaining difference of 0.3mm/year is not explained. We note that the trends of CLS and Altimetrics orbit or range cyclic mean computed separately are very different. Altimetrics sees the Envisat platform rising by 46m/years whereas CLS sees a rise of 7m/year. This highlights a difference of processing and/or a difference of coverage.

2) SSB

The trend of the difference is +0.7mm/year.

This difference is probably induced by a trend between the CLS and Altimetrics SWH of 1.4cm/year. There is no reason for having a different trend on SWH. Only the processing can explain it.

3) Wet troposphere correction

The trend of the difference is -0.7mm/year with an acceleration at the end of the period. The correction used are not the same, ECMWF model in CLS case, radiometer with adjusted 23.8GHz TB in Altimetrics case. Note that the Altimetrics radiometer wet troposphere correction seems to be quite different from the Altimetrics ECMWF model wet troposphere (trend opposed).

4) dry troposphere correction
The trend of the difference is -0.4mm/year.
There are two jumps in the difference around cycle 38 and 45. This jump is in the GDR products time series which are used by Altimetrics. The first corresponds to the change of CMA version (CMA version 7) since when new S1 and S2 atmospheric tides are applied. The second jump is due to a change of the ECMWF model affecting Gaussian grids. The CLS is using the ECMWF model in Cartesian grids, which are not affected by a change of version.

5) ionosphere correction
The trend of the difference is -0.3mm/year.
There is a 1.5mm jump in the difference around cycle 41 which explains the trend difference. This jump is in the GDR field used in CLS time series. This jump is due to the change of SSB tables used in the computation of the corrected range in input of the dual ionospheric correction algorithm. Before cycle 41 the same SSB table is used to correct the Ku and S-band range. From cycle 41 onwards, a specific SSB has been used for the S-Band range.

8.5.2.4 Conclusion

The conclusion of this study is that the MSL trend differences have several causes. The two potential causes of discrepancies that have to be investigated on CLS side are first the ionosphere correction and the then the orbit. A detailed analysis of these two parameters are detailed in the following parts.

8.5.3 Impact of the updated Ionospheric correction

This update consists in correcting the S-band range from a suitable SSB on cycles 10-41 before computing the dual ionosphere correction. The impact of using the homogeneous ionosphere correction for Envisat on the global MSL is plotted on Figure 66 and 67. Before cycle 41, the new MSL is slighly lower (about -1.5 mm) compared to the old one. The new MSL trend increases by 0.4mm/year when looking at the whole time series and 0.5mm/year without the first year. This is a positive change: Envisat CLS MSL is now closer to Altimetrics from the one hand and to Jason-1 MSl in the other hand.

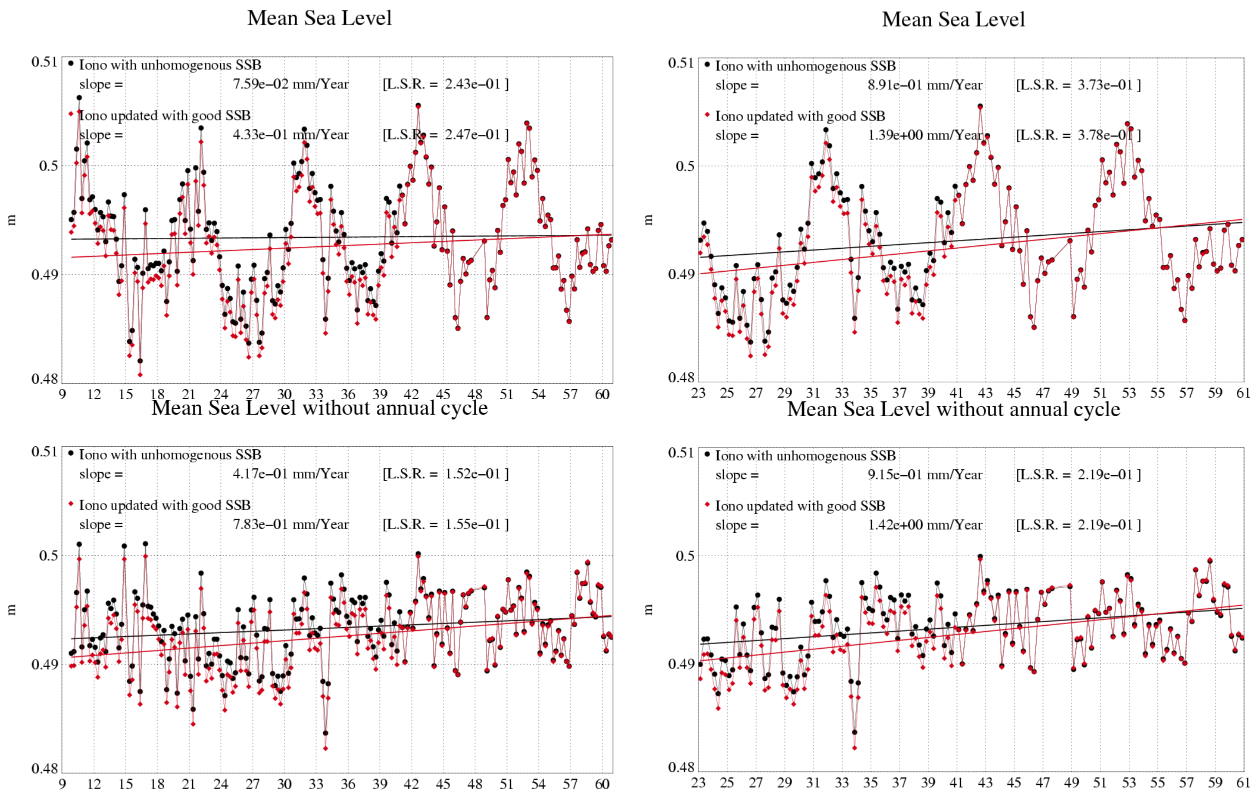

Figure 66: *MSL trend at CLS with Updated Ionospheric correction (A,top-left), A + without the first cycles (B,top-right), A + a removal of the annual signals (C,bottom-left), C + without the first cycles (bottom-right)*

Figure 68 shows the global MSL trend for Jason-1 and Envisat on the whole Envisat period (2003-2007). The Envisat curve shows a 0.8mm/year trend while Jason-1 leads to an increasing trend of about 2.3 mm/year. The trend difference of -1.4mm/year on the whole period is reduced to -0.7mm/year when looking at the period 23-61 (Figure 68 and 69) with a new MSL trend for Envisat of 1.4mm/year. Figure 70 shows the global MSL trend for the last two years (2005-2007) where both missions are consistent, both around 0.0mm/year.

The new Envisat MSL is increased by about 0.5mm per year over the period 2004-2007 (cycles Envisat 23 to 62), which improves the consistency between both missions.

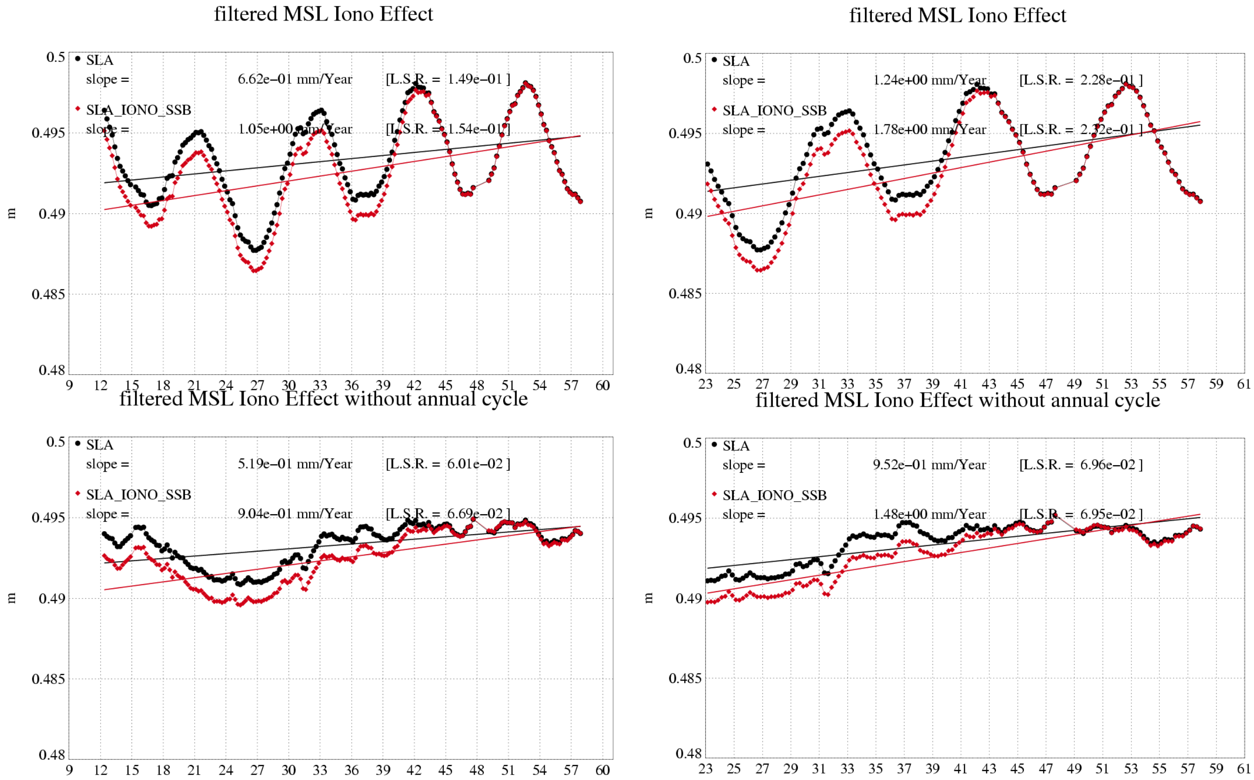

Figure 67: *Filtered MSL trend at CLS with Updated Ionospheric correction (A,top-left), A + without the first cycles (B,top-right), A + a removal of the annual signals (C,bottom-left), C + without the first cycles (bottom-right)*

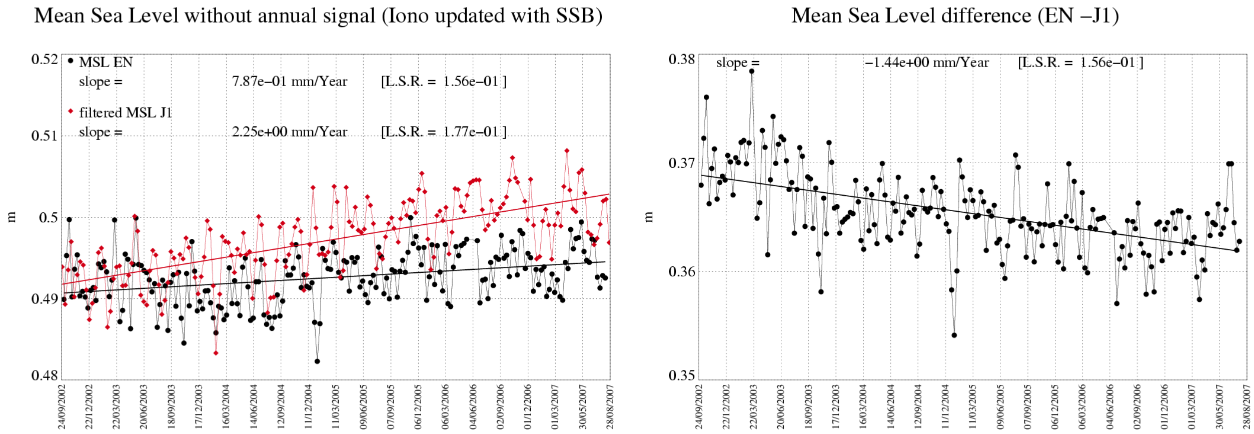

Figure 68: *Envisat updated and Jason-1 MSL trend over the period 2003-2007 (cycles Envisat 9 to 62) (left), Envisat - Jason-1 MSL trend (right)*

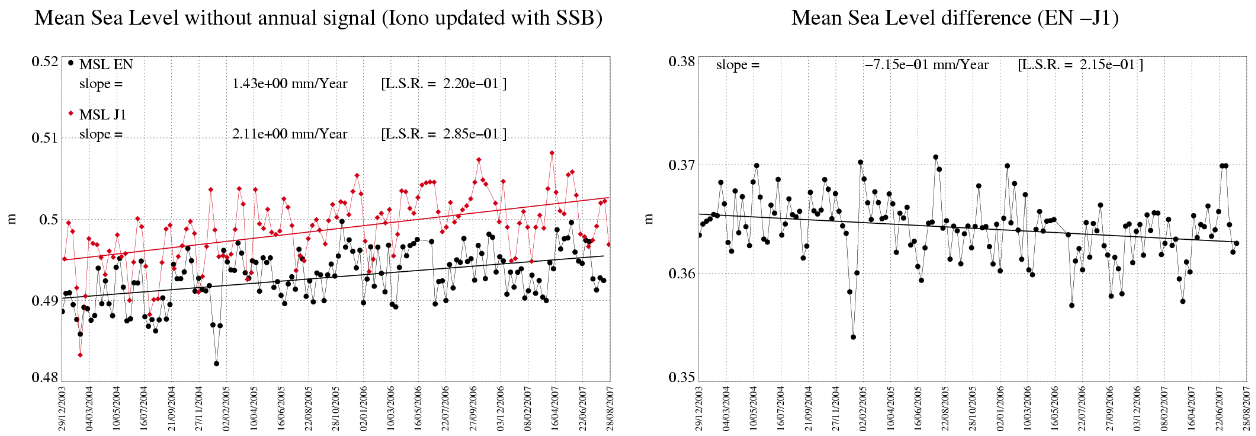

Figure 69: *Envisat updated and Jason-1 MSL trend over the period 2004-2007 (cycles Envisat 23 to 62) (left), Envisat - Jason-1 MSL trend (right)*

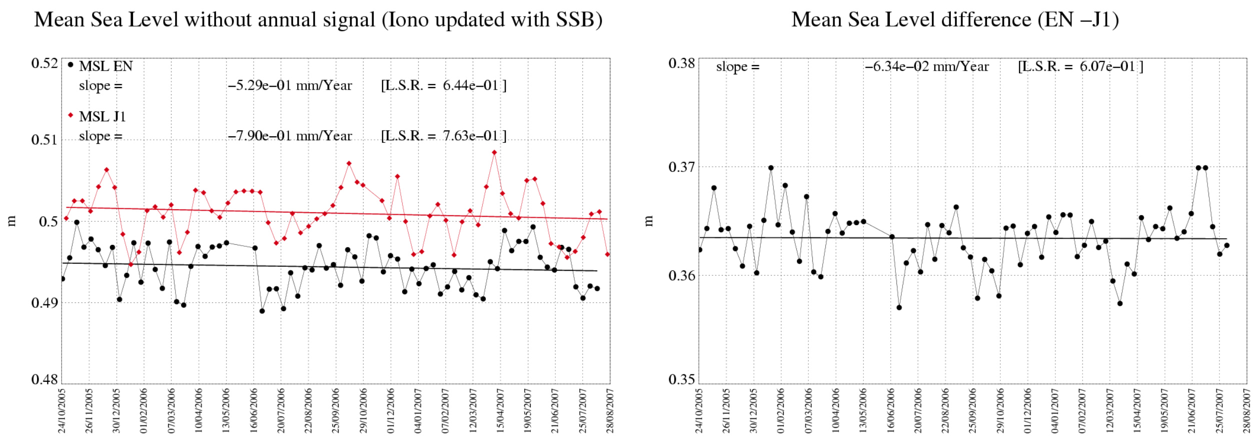

Figure 70: *Envisat updated and Jason-1 MSL trend over the period 2006-2007 (cycles Envisat 42 to 62) (left), Envisat - Jason-1 MSL trend (right)*

8.5.4 Impact of the orbit

When using the CNES orbit in the MSL Trend computation, part of the trend might be explained by the fact that the CNES orbit is not homogeneous on the whole data set (GRIM5 orbits before cycle 41). The CNES orbit was replaced by two other solutions, Delft orbit and ESOC orbit both homogeneous on the whole time series. The orbits as well as the processing are described in part 8.4. The impact on the MSL of using the ESOC orbit instead of the GDR orbit is -0.3mm/year on the trend estimation (Figure 71 B and 72 B) and -0.4mm/year using Delft orbit. The main comment is that the use of an orbit homogeneously processed over the whole periods does not improve the consistency with Jason-1. On the contrary, it increases the difference in both cases.

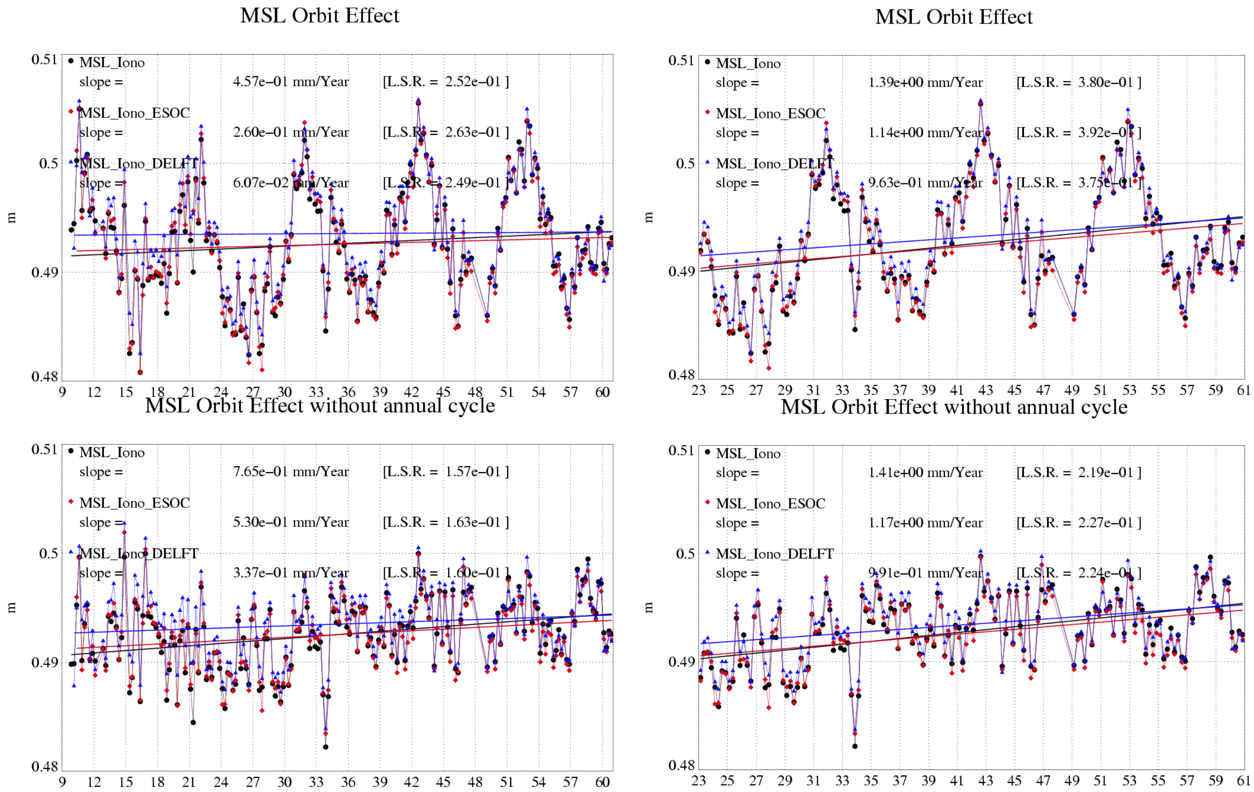

Figure 71: *MSL trend at CLS with Updated Ionospheric correction using CNES, Delft and DEOS Orbit (A,top-left), A + without the first cycles (B,top-right), A + a removal of the annual signals (C,bottom-left), C + without the first cycles (bottom-right)*

Figure 73, 75 and 74 show the Envisat MSL respectively using CNES, Delft and ESOC orbit separating ascending and descending passes. The MSL trend is surprisingly different on ascending and descending passes using CNES and ESOC. Delft orbit only allow ascending and descending Envisat MSL trends to be consistent.

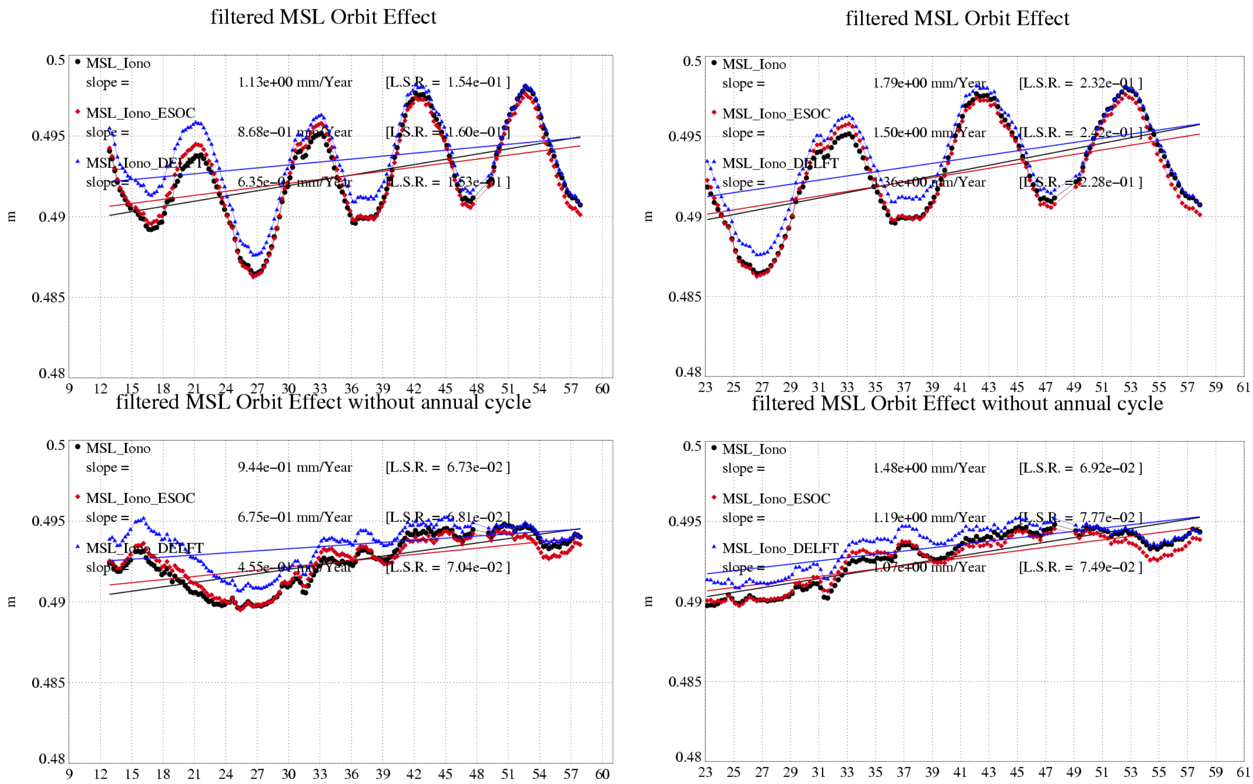

Figure 72: *Filtered MSL trend at CLS with Updated Ionospheric correction using CNES, Delft and DEOS Orbit (A,top-left), A + without the first cycles (B,top-right), A + a removal of the annual signals (C,bottom-left), C + without the first cycles (bottom-right)*

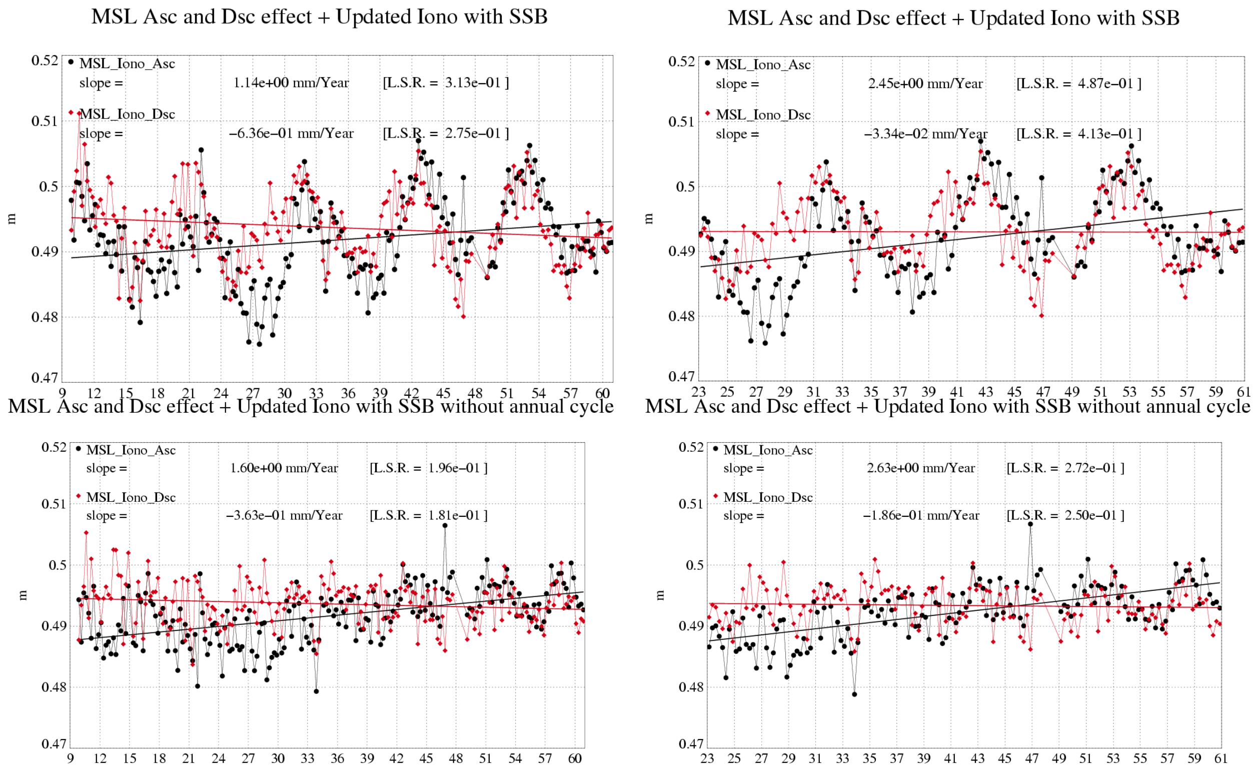

Figure 73: *MSL trend at CLS with Updated Ionospheric correction and CNES Orbit (A,top-left), A + without the first cycles (B,top-right), A + a removal of the annual signals (C,bottom-left), C + without the first cycles (bottom-right)*

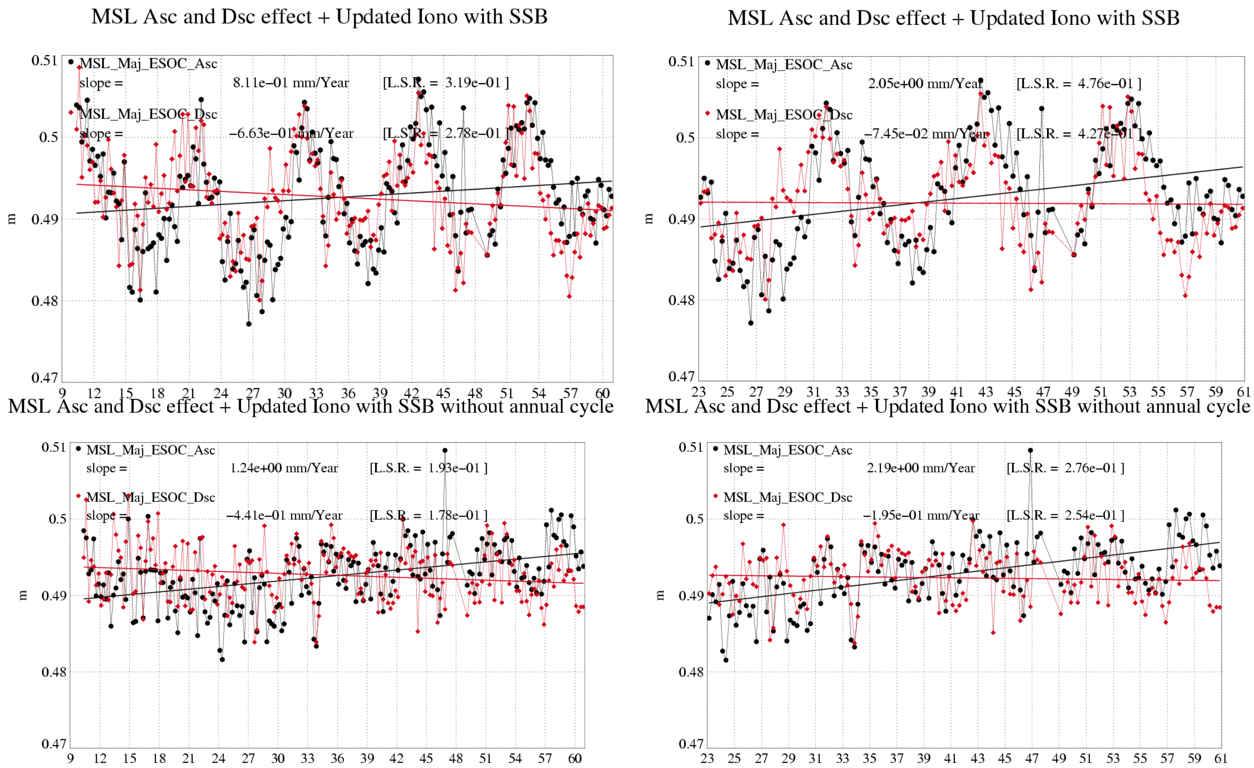

Figure 74: *MSL trend at CLS with Updated Ionospheric correction and ESOC Orbit (A,top-left), A + without the first cycles (B,top-right), A + a removal of the annual signals (C,bottom-left), C + without the first cycles (bottom-right)*

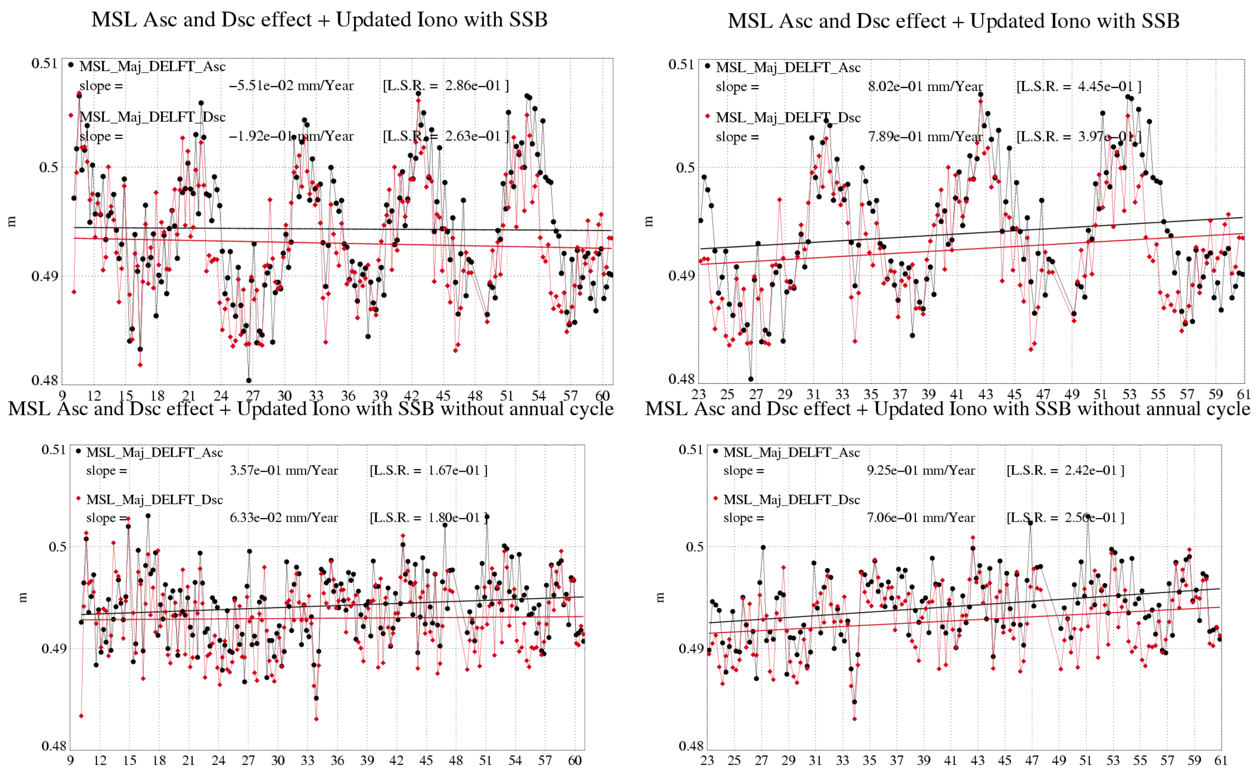

Figure 75: *MSL trend at CLS with Updated Ionospheric correction and Delft Orbit (A,top-left), A + without the first cycles (B,top-right), A + a removal of the annual signals (C,bottom-left), C + without the first cycles (bottom-right)*

The results of this part are summed up in the Table 8.

MSL Trend	Cycles 9 to 61	Cycles 23 to 61
JASON	+2.4	+2.3
ENVISAT orbit CNES	+0.4	+0.9
ENVISAT Iono update orbit CNES	+0.8	+1.4
ENVISAT Iono update orbit ESOC	+0.5	+1.2
ENVISAT Iono update orbit Delft	+0.3	+1.0
ENVISAT Iono update Ascending Tracks orbit CNES	+1.6	+2.6
ENVISAT Iono update Descending Tracks orbit CNES	-0.4	-1.85
ENVISAT Iono update Ascending Tracks orbit ESOC	+1.2	+2.2
ENVISAT Iono update Descending Tracks orbit ESOC	-0.4	-1.95
ENVISAT Iono update Ascending Tracks orbit Delft	+0.35	+0.9
ENVISAT Iono update Descending Tracks orbit Delft	+0.06	+0.7

Table 8: *T*rend estimated from different MSL. (mm/year)

8.5.5 Conclusions and perspectives

The conclusion of this study is first that there are a lot of potential causes for the inconsistency between the CLS Envisat MSL and the Altimetrics Envisat MSL or the Jason-1 MSL. Two potential sources of error have been identified on CLS side, the ionosphere correction and the orbit. But if the update of the ionosphere correction allows us to reduce the inconsistency by 0.4mm/year, the use of other orbits, though homogeneous on the whole time series, degrades it.

8.6 J1/EN SSH differences at crossovers

8.6.1 Introduction

Since September 2005, the Envisat and Jason-1 GDR "version b" products have been dissaminated to users. Envisat/Jason-1 cross-calibration analyses based on 1 year shown that the consistency between the two satellites was greatly improved with this new version (see [26]). Now, longer time series are necessary to investigate finely the residual differences between Envisat and Jason-1.

The full reprocessing of Jason-1 products in b version was completed mid-2007 whereas Envisat products have not been reprocessed yet. However, Most of the Envisat GdrB upgrade can be implemented in this data-base. Only the new CNES EIGEN-CG03C POE orbit, one of the major changes in the GDR product, can't be updated in this data base.

A POE orbit using recent standard, including notably the use of a Grace Gravity model, has been reprocessed at ESOC over a long period (cycles 10-60) especially for this analysis. The aim of this study is to use these reprocessed orbits in order to have a homogeneous Envisat data set. On Jason-1 side the orbits distributed by the Goddard Space Flight Center ([5]) are also tested.

The purpose of this analysis is to describe the geographical features of EN/J1 SSH Differences at 10-day crossovers on a long homogeneous time series. The main idea is thus to use the ESOC orbit (described in a previous part) fully reprocessed in an homogeneous version in November 2007.

8.6.2 SSH computation

The same SSH formulae as for 7 is used. The sentivity to the type of wet troposphere correction (ECMWF model versus radiometer), ionosphere correction (dual frequency versus GIM model) and tide correction (GOT 2000 versus FES 2004) have also been analysed.

8.6.3 Impact of the use of ESOC orbit on the period 41-52

The map of statistics of the SSH differences at crossovers are shown in Figure 76, 77 and 78. The global mean difference has been removed in order to have differences centered around zero. As expected from the CNES/ESOC orbit comparisons shown previously, the use of ESOC has very few impact on the EN/J1 consistency. The difference is negative over the Indian and West Pacific Ocean, and positive over the East Pacific and Atlantic ocean except at high latitude. A positive pattern is also visible around central America. On the normalized variance map, an interresting pattern is noticeable signal around the geomagnetic equator.

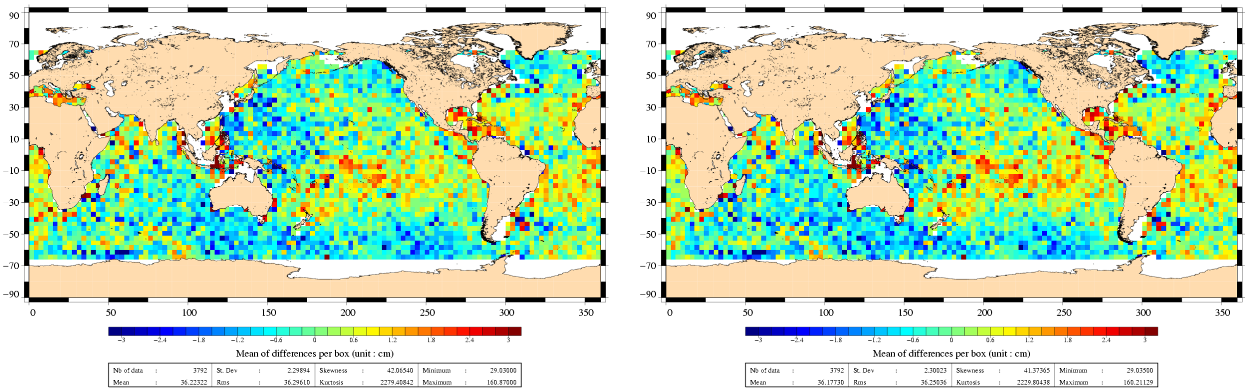

Figure 76: *Mean of cyclic mean map of [EN-J1] using CNES orbit (left) and ESOC orbit (right)*

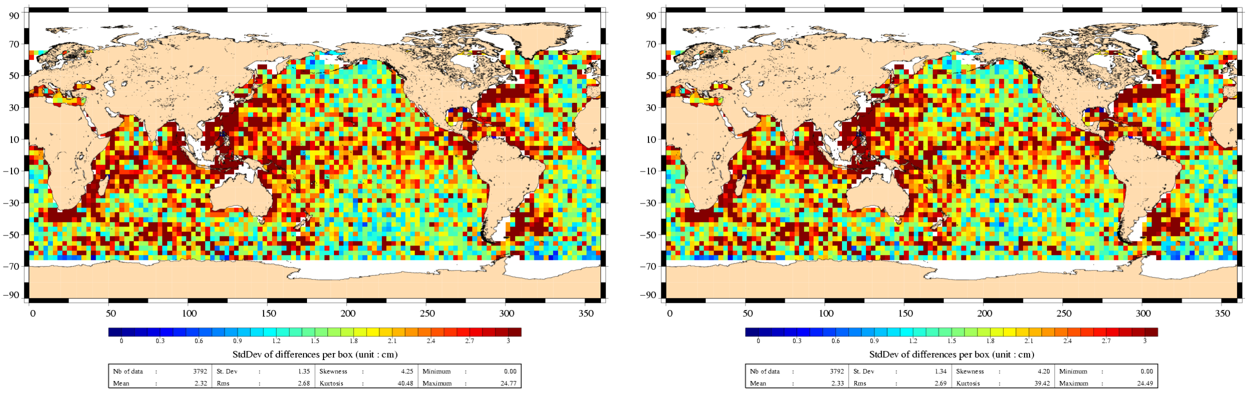

Figure 77: *Standard deviation of cyclic mean map of [EN-J1] using CNES orbit (left) and ESOC orbit (right)*

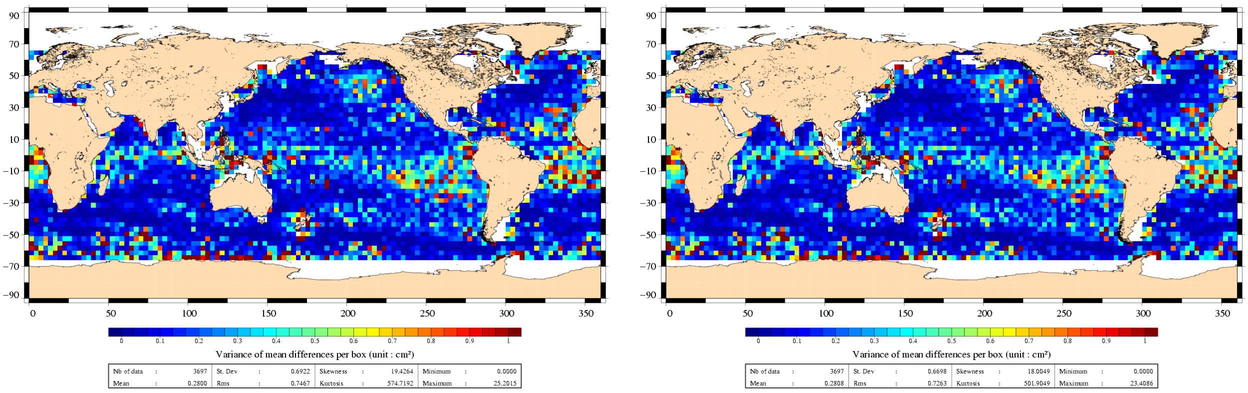

Figure 78: *Ratio of the [variance /variance oceanic signal] of cyclic mean map of [EN-J1] using CNES orbit (left) side and ESOC orbit (right)*

8.6.4 Analysis using ESOC orbit on the period 13-51

The map of statistics of the SSH differences at crossovers using ESOC orbit on the period 13-51 are shown in Figure 79, 80 and 81. With a long time series, the differences are less noisy. The North/South structure now dominates the difference: negative differences are observed in the Southern Hemisphere at high latitudes. The positive pattern around central America is still visible. A correlation with the mean oceanic waves distribution could be done (see figure 82). The impact several geophysical corrections are also analysed:
-Using the radiometer correction instead of the model increases the inconsistency. Note that the Envisat MWR correction is not homogeneous on the whole mission (side lobe correction from cycle 41 onwards). The exact impact of using the radiometer on both mission is given in figure 83.
-Using the GIM correction instead of the dual frequency ionosphere correction has few impact. The exact impact of using the GIM model on both mission is givent in figure 83.
-Using the FES2004 model instead of the GOT00 model changes the differences in Indonesia and seems to correct a systematic discontinuity near Antartica (longitude 50).

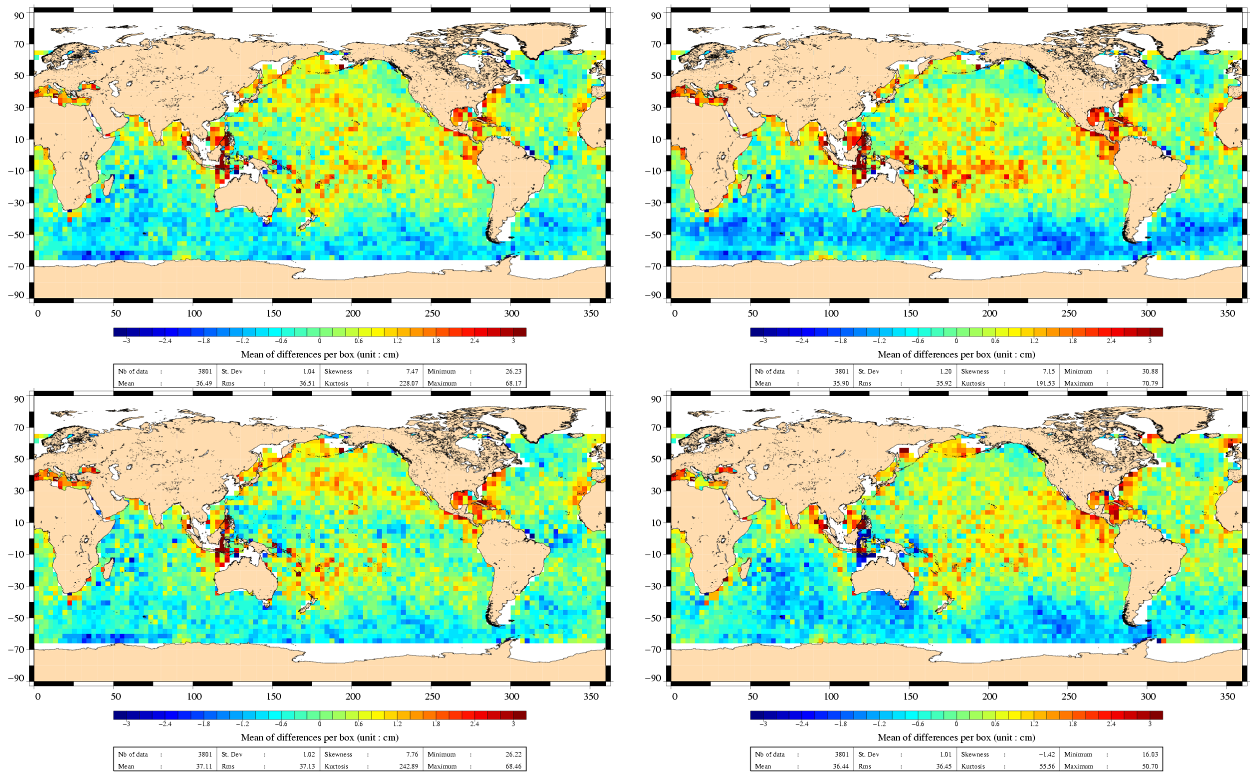

Figure 79: *Mean of cyclic mean map of [EN-J1] using reference SSH (top-left), using radiometer wet troposphere correction (top-right), using GIM ionosphere correction (bottom-left), asing FES04 ocean tide model correction (bottom-right)*

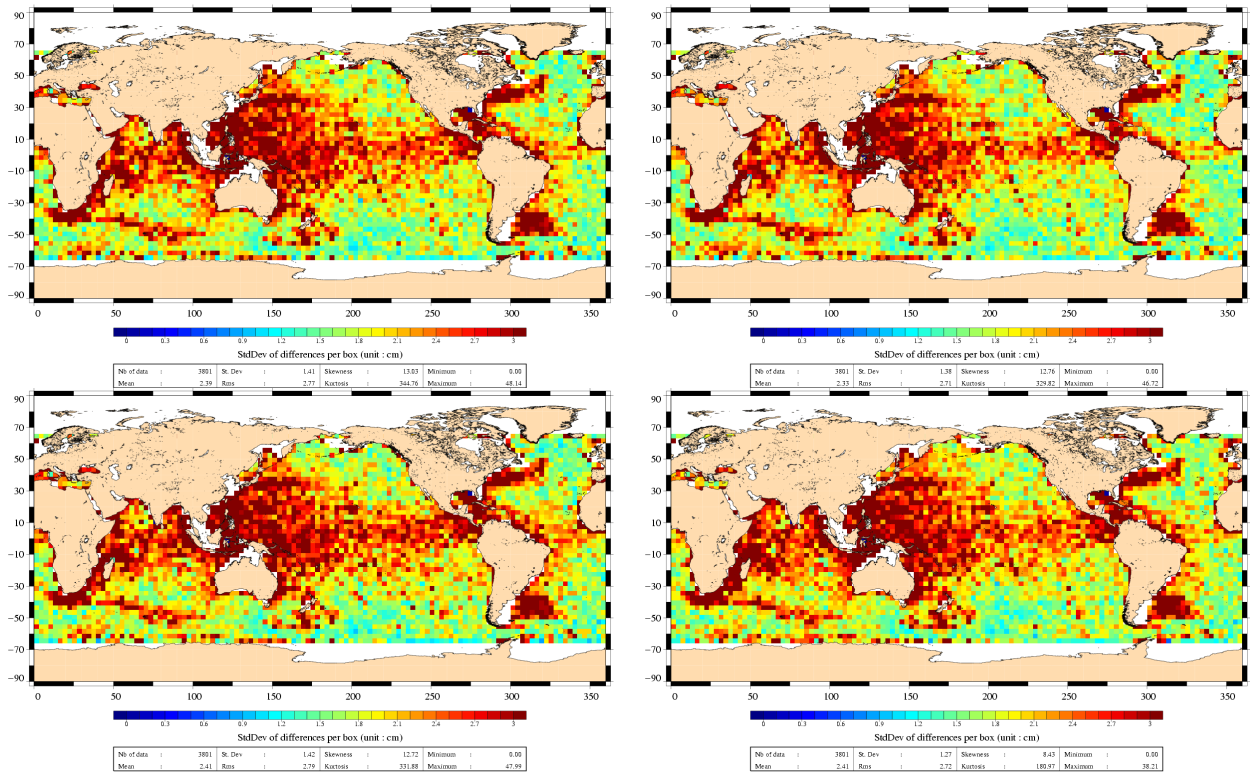

Figure 80: *Standard deviation of cyclic mean map of [EN-J1] using reference SSH (top-left), using radiometer wet troposphere correction (top-right), using GIM ionosphere correction (bottom-left), asing FES04 ocean tide model correction (bottom-right)*

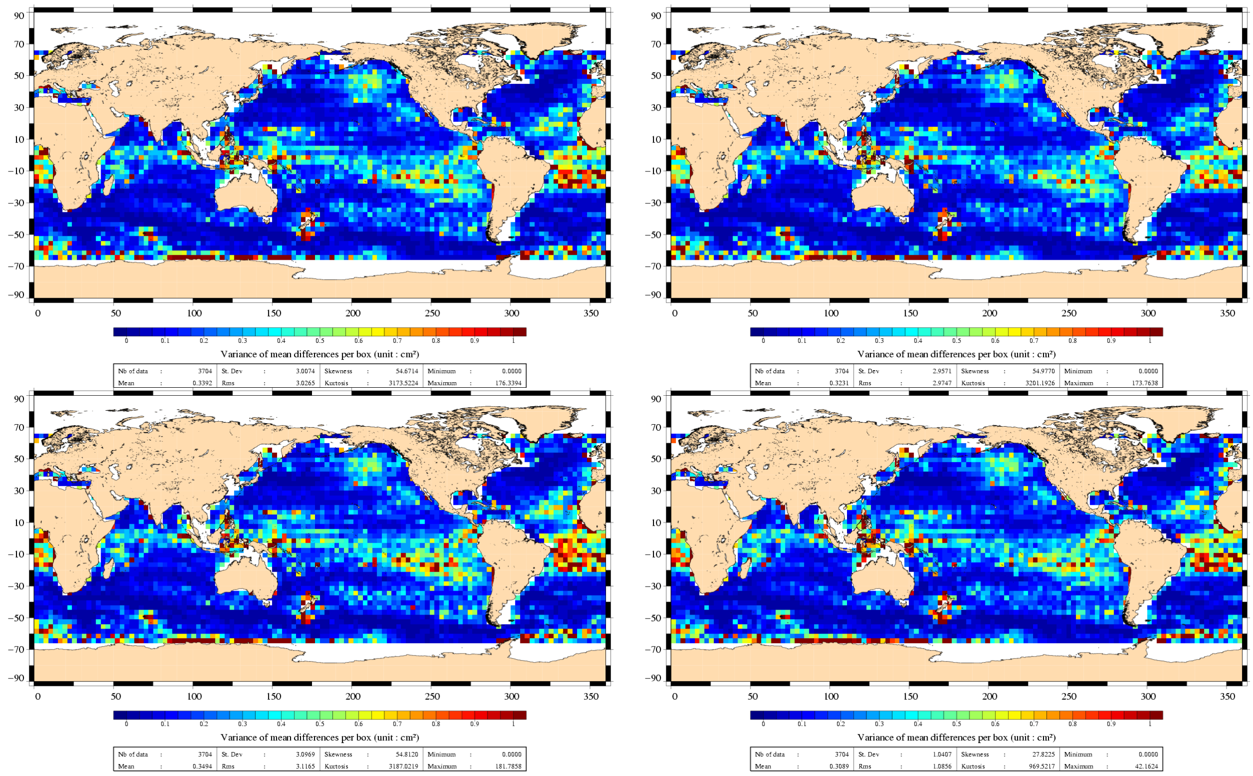

Figure 81: *Ratio of the [variance/variance oceanic signal] of cyclic mean map of [EN-J1] using reference SSH (top-left), using radiometer wet troposphere correction (top-right), using GIM ionosphere correction (bottom-left), asing FES04 ocean tide model correction (bottom-right)*

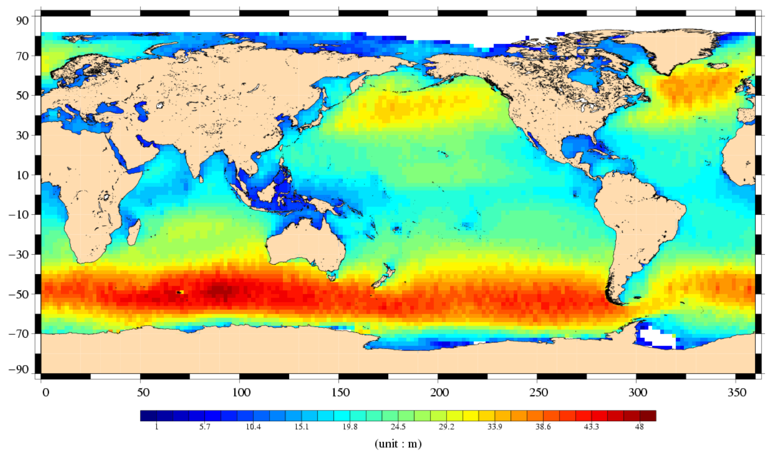

Figure 82: *Mean SWH map on Envisat, cycle 13-53*

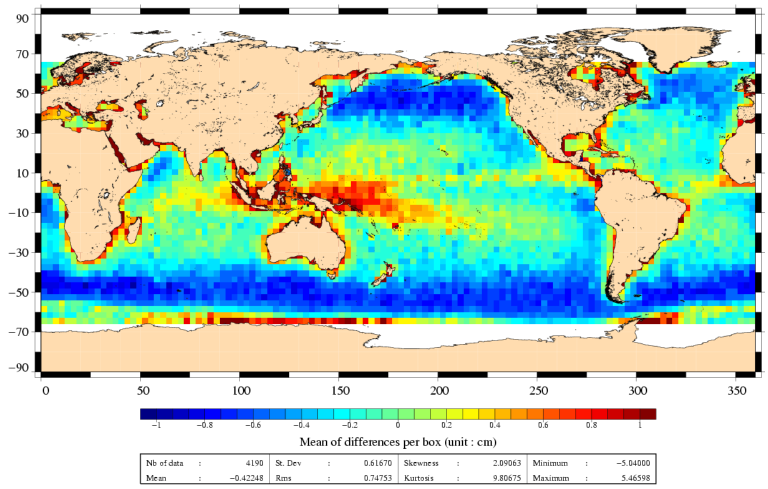

Figure 83: *Mean [Envisat[Radiometer-ECMWF]-Jason-1[Radiometer-ECMWF]] wet troposphere correction differences at Envisat/Jason-1 crossovers, cycle 13-53*

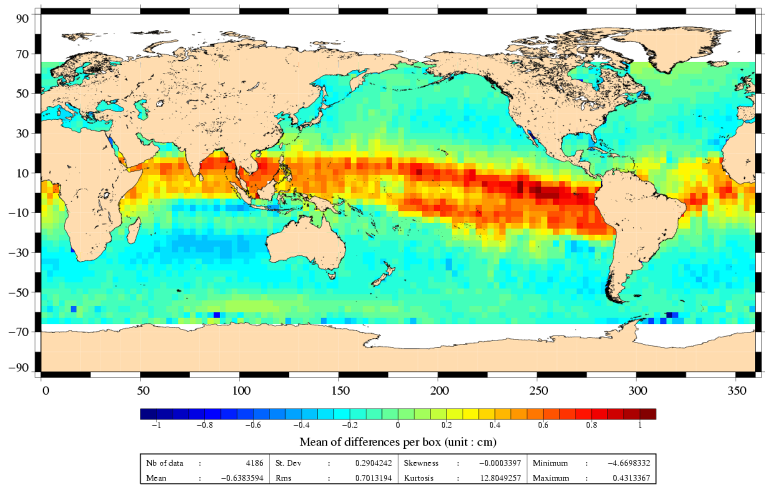

Figure 84: *Mean [Envisat[Dual-GIM]-Jason-1[Dual-GIM]] ionosphere correction differences at Envisat/Jason-1 crossovers, cycle 13-53*

8.6.5 Impact of separating ascending and descending Envisat passes

The map of statistics of the SSH differences at crossovers using ESOC orbit on the period 13-51 and separating ascending and descending Envisat passes are shown in Figure 85, 86 and 87. The main comment is that Jason-1 is more consistent with Envisat descending passes than ascending passes in terms of geographically correlated biases.

(cycles 13 to 52) ESOC orbit

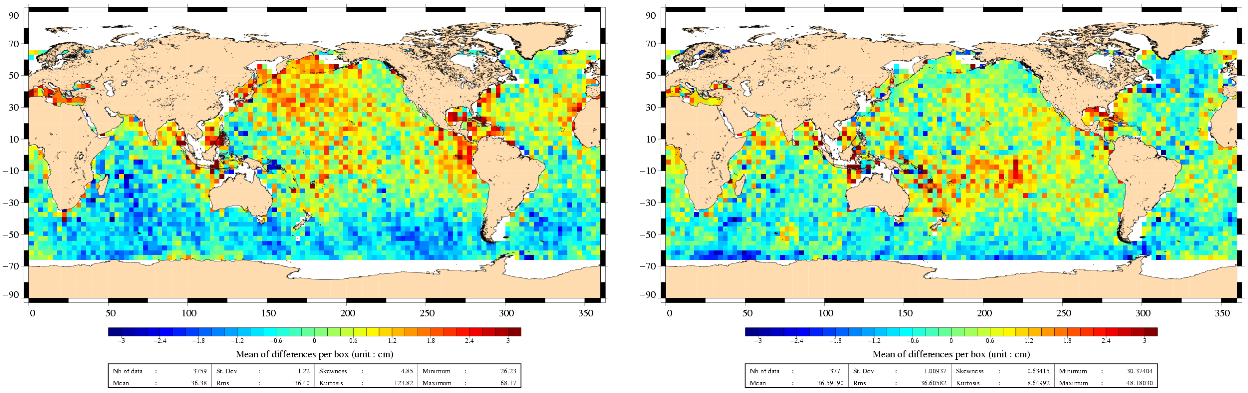

Figure 85: *Mean of cyclic mean map of [EN-J1] on ascending EN (left) and descending passes EN (right)*

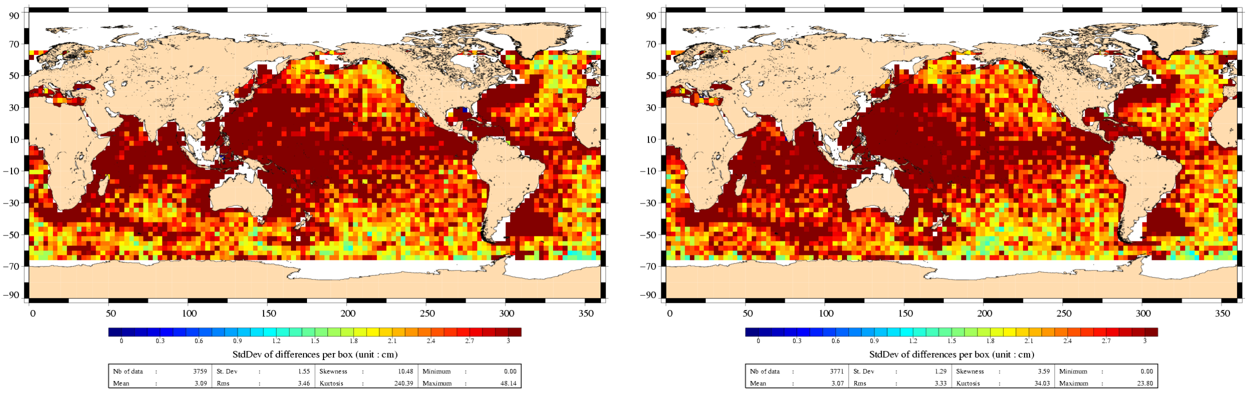

Figure 86: *Standard deviation of cyclic mean map of [EN-J1] on ascending EN (left) and descending passes EN (right)*

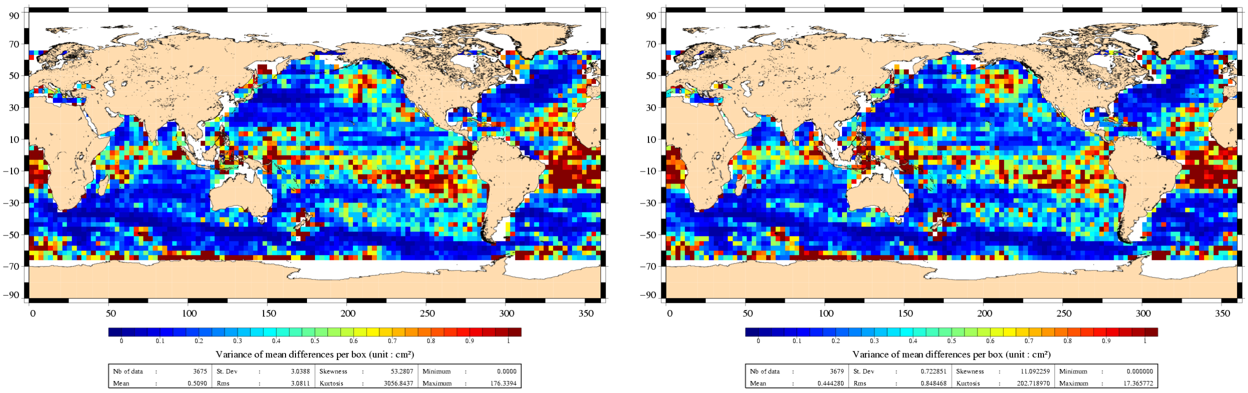

Figure 87: *Ratio of the [variance/variance oceanic signal] of cyclic mean map of [EN-J1] on ascending EN (left) and descending passes EN (right)*

8.6.6 Impact of using GSFC orbit for Jason-1

The map of statistics of the SSH differences at crossovers using ESOC orbit for Envisat and using the GSFC orbit for Jason-1 on the period 13-51 are shown in figure 88, 89 and 90 (right). The use of the GSFC orbit, based on the ITRF2005 reference system as the ESOC orbit, induce a better homogeneity between the two satellites. The main remaining pattern is a positive bias in the tropical South Pacific ocean and, as before, a strong positive pattern around central America.

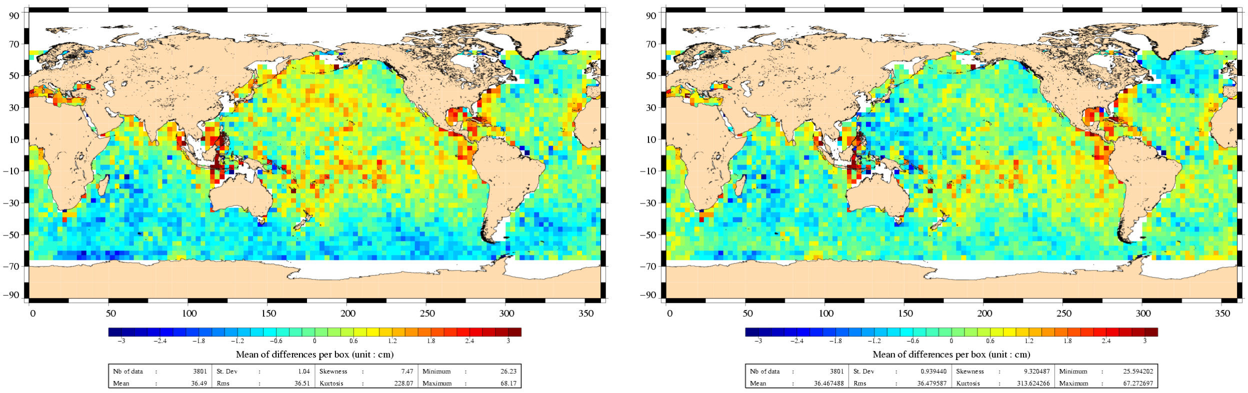

Figure 88: *Mean of cyclic mean map of [EN-J1] using ESOC(EN)/CNES(J1) orbit (left) and ESOC(EN)/GSFC(J1) orbit (right)*

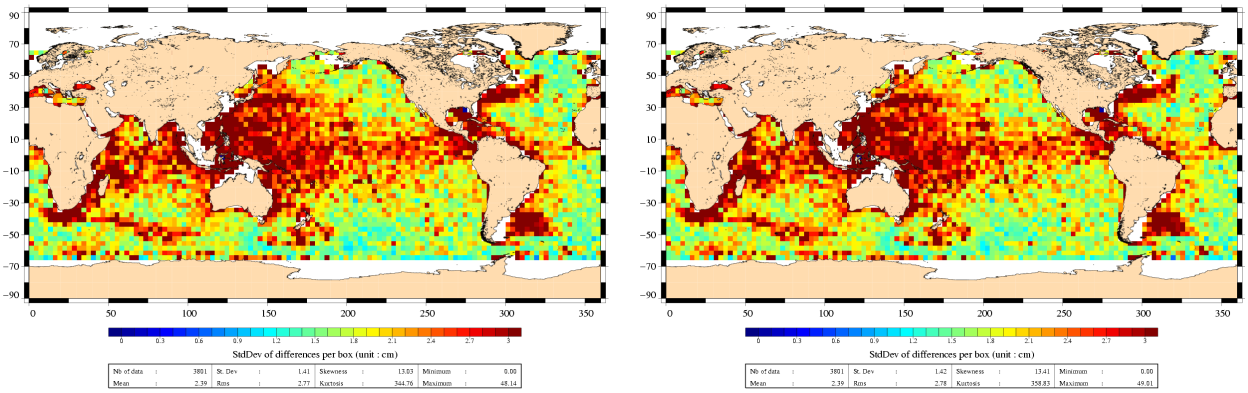

Figure 89: *Standard deviation of cyclic mean map of [EN-J1] using ESOC(EN)/CNES(J1) orbit (left) and ESOC(EN)/GSFC(J1) orbit (right)*

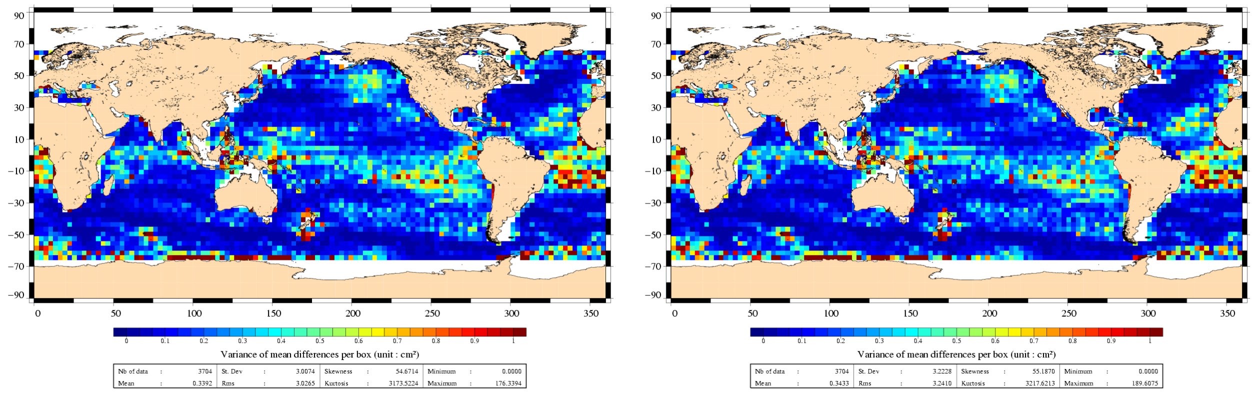

Figure 90: *Ratio of the [variance /variance oceanic signal] of [EN-J1] using ESOC(EN)/CNES(J1) orbit (left) and ESOC(EN)/GSFC(J1) orbit (right)*

8.7 Quality Assessment of Side B

The instrument sub-system Radio Frequency Module was switched to B-side during 37 days, from the 15/05/2006 14:21:50 to the 21/06/2006 11:37:32 (cycle 47 pass 794 to cycle 48 pass 847). The S-band transmission power dropped on the 20/05/2006 13:24:57 (Cycle 47 pass 936), making all the S Band related parameters meaningless from this date.

Present and missing measurements:

- 199 passes produced on Cycle 47 B-side. 10 passes are missing :
  5 passes (903-907) are missing due to : RA2 in RS/WT/INI due to an SEU anomaly
  5 passes (909-913) are missing due to : RA2 in RS/WT/INI due to an SEU anomaly
- 738 passes produced on Cycle 48 B-side. 109 passes are missing :
  81 passes (107 à 187) are missing due to : RA-2 was commanded to Heater-1 for the weekend, back to operations again with RFSS configured to side B.
  10 passes (200-209) are missing due to : missing Level1B
  5 passes (335-339) are missing due to : RA-2 RETURN TO OPERATIONS
  1 pass (473) is missing due to: missing Level1B
  1 pass (475) is missing due to: missing Level1B
  1 pass (499) is missing due to: missing Level1B
  10 passes (664-673) are missing due to : RA-2 switched to Reset/Wait after an SEU anomaly, back to operations again with RFSS configured to side B.

Edited measurements on B-side :

- 2 passes (cycle 47 passes 872-873) are entirely edited on the radiometer land flag (no MWR correction)

Performances:

Nominal performances for cycle 48 of data :
$StDev(Crossover, Bathy < -1000m/Var < 20cm/|latitudes| < 50deg)$=6.68cm
$StDev(SSH - MSS, Bathy < -1000m/Var < 20cm/|latitudes| < 50deg)$=9.29cm

Particular investigations on altimeter parameters:

- The USO anomaly present on A-side data is not visible on B-Side data.
- A 0.0029 deg2 bias is noticed on the square of off nadir angle:
- The standard deviation of Ku 20Hz measurements is nominal:
- A 0.1dB bias is noticed on the Ku Sigma0 parameter:
- The Ku SWH is nominal:
- A 0.5 m/s bias is noticed on the wind speed (due to the 0.1dB bias on Sigma0):
- The performance of SLA is nominal. The bias relative to the MSS is about 50.3 cm using the GIM ionosphere correction. This bias is around 0.9 cm higher than the Side A SLA.:

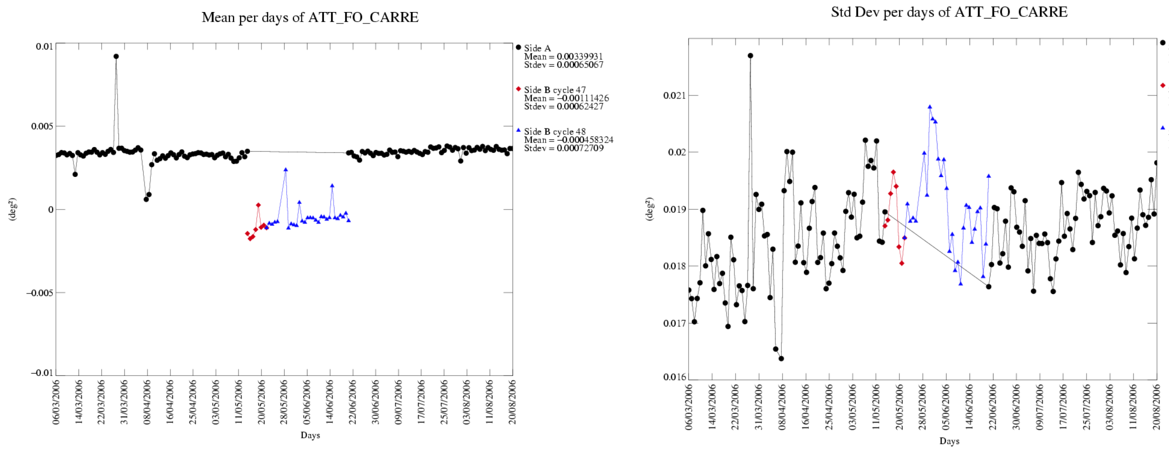

Figure 91:

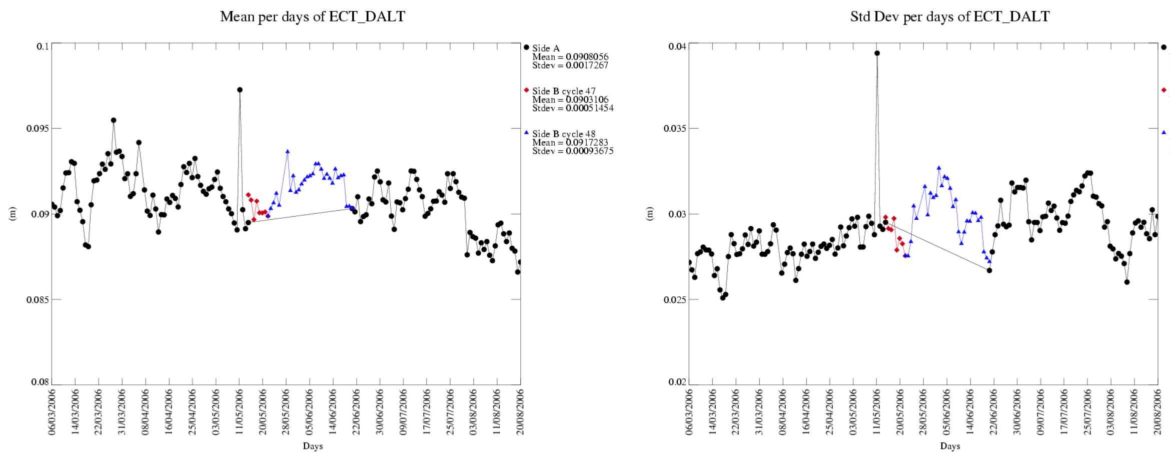

Figure 92:

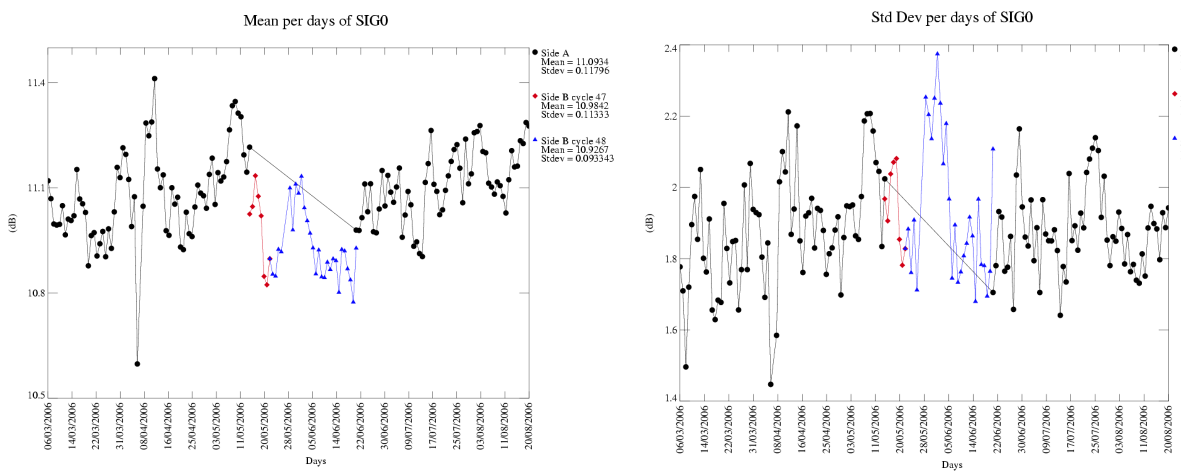

Figure 93:

Warning :

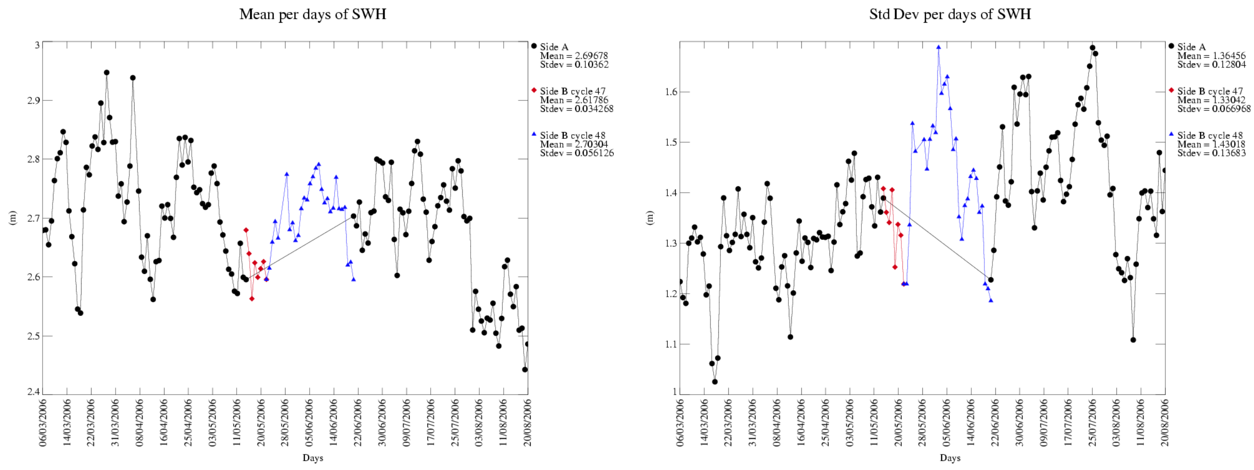

Figure 94:

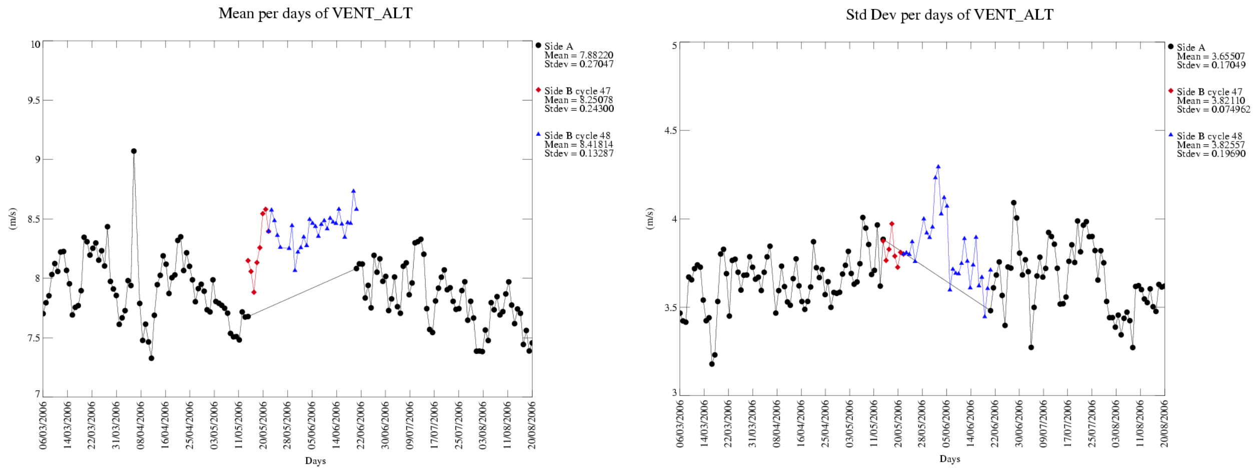

Figure 95:

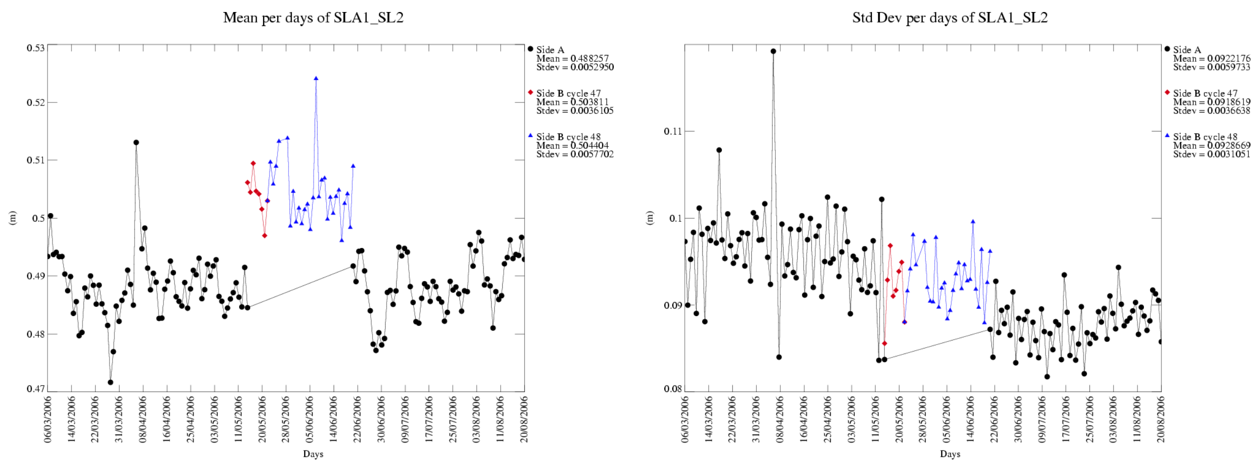

Figure 96:

- Users must not use the S-Band parameters from 20/05/2006 13:24:57 onwards (Cycle 47 pass 936)

Conclusion : The Ku-band side B altimeter parameters have a nominal quality from CALVAL point of view.

9 Conclusion

A statistical evaluation of Envisat altimetric measurements over ocean has been presented in this report. With more than five years of data now available in Geophysical Data Record (GDR) products, Envisat altimetric measurements show good general results:

- The S-Band anomaly has been solved and the USO anomaly is still affecting Ra-2 data which can be corrected and used even during anomaly periods.
- The ocean-1 altimeter and radiometer parameters are consistent with expected values
- The current standards (orbit configuration, instrumental and geophysical correction) used since September 2005 in the IPF/CMA, allow Envisat products to have a high geophysical quality.
- The SLA performance is very good, at the same level as Jason-1.
- The Envisat Mean Sea Level trend is still an issue, though on the two last years, Envisat and Jason-1 have the same MSL trend, which is encouraging.

A reprocessing of the whole Envisat altimetric mission is expected in mid-2007. The major evolutions will be a new precise orbit based on recent Grace data and new ITRF model, better ECMWF meteo fields, new geophysical and instrumental (USO) corrections, new SSB correction, updated wet tropospheric correction. Besides it is planned to re-process ERS-2 data with similar algorithms. Then, performances and comparisons will be carried out again using these new data in order to assess the consistency between Envisat and ERS-2 parameters.

These new products will further improve the high quality level of the Envisat altimetric mission and will make easier the data fusion for multi-mission altimetry, as it is essential for oceanography and applications.

10 Bibliography

References

[1] Abdalla, S., "A wind retrieval algorithm for satellite radar altimeters", ECMWF Technical Memorandum, in preparation, 2006.

[2] Ablain, M., G. Pontonnier, B. Soussi, P. Thibaut, M.H. de Launay, J. Dorandeu, and P. Vincent. 2004. Jason-1 GDR Quality Assessment Report. Cycle 079. SALP-RP-P2-EX-21072-CLS079, May.

[3] M. Ablain., S. Philipps, Dorandeu J., 2006: Jason-1 validation and cross calibration activities. Yearly report. Technical Note CLS.DOS/NT/06-302, Contract N° 03/CNES/1340/00-DSO310 - lot2.C http://www.jason.oceanobs.com/documents/calval/validation_report/annual_report_j1_2006.pdf

[4] M. Ablain., S. Philipps, 2007: Jason-1 validation and cross calibration activities. Yearly report. Technical Note CLS.DOS/NT/06-302, Contract N° 03/CNES/1340/00-DSO310 - lot2.C http://www.jason.oceanobs.com/documents/calval/validation_report/annual_report_j1_2007.pdf

[5] Beckley, B. D., F. G. Lemoine, S. B. Luthcke, R. D. Ray, and N. P. Zelensky A reassessment of global and regional mean sea level trends from TOPEX and Jason-1 altimetry based on revised reference frame and orbits, Geophys. Res. Lett., 34, L14608, 2007, doi:10.1029/2007GL030002.

[6] Carrère, L., and F. Lyard, Modeling the barotropic response of the global ocean to atmospheric wind and pressure forcing - comparisons with observations. 2003. Geophys. Res. Lett., 30(6), 1275, doi:10.1029/2002GL016473.

[7] Cazenave, A., et al.,1999: Sea Level Change from Topex/Poseidon altimetry and tide gauges, and vertical crustal motions from DORIS, G. Res. Let., 26, 2077-2080.

[8] Celani C., B. Greco, A. Martini, M. Roca, 2002: Instruments corrections applied on RA-2 Level-1B Product. 2002: Proceeding of the Envisat Calibration Workshop.

[9] Chambers, D., P., J. Ries, T. Urban, and S. Hayes. 2002. Results of global intercomparison between TOPEX and Jason measurements and models. Paper presented at the Jason-1 and TOPEX/Poseidon Science Working Team Meeting, Biarritz (France), 10-12 June.

[10] Dedieu M., L. Eymard, E. Obligis, N. Tran, F. Ferreira, 2005: ENVISAT Microwave Radiometer Assessment Report Cycle 039, Technical Note CLS.DOS/NT/05.147 Available at http://earth.esa.int/pcs/envisat/mwr/reports/

[11] Dorandeu, J. and P.Y. Le Traon, 1999: Effects of Global Atmospheric Pressure Variations on Mean Sea Level Changes from TOPEX/Poseidon. J. Atmos. Technol., 16, 1279-1283.

[12] Dorandeu J., Y. Faugere, F. Mertz, F. Mercier, N. Tran, 2004a: Calibration / Validation Of Envisat GDRs Cross-calibration / ERS-2, Jason-1 Envisat and ERS Symposium, Salzburg, Austria.

[13] Dorandeu, J., M. Ablain, Y. faugere, F. Mertz, B. Soussi, 2004b, Jason-1 global statistical evaluation and performance assessment. Calibration and cross-calibration results Mar. Geod. 27(3-4): 345-372.

[14] Doornbos E., Scharroo R., 2005: Improved ERS and Envisat precise orbit determination, Proc. of the 2004 Envisat and ERS Symposium, Salzburg, Austria.

[15] ECMWF, The evolution of the ECMWF analysis and forecasting system Available at: http://www.ecmwf.int/products/data/operational_system/evolution/

[16] EOO/EOX, October 2005, Information to the Users regarding the Envisat RA2/MWR IPF version 5.02 and CMA 7.1 Available at http://earth.esa.int/pcs/envisat/ra2/articles/

[17] EOP-GOQ and PCF team, 2005: Envisat Cyclic Altimetric Report, Technical Note ENVI-GSOP-EOPG-03-0011 Available at: http://earth.esa.int/pcs/envisat/ra2/reports/pcs_cyclic/

[18] Eymard L., E. Obligis, N. Tran, February 2003, ERS2/MWR drift evaluation and correction, CLS.DOS/NT/03.688

[19] Faugere Y., Mertz F., Dorandeu J., 2003: Envisat GDR quality assessement report (cyclic), Cycle 015. SALP-RP-P2-EX-21072-CLS015, May. Available at http://www.aviso.oceanobs.com/html/donnees/calval/validation_report/en/welcome_uk.html

[20] Faugere Y., Mertz F., Dorandeu J., 2003: Envisat validation and cross calibration activities during the verification phase. Synthesis report. Technical Note CLS.DOS/NT/03.733, ESTEC contract N°16243/02/NL/FF WP6, May 16 2003 Available at http://earth.esa.int/pcs/envisat/ra2/articles/Envisat_Verif_Phase_CLS.pdf

[21] Faugere Y., Mertz F., Dorandeu J., 2004: Envisat RA-2/MWR ocean data validation and cross-calibration activities. Yearly report. Technical Note CLS.DOS/NT/04.289, Contract N° 03/CNES/1340/00-DSO310 Available at http://earth.esa.int/pcs/envisat/ra2/articles/Envisat_Yearly_Report_2004.pdf

[22] Faugere Y., Estimation du bruit de mesure sur jason-1, December 2002, CLS.ED/NT.

[23] Y.Faugere, J.Dorandeu, F.Lefevre, N.Picot and P.Femenias, 2005: Envisat ocean altimetry performance assessment and cross-calibration. Submitted in the special issue of SENSOR 'Satellite Altimetry: New Sensors and New Applications'

[24] Faugere Y., Mertz F., Dorandeu J., 2005: Envisat RA-2/MWR ocean data validation and cross-calibration activities. Yearly report. Technical Note CLS.DOS/NT/04.289, Contract N° 03/CNES/1340/00-DSO310 http://www.jason.oceanobs.com/documents/calval/validation_report/en/annual_report_en_2005.pdf

[25] Faugere Y., Granier N., Ollivier A., 2006: Envisat RA-2/MWR ocean data validation and cross-calibration activities. Yearly report. Technical Note CLS.DOS/NT/04.289, Contract N° 03/CNES/1340/00-DSO310 http://www.jason.oceanobs.com/documents/calval/validation_report/en/annual_report_en_2006.pdf

[26] Faugere, Y., J. Dorandeu, N. Picot, P. Femenias. 2007. Jason-1 / Envisat Cross-calibration, presentation at the Hobart OSTST meeting

[27] Faugere, Y., Ollivier, A., 2007, Investigation on the differences between CLS and Altimetrics Envisat MSL trend, CLS.DOS/NT07-261

[28] Faugere, Y., Ollivier, A., 2008, Investigation on the High frequency content of Jason and Envisat, CLS.DOS/NT08-119

[29] Dibarbour, G., Bruit Jason et Analyse spectrale, March 2001, CLS.ED/NT

[30] Labroue, S. and P. Gaspar, 2002: Comparison of non parametric estimates of the TOPEX A, TOPEX B and JASON 1 sea state bias. Paper presented at the Jason 1 and TOPEX/Poseidon SWT meeting, New-Orleans, 21-12 October.

[31] Labroue S. and E. Obligis, January 2003, Neural network retrieval algorithms for the ENVISAT/MWR, Technical note CLS.DOS/NT/03.848

[32] Labroue S., 2003: Non parametric estimation of ENVISAT sea state bias, Technical note CLS.DOS/NT/03.741, ESTEC Contract n°16243/02/NL/FF - WP3 Task 2

[33] Labroue S., 2004: RA-2 ocean and MWR measurement long term monitoring, Final report for WP3, Task 2, SSB estimation for RA-2 altimeter, Technical Note CLS-DOS-NT-04-284

[34] Labroue S., 2005: RA2 ocean and MWR measurement long term monitoring 2005 report for WP3, Task 2 SSB estimation for RA2 altimeter, Technical Note CLS-DOS-NT-05-200

[35] Labroue S., 2006: Estimation du Biais d'Etat de Mer pour la mission Jason-1, Technical note CLS-DOS-NT-06-244

[36] Laxon and M. Roca, 2002: ENVISAT RA-2: S-BAND PERFORMANCE, S., Proceedings of the ENVISAT Calibration Workshop, Noordwijk

[37] Le Traon, P.-Y., J. Stum, J. Dorandeu, P. Gaspar, and P. Vincent, 1994: Global statistical analysis of TOPEX and POSEIDON data. J. Geophys. Res., 99, 24619-24631.

[38] Le Traon, P.-Y., , F. Ogor, 1998: ERS-1/2 orbit improvement using TOPEX/POSEIDON: the 2 cm challenge. J. G. Res., VOL 103, p 8045-8057, April 15, 1998.

[39] Lefèvre, F., and E. Sénant, 2005: ENVISAT relative calibration, Technical Note CLS-DOS-NT-05.074.

[40] Lillibridge J, R. Scharroo and G. Quartly, 2005: rain and ice flagging of Envisat altimeter and MWR data, Proc. of the 2004 Envisat and ERS Symposium, Salzburg, Austria

[41] Luthcke. S. B., N. P. Zelinsky, D. D. Rowlands, F. G. Lemoine, and T. A. Williams. 2003. The 1-Centimeter Orbit: jason-1 Precision Orbit Determination Using GPS, SLR, DORIS, and Altimeter Data. Mar. Geod. 26(3-4): 399-421.

[42] Martini A. and P. Féménias, 2000: The ERS SPTR2000 Altimetric Range Correction: Results and Validation. ERE-TN-ADQ-GSO-6001. 23 November 2000.

[43] Martini A., 2003: Envisat RA-2 Range instrumental correction : USO clock period variation and associated auxiliary file, Technical Note ENVI-GSEG-EOPG-TN-03-0009 Available at http://earth.esa.int/pcs/envisat/ra2/articles/USO_clock_corr_aux_file.pdf http://earth.esa.int/pcs/envisat/ra2/auxdata/

[44] A. Martini, P. Feminias, G. Alberti, M.P.Milagro-Perez, 2005: RA-2 S-Band Anomaly: Detection and waveform recontruction. Proc. of 2004 Envisat & ERS Symposium, Salzburg, Austria. 6-10 September 2004 (ESA SP-572, April 2005).

[45] Mertz, F., Y. Faugere and J. Dorandeu, 2003: Validation of ERS-2 OPR cycle 083-086. CLS.OC.NT/03.702 issue 083-086.

[46] Mertz F., J. Dorandeu, N. Tran, S. Labroue, 2004, ERS-2 OPR data quality assessment. Long-term monitoring - particular investigations, Report of task 2 of IFREMER Contract n° 04/2.210.714. CLS.DOS/NT/04.277.

[47] Mitchum, G., 1994: Comparison of TOPEX sea surface heights and tide gauge sea levels, J. Geophys. Res., 99, 24541-24554.

[48] Mitchum, G., 1998: Monitoring the stability of satellite altimeters with tide gauges, J. Atm. Oceano. Tech., 15, 721-730.

[49] Obligis E., L. Eymard, N. Tran, S. Labroue, 2005: Three years of Microwave Radiometer aboard Envisat: In-flight Calibration, Processing and validation of the geophysical products, submitted

[50] R D Ray and R M Ponte, 2003: Barometric tides from ECMWF operational analyses, Annales Geophysicae, 21: 1897-1910.

[51] Roca M., A. Martini, 2003: Level 1b Verification updates, Ra2/MWR CCVT meeting, 25-26 March 2003, ESRIN, Rome

[52] Rudolph A., D.Kuijper, L.Ventimiglia, M.A. Garcia Matatoros, P.Bargellini, 2005: Envisat orbit control - philosophy experience and challenge, Proc. of the 2004 Envisat and ERS Symposium, Salzburg, Austria

[53] R. Scharroo and P. N. A. M. Visser, 1998: Precise orbit determination and gravity field improvement for the ERS satellites, J. Geophys. Res., 103, C4, 8113-8127

[54] Scharroo R., A decade of ERS Satellite Orbits and Altimetry, 2002: Phd Thesis, Delft University Press science

[55] Scharroo R., December 12, 2002, Routines for iono corrections, internet communication to the CCVT community

[56] Scharroo R., J. L. Lillibridge, and W. H. F. Smith, Cross-Calibration and Long-term Monitoring of the Microwave Radiometers of ERS, TOPEX, GFO, Jason-1, and Envisat, **Marine Geodesy, 27:279-297**, 2004.

[57] Scharroo, R., RA-2 USO Anomaly: predictive correction model, Tech. Rep. N1-06-002, Altimetrics LLC, Cornish, New Hampshire, May 2006.

[58] Stum J., F. Ogor, P.Y. Le Traon, J. Dorandeu, P. Gaspar and J.P. Dumont, 1998: "An intercalibration study of TOPEX/POSEIDON, ERS-1 and ERS-2 altimetric missions", Final report of IFREMER contract N_97/2 426 086/C CLS.DOS/NT/98.070.

[59] Tran, N., D. W. Hancock III, G.S. Hayne. 2002: "Assessment of the cycle-per-cycle noise level of the GEOSAT Follow-On, TOPEX and POSEIDON." J. of Atmos. and Oceanic Technol. 19(12): 2095-2117.

[60] Tran N. and E. Obligis, December 2003, Validation of the use of ENVISAT neural algorithm on ERS-2. CLS-DOS-NT-03.901.

[61] Tran N., E. Obligis and L. Eymard, 2006, Envisat MWR 36.5 GHz drift evaluation and correction. CLS-DOS-NT-05.218.

[62] Vincent, P., S. D. Desai, J. Dorandeu, M. Ablain, B. Soussi, P. S. Callahan, and B. J. Haines 2003. Jason-1 Geophysical Performance Evaluation. Mar. Geod. 26(3-4): 167-186.

[63] Witter, D. L., D. B. Chelton, 1991: "A Geosat altimeter wind speed algorithm development", J. of. Geophys. Res. (oceans), 96, 8853-8860, 1991.

[64] Zanife, O. Z., P. Vincent, L. Amarouche, J. P. Dumont, P. Thibaut, and S. Labroue, 2003. Comparison of the Ku-band range noise level and the relative sea-state bias of the Jason-1, TOPEX and Poseidon-1 radar altimeters. Mar. Geod. 26(3-4): 201-238.

11 Appendix 1: Instrument and plateform status

11.1 ACRONYMS

The main acronyms used to described the events are explained below.
CMA: Centre Multimission Altimetrique
CTI tables: Configuration Table Interface. They Contain the setting of the instruments and are uploaded on board after a switch off, a reset
HTR Refuse: Heater Refuse
ICU: Instrument Control Unit, a part of the distributed command and control function implemented on ESA spacecraft. The unit receives, decodes and executes high-level commands for its instrument, and autonomously performs health-checking and parameter monitoring. In the event of anomalies it takes autonomous recovery actions.
IPF: Instrument Processing Facilities
MCMD: Macrocommand
OBDH: On Board Data Handling
OCM: Orbit Controle Mode/maneuvre
P/L SOL: Payload Switch Off Line
SEU: Single Event Upset
SM-SOL by PMC: SM Switch Off Line by Payload Main Computer
SW: Software
TM: Telemetry
USO: Ultra Stable Oscillator

11.2 Cycle 010

- RA-2 went to STBY/Refuse (2002/10/09 09 13:34:22 to 2002/10/10 08:56:53)

11.3 Cycle 011

- Ra2 switch-down - Planned SM-SOL by PMC1 (2002/11/18 04:38:00 to 2002/11/19 19:19:21,Pass 382-429)
- DORIS Navigator switch-down - Planned SM-SOL by PMC1 (2002/11/18 04:38:02 to 2002/11/22 12:40:00, Pass 382-505)
- MWR switch-down - Planned SM-SOL by PMC1 (2002/11/18 04:37:59 to 2002/11/20 12:20:06, Pass 382-448)
- Orbit Maintenance Maneuver (2002/11/07 18:15:51 to 2002/11/07 21:06:17,Pass 83-85)
- Orbit Maintenance Maneuver (2002/11/29 03:35:30 to 2002/11/29 06:25:57,Pass 696-698)

11.4 Cycle 012

- RA-2 went to HTR-0 Refuse (2002/12/21 04:31:26 to 2002/12/21 12:52:00, Pass 325-333)
- Orbit Inclination Maneuver (2002/12/18 04:28:18 to 2002/12/18 06:36:46, Pass 238-240)
- Orbit Maintenance Maneuver (2002/12/18 22:17:22 to 2002/12/19 00:17:34, Pass 259-261)

11.5 Cycle 013

- RA-2 went to HTR-0 Refuse (2003-01-16 01:52:36 to 2003-01-17 17:00:35)
- RA-2 went to suspend mode (2003-01-25 23:56:36 to 2003-01-27 19:54:02)
- Orbit Maintenance Maneuver (2003/01/14 00:55:17 to 2003/01/14 03:45:42 TAI)
- Orbit Maintenance Maneuver (2003/02/11 23:04:49 to 2003/02/12 01:04:57 TAI)

11.6 Cycle 014

- SEU's caused a Software Anomaly (2003/03/02 02:46:44 to 2003/03/03 16:46:35).
- Subsystems unavailable - Autonmous P/L switch-off (2003/03/15 04:21:08 to 2003/03/17 19:00:13)
- RA2 in HTR0/Refuse due to HPA primery bus undercurrent (2003/03/17 21:09:32 to 2003/03/18 18:50:40)
- Orbit Maintenance Maneuver (2003/02/21 03:42:57 to 2003/02/21 05:53:24)
- Orbit Maintenance Maneuver (2003/03/03 23:51:14 to 2003/03/04 01:51:22)

11.7 Cycle 015

- Wrong setting of Ra2 parameters (no CTI tables have been up-loaded on-board) from 18 Mar 2003 18:50:40 to 9 Apr 2003 17:12:24, Pass 1 to 452
- RA-2 unavailability (Format Header Error forcing ICU to RS/WT/INI) from 8 Apr 2003 15:08:57.000 to 9 Apr 2003 17:12:24.000, Pass 437 to 452
- RA-2 unavailability (Format Header Error forcing ICU to RS/WT/INI) from 8 Apr 2003 15:08:57.000 to 9 Apr 2003 17:12:24.000, Pass 613 to 624
- RA-2 unavailability: Multiple SEU caused ICU switchdown (2003/04/24 13:20:09 to 2003/04/25 09:15:36,879 to 901)
- Orbit Maintenance Maneuver (2003/04/04 00:40:48 to 2003/04/04 02:40:56 TAI)

11.8 Cycle 016

- RA2 unavailability (known SEU failure) (from 5 May 2003 12:30:17.000 to 6 May 2003 10:01:10.000, Pass 191 to 215)
- RA-2 unavailability (ICU in SUSPEND due to TM FMT Error when a Reduced FMT was requested) (from 11 May 2003 11:06:33.000 to 12 May 2003 10:14:35.726, Pass 361 to 387)
- Orbit Maintenance Maneuver (from 2003/05/14 22:40:13 to 2003/05/15 00:40:19 TAI, Pass 460 to 462)
- RA-2 unavailability (Switch-down for PMC SW upgrade and OCM) from 18 May 2003 06:25:17.000 to 19 May 2003 15:59:28.000, Pass 548 to 602)
- MWR unavailability (Switch-down for PMC SW upgrade and OCM) from 18 May 2003 06:25:24.000 to 19 May 2003 14:45:40.000, Pass 548 to 602)
- DORIS unavailability (Switch-down for PMC SW upgrade and OCM) from 18 May 2003 06:25:25.000 to 19 May 2003 13:21:28.000, Pass 548 to 602)
- Orbit Inclination Maneuver (from 2003/05/20 04:11:53 to 2003/05/20 06:23:31 TAI, Pass 610 to 612)
- RA-2 unavailability (ICU went to RS/WT/INI) from 1 Jun 2003 14:36:40.000 to 2 Jun 2003 09:20:35.000, Pass967 to 987

11.9 Cycle 017

- Orbit Maintenance Maneuver (from 2003/06/07 01:08:16 to 2003/06/07 03:08:23 TAI, Pass 119 to 122)

11.10 Cycle 018

- Orbit Maintenance Maneuver (from 2003/07/11 0:58:45 to 2003/07/11 03:49:08 TAI, Pass 90 to 94)
- RA2 unavailability (RA-2 in STBY/REF due to MCMD timeout) (from 26 Jul 2003 15:28:11 to 26 Jul 2003 17:25:35, Pass 538)
- RA2 unavailability (RA-2 picked up Mission Planning schedule) (from 31 Jul 2003 16:11:02 to 31 Jul 2003 18:06:30, Pass 682)
- Orbit Maintenance Maneuver (from 2003/07/11 0:58:45 to 2003/07/11 03:49:08 TAI), Pass 91 to 94)

11.11 Cycle 019

- Orbit Maintenance Maneuver (from 2003/08/15 1:31:29 to 2003/08/15 03:31:35 TAI, Pass 91 to 93)
- RA-2 went to STBY/Refuse due to Individual Echoes MCMD Timeout (from 2003-08-15 16:40:21 to 2003-08-15 18:35:35, Pass 110)
- RA-2 went to STBY/Refuse due to Individual Echoes MCMD Timeout (from 2003-08-30 15:28:00 to 2003-08-30 20:47:35, Pass 538 to 543)
- PLSOL . Instrument Switch OFF/ON (from 2003-09-04 22:52:52 to 2003-09-06 16:41:09, Pass 689 to 738)

11.12 Cycle 020

- RA-2 in STANDBY / REFUSE MODE (from 2003-09-21 15:36:40 to 2003-09-21 17:33:30, Pass 166 to 167)
- RA-2 is in RS/WT/INT mode (from 2003-09-27 00:28:08 to 2003-09-27 12:52:00, Pass 320 to 333)
- Wrong setting of Ra2 parameters (no CTI tables have been up-loaded on-board) (from 2003-09-27 12:52:00 to 2003-09-30 12:45:00, Pass 334 to 407)
- Orbit Maintenance Maneuver (2003/09/30 00:40:53 to 2003/09/30 02:41:00 TAI, Pass 405 to 407)

11.13 Cycle 021

- Orbit Inclination Maneuver (2003/10/28 04:56:18 to 2003/10/28 07:09:44 TAI, Pass 210 to 212)
- RA-2 is in RS/WT/INT mode. 29 Oct 2003 06 :47 :04 to 29 Oct 2003 12 :58 :35, Pass 242 to 247)
- Orbit Maintenance Maneuver (2003/10/31 01:13:10 to 2003/10/31 03:13:25 TAI, Pass 291 to 293)
- RA-2 is in RS/WT/INT mode. TM format header error (02 Nov 2003 15 :16 :56 to 03 Nov 2003 12 :08 :35, Pass 366 to 389)
- Orbit Maintenance Maneuver (2003/11/18 23:02:30 to 2003/11/19 01:52:55 TAI, Pass 833 to 835)

11.14 Cycle 022

- RA-2 is in RS/WT/INT mode (2003-11-26 13:31:20 to 2003-11-26 19:39:35, Pass 49 to 54)
- RA-2 PLSOL . Instrument Switch OFF/ON (2003-12-03 07:18:43 to 2003-12-05 16:35:05, Pass 241 to 308)
- MWR PLSOL . Instrument Switch OFF/ON (2003-12-03 07:18:43 to 2003-12-04 18:45:41)
- RA-2 is in RS/WT/INT mode. (2003-12-06 15:55:52 to 2003-12-10 19:16:36, Pass 338 to 455)
- Orbit Maintenance Maneuver (2003/12/15 21:02:28 to 2003/12/15 23:02:36, Pass 601 to 603)
- Orbit Maintenance Maneuver (2003/12/26 21:03:30 to 2003/12/26 23:03:34, Pass 916 to 918)

11.15 Cycle 023

Orbit Maintenance Maneuver (2004/01/21 23:54:27 to 2004/01/22 01:54:37))

- Orbit Maintenance Maneuver (2004/01/26 22:26:07 to 2004/01/27 00:26:11))

11.16 Cycle 024

- Orbit Inclination Maneuver (2004/02/04 04:46:39 to 2004/02/04 06:58:05)
- Orbit Maintenance Maneuver (2004/02/05 11:17:21 to 2004/02/05 13:17:23)
- Orbit Maintenance Maneuver (2004/02/24 11:48:39 to 2004/02/24 13:48:45)

11.17 Cycle 025

- Orbit Maintenance Maneuver (2004/04/07 20:05:30 to 2004/04/07 22:05:34)

11.18 Cycle 026

- RA-2 in STANDBY/REF DUE TO MCMD H202 FAILURE (2004-22-04 15:15:36 2004-22-04 17:07:05)
- RA-2 Switch down to RESET/WAIT due to too many SEU's reported. (2004-05-10 02:06:31 2004-05-10 11:27:30)
- Orbit Inclination Maneuver (2004/04/14 04:43:02 2004/04/14 06:55:00)
- Orbit Maintenance Maneuver (2004/05/07 01:08:56 2004/05/07 03:09:04)

11.19 Cycle 027

- RA2 went to suspend owing to repeated type 10 entries in report format (2004/05/31 02:45:27 to 2004/05/31 12:01:50)
- No DORIS data from 2004/06/06 13:00:00 to 2004/06/14 14:52:00. Following an onboard incident, Doris instrument has been switched to the redundant chain. Doris data are unavailable from June, 6th to June, 14th. To allow GDR production, POE with laser only data have been produced during this period.
- RA2 in SUSPEND Mode (2004/06/21 14:47:51 to 2004/06/21 19:24:30, Pass 995 to 999)

11.20 Cycle 028

- RA2 in ICU rs/wt/ini (2004/07/18 13:47:03 to 2004/07/18 19:59:00, Pass 765 to 771)
- Orbit Maintenance Maneuver (2004/06/30 08:08:29 to 2004/06/30 10:08:35, Pass 242 to 244)

11.21 Cycle 029

RA2 in ICU RS/WT/INI. (SDU problem in RAM) (2004/08/10 15:00:39 to 2004/08/11 10:59:30, Pass 423 to 445)

- Orbit Maintenance Maneuver (2004/08/17 02:04:20 to 2004/08/17 04:04:26 , Pass 607 to 609)

11.22 Cycle 030

- RA2 in ICU RS/WT/INI. (SDU problem in RAM) (2004/09/26 13:39:50 to 2004/09/27 16:23:30, Pass 765-795)
- Abnormal behaviour of the RA-2 sensor (2004/09/27 16:23:30 to 2004-09-29 10:21:07, Pass 796-846)
- Collision avoidance Maneuver (2004/09/01 22:52:27 to 2004/09/02 00:52:37, Pass 60-62)
- Collision avoidance Maneuver (2004/09/02 23:44:27 to 2004/09/03 01:44:37, Pass 89-91)
- Orbit Inclination Maneuver (2004/09/21 04:14:37 to 2004/09/21 06:29:19, Pass 610-612)
- Orbit Maintenance Maneuver (2004/09/24 03:53:38 to 2004/09/24 05:53:46, Pass 695-697)

11.23 Cycle 031

- Collision avoidance Maneuver (2004/10/22 03:20:22 to 2004/10/22 07:00:41, Pass 495-498)
- High solar activity (Pass 974-1002)

11.24 Cycle 032

- RA2 in RS/WT/INI. 2004/11/23 13:25:58 to 2004/11/24 14:10:10, Pass 421-449
- RA2 Format header error. 2004/12/01 10:22:30 to 2004/12/01 15:34:29, Pass 647-651
- Orbit Maintenance Maneuver (2004/11/12 01:07:57 to 2004/11/12 03:08:06,Pass 91-93)

11.25 Cycle 033

- RA-2 went to RS/WT/INI due RBI (2004/12/27 02:49:10 to 2004/12/27 13:49:30, 380 to 391)
- Orbit Maintenance Maneuver (2004/12/17 01:03:48 to 2004/12/17 03:03:52, 91 to 93)
- Orbit Maintenance Maneuver (2005/01/05 23:10:28 ro 2005/01/06 01:10:36, 661 to 663)
- Orbit Inclination Maneuver (2005/01/07 04:25:17 to 2005/01/07 06:38:53, 696 to 698)

11.26 Cycle 034

- RA-2 went to RS/WT/INI Mode (2005/01/26 15:50:30 to 2005/01/26 21:07:30, 252 to 257)
- Orbit Maintenance Maneuver (2005/02/18 01:23:24 to 2005/02/18 03:23:28, 893 to 894)

11.27 Cycle 035

- RA-2 went to RS/WT/INI Mode (2005/03/18 04:35:34 to 2005/03/18 12:58:00, 697 to 705)
- Orbit Maintenance Maneuver (2005/03/17 04:51:26 to 2005/03/17 07:06:31, 668 to 669)

11.28 Cycle 036

- RA-2 went to RS/WT/INI mode (2005/04/18 05:01:10 to 2005/04/18 13:22:32, 583 to 591)
- RA-2 went to RS/WT/INI mode (2005/04/18 37:58:10 to 2005/04/24 11:42:30, 742 to 761)

11.29 Cycle 037

- RA-2 went to ICU in RS/WT/INI (RBI ERR 71) (2005/05/14 23:56:37 to 2005/05/15 10:53:45, 348 to 359)
- RA-2 went to ICU in RS/WT/INI (2005/05/21 00:10:45 to 2005/05/21 10:55:35, 520 to 531)

11.30 Cycle 038

- RA-2 went to ICU in RS/WT/INI (2005/07/04 04:41:10 to 2005/07/04 11:19:39, 783 t0 789)

11.31 Cycle 039

- RA-2 went to ICU in RS/WT/INI (2005/07/16 13:32:21 to 2005/07/16 19:58:52,135 to 141)
- RA-2 went to ICU in RS/WT/INI (2005/07/17 14:43:49 to 2005/07/17 19:20:30,165 to 169)
- RA-2 went to ICU in RS/WT/INI (2005/07/29 00:41:41 to 2005/07/29 09:58:30,492 to 501)
- Orbit Maintenance Maneuver (2005/08/09 22:45:44 to 2005/08/10 00:45:50 TAI)

11.32 Cycle 040

- RA-2 went to ICU in RS/WT/INI (2005/08/16 16:41:57 to 2005/08/16 20:22:30,24 to 27)
- RA-2 went to ICU in RS/WT/INI (2005/08/30 16:01:25 to 2005/08/30 19:43:00,424 to 427)
- RA-2 went to ICU in RS/WT/INI (2005/09/12 15:53:09 to 2005/09/12 19:47:00,796 to 799)
- Orbit Maintenance Maneuver (2005/09/07 05:19:53 to 2005/09/07 07:36:31 TAI)

11.33 Cycle 041

- RA-2 went to ICU in RS/WT/INI (2005/09/20 12:19:17 to 2005/09/20 18:56:00,19 to 25)
- RA-2 went in RS/WT/INI (2005/10/04 12:47:33 to 2005/10/04 16:35:30,420 to 423)
- Orbit Maintenance Maneuver (2005/10/06 02:19:10 to 2005/10/06 02:19:14 TAI)

11.34 Cycle 042

- RA-2 went in RS/WT/INI following Uncontrolled S/W Action (2005/10/28 05:34:13 to 2005/10/28 10:39:00,97 to 101)

11.35 Cycle 043

- RA-2 went in RS/WT/INI following Uncontrolled S/W Action (2006/01/02 12:56:35 2006/01/02 18:09:30,993 to 997)

11.36 Cycle 044

- RA-2 went in RS/WT/INI following Multiple SEU Anomaly (ref AR-614) (2006/01/12 14:20:35 to 2006/01/12 19:12:30,279 to 283)
- RA-2 went in RS/WT/INI(2006/01/30 02:07:15 to 2006/01/30 11:29:00,780 to 789)
- RA-2 went in RS/WT/INI following Uncontrolled S/W Action (2006/02/01 05:17:56 to 2006/02/01 12:04:30,841 to 847)
- RA-2 went in RS/WT/INI following Uncontrolled S/W Action (2006/02/01 16:30:28 to 2006/02/01 18:36:30,854 to 855)
- Orbit Inclination Maneuver (2006/01/10 05:54:24 to 2006/01/10 06:11:24)

11.37 Cycle 045

- RA-2 went in RA2 back to operations following TM format anomaly (2006/03/13 09:36:51 to 2006/03/13 17:40:00,989 to 997))

11.38 Cycle 046

- RA-2 switch to STBY and back to measurement to get useful telemetry related to USO (2006/03/17 12:04:00 to 2006/03/17 13:26:00,104 to 107)
- Orbit Inclination Manoeuvre (2006/03/28 05:33:20 to 2006/03/28 05:52:11 TAI)
- Payload anomaly DORIS MVR switch off (no data from) (2006/04/06 02:09:00 to 2006/04/08 12:40:00 TAI)
- RA2 back to operations following TM format anomaly (2006/04/06 12:31:00 to 2006/04/08 12:31:00,664 to 735)
- Doris Doppler Instrument nominal mode with median frequency bandwith pre-positionning (required for DORIS incident recovery) (2004/04/08 12:40:00 to 2006/04/14 09:00:00 TAI)
- Payload anomaly DORIS Reset (2006/04/14 09:00:09)

11.39 Cycle 047

- On 12th-13th May, a special operation was executed to limit RA-2 Chirp Bandwidth to 80MHz (starting from 12/05/2006 at 15:51:37, pass 710) and then 20 MHz (starting from 13/05/2006 at 03:57:57, Pass 724). The instrument was returned to 320MHz on 13/05/2006 at 15:10:17, Pass 738. Users are strongly advised not to use passes 710-738
- The instrument sub-system Radio Frequency Module (RFM) was switched to its B-side on 15 May 2006 at 14:21:50, Pass 790
- RA-2 BACK TO OPERATIONS AFTER 2 CONSECUTIVE SEU ANOMALIES (19 May 2006 09:24:32 and 19 May 2006 19:13:00)

11.40 Cycle 048

RFM switched to its nominal configuration side (A-side) on the 2006/06/21 at 13:20:15, Pass 850

- RA-2 Back to Measurement following Uncontrolled S/W Action (2006/06/25 15:01:36 to 2006/06/25 19:46:00, passes 967-971)

11.41 Cycle 049

- none

11.42 Cycle 050

- RA-2 Back to Measurement following Multiple SEU Anomaly (2006/08/01 01:14:40 to 2006/08/01 08:54:30,6 to 13)
- Foccserver have been re-booted and is up and running. The problem was probably due to a HW failure at ESRIN (IECF) which caused all the user slots to be occupied(2006/08/17 00:00:41 to 2006/08/17 11:10:00,TAI)

11.43 Cycle 051

- RA-2 Back to Measurement following a Service Module Anomaly (2006/09/7 16:40:30 to 2006/09/10 15:47:30,80 to 166)
- Orbit Inclination Maneuver (2006/09/13 05:22:17 to 2006/09/13 05:40:29)
- Interruption of the Envisat data transmission via the ESA Data Relay Satellite Artemis (anomaly with Envisat Ka-band antenna) from 2006/09/26 until 2006/10/1,630 to 641, 658 to 669, 686 to 697, 716 to 725, 744 to 755)

11.44 Cycle 052

- RA-2 Back to Measurement following a Service Module Anomaly (2006/10/26 04:02:43 to 2006/10/26 10:32:00,467 to 473)
- RA-2 Back to Measurement following a Service Module Anomaly (2006/11/02 15:20:19 to 2006/11/02 20:07:00,681 to 685)

11.45 Cycle 053

- RA-2 Back to Measurement following Multiple SEU Anomaly (2006/11/26 08:01:06 to 2006/11/26 17:32:00, 358-367)
- Available again in Measurement after SM Memory Maintenance (2006/11/28 07:40:00 to 2006/11/29 17:23:00,413-469)
- The entire payload switched off (Due to a LVL 3 PROTOCOL ERROR AND INTERRUPT) (2006/12/12 18:02:17 to 2006/12/15 15:54:00,826-909)

11.46 Cycle 054

- HSM input reset (2006/12/27 14:18:50 to 2006/12/28 10:51:48)

11.47 Cycle 055

- Orbit Inclination Maneuver (2007/01/23 04:33:06 to 2007/01/23 04:51:50; 9)
- RA-2 recovered from STANDBY / REFUSE MODE and back to MEASUREMENT (2007/02/01 15:15:30 to 2007/02/01 17:11:30, 280-281)
- RA-2 return to operation from RESET/WAIT due to MCMD Transfer Acknowledge Error (2007/02/16 00:47:49 to 2007/02/16 11:07:00, 692-703)
- RA-2 return to operation from HT0/REF due to low HPA PBC current (2007/02/17 00:45:47 to 2007/02/19 11:11:00, 721-789)

11.48 Cycle 056

- No event

11.49 Cycle 057

- Orbit Inclination Maneuver (2007/04/03 04:34:42 to 2007/04/03 04:50:14)
- RA-2 Return to Mesurement from HEATER 0 / REFUSE MODE due to HPA bus current OOL (2007/04/03 12:37:27 3 to 2007/04/03 13:48:00)
- RA-2 Return to Measurement after HEATER 0 / REFUSE MODE due to HPA bus current OOL (2007/04/04 09:49:12 to 2007/04/04 11:30:00)
- RA-2 back to measurement from STBY/REFUSE following HTR0/REFUSE MODE (2007/04/09 05:08:51 to 2007/04/09 10:36:30)

11.50 Cycle 058

- The MWR instrument switched into Stand-by/Refuse mode following an on-board anomaly (2007/05/26 13:20:29 to 2007/05/30 13:41:06, 535-649)

11.51 Cycle 059

- RA-2 recovered back to measurement from HTR1/REF0 (2007/06/30 00:37:55 to 2007/06/02 09:51:00,520-587)

11.52 Cycle 060

- RA-2 returned to Measurement from HTR1/REF due to a Telemetry error.(2007/07/19 01:08:026 to 2007/07/19 07:38:00,63-69)
- Orbit Inclination Maneuver (2007/07/17 04:41:26 to 2007/07/17 04:43:42,9)

11.53 Cycle 061

- Payload switch-off due to Service Module Anomaly (Global AOCS Surveillance triggered) (24 Sep 2007 12:27:00 to 27 Sep 2007 11:13:30,993-1002)

11.54 Cycle 062

- Payload switch-off due to Service Module Anomaly (Global AOCS Surveillance ered).(24 Sep 2007 12:27:00 to 27 Sep 2007 11:13:30,1-7)
- Orbit Inclination Maneuver (27 Sep 2007 05:16:25 to 27 Sep 2007 05:31:15)
- Orbit Maintenance Maneuver (28 Sep 2007 03:16:04 to 28 Sep 2007 03:16:08)
- MCMD Transfer Acknowledge Error caused the ICU to be put into Reset/Wait Mode. This is one of the cexpected anomalies and RA-2 was back to measurement on the same day. (2 Oct 2007 16:15:55 to 2 Oct 2007 20:09:30,224-227)

12 Appendix 2: Proceeding of the 2007 Envisat Symposium, Montreux

AN OPERATIONAL CORRECTION FOR THE RA2 SIDE A USO ANOMALY: METHOD AND PERFORMANCE ASSESSMENT

Yannice Faugère [1], Annabelle Ollivier [1], Ouan Zan Zanifé [1], Remko Scharroo [2], Annalisa Martini [3], Mónica. Roca [4], Pierre Femenias [5]

(1) CLS, 8-10 rue Hermes, Parc Technologique du Canal, 31526 Ramonville Saint-Agne, France
(2) Altimetrics, LLC 330a Parsonage Road, Cornish NH 03745, USA
(3) Serco SpaVia Sciadonna, 24/26 00044 Frascati (Roma) - Italy
(4) IsardSat, Barcelona, Spain
(5) ESA, EO Ground Segment Department, ESA/ESRIN EOP-GOQ, Via Galileo Galilei CP64, Frascati, Italy

ABSTRACT

For an unknown reason a change of behaviour of the Ultra Stable Oscillator (USO) clock frequency occurred on September 2004 lasting 2 days and on February 2006, lasting 9 days. Between March 2006 and March 2007, all the RA-2 A-side data have been impacted by the USO anomaly. Translated into range, the anomaly consists in an oscillating signal with an orbital period and an amplitude of 30cm around a 5.6m mean bias.

This paper presents the method implemented temporarily to correct the anomalous data as well as the assessment of the quality and performance of the corrected data through two analyses: first, an extensive geophysical validation study over ocean, then a comparison of the operational correction method to a predictive model based one.

Auxiliary files are available on all surfaces, for real time and off-line data, at the same time as the products themselves and enable Ra2 data to recover their high level of accuracy. Soon, a finalized correction will be included in the products themselves.

1. INTRODUCTION

For an unknown reason a change of behaviour of the Ultra Stable Oscillator (USO) clock frequency occurred on September 2004 lasting 2 days and on February 2006, lasting 9 days. Between March 2006 and March 2007, all the RA-2 A-side data have been impacted by the USO anomaly.

An operational correction procedure has been implemented by the altimetry Data Processing and Quality Control (DPQC) team. This paper aims at presenting this correction method.

After a description of the anomaly since september 2004, the method used to correct the data is presented. Then, a quality assessment of the corrected data is performed over ocean during the anomaly period. On the same period, a comparison is then performed with another solution, a model based correction. Finally, the method is tested on a stable period in order to check that the proposed method enables to moitor the USO device long term effects. To finish with, the last section deals with the practical details necessary to use the correction.

2. ANOMALY DESCRIPTION

When the anomaly occurs, the USO period increases rapidly during several hours to reach about 12500.090 picoseconds and from then starts to oscillate with a 0.005 ps amplitude. This change of frequency has a direct impact on the altimetric range measurement in both Ku and S bands. Translated into range, the anomaly consists in an oscillating signal with an orbital period and an amplitude of 30cm around a 5.6m mean bias. It is noticeable on the Sea Level Anomaly (SLA) map in Figure 1 that without the correction, all the oceanic structures would be hidden by the anomaly.

The change of behaviour of the Ultra Stable Oscillator (USO) clock frequency occurred on September 2004 lasting 2 days and on February 2006, lasting 9 days as shown in Figure 2. Furthermore, between March 2006 and 2007, the USO correction does not have a stable behaviour concerning its average per day. It varies between 5.2 and 5.8m. Jumps can also be noticed after each platform or instrument event. Since the beginning of March 2007 the USO period bias and orbital variations disappeared, coming back to the nominal behaviour. The reason remains unexplained as well.

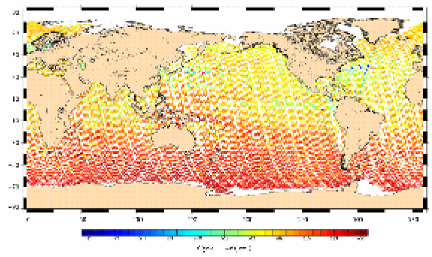

Figure 1. SLA without the USO Correction on cycle 46 affected by the anomaly.

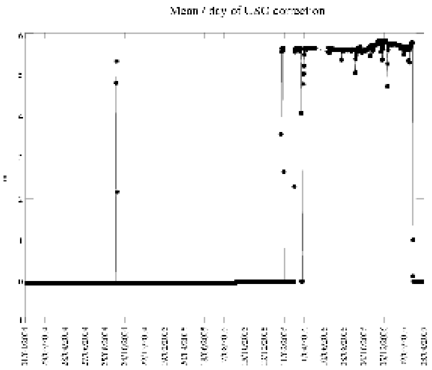

Figure 2. Daily mean Period converted into range (m) since September 1st of 2004

3. USO RANGE CORRECTION METHOD

The proposed method to estimate the true USO period is based on a reference with the on board clock ([1]). The USO period is calculated by finite difference:

$$Period(t) = \frac{OBDH(t - step/2) - OBDH(t + step/2)}{USO_{count}(t - step/2) - USO_{count}(t + step/2)} \quad (1)$$

(1)

Where OBDH is the on-board clock time, USOcount the count of the altimeter clock and step=100s. The method is fully described in [2] and [3]. To compute a corrected tracker range an approximated method is used. The range used comes from an already computed tracker range with a wrong USO clock period (using Level1B data instead of Level0). It is demonstrated in [4], that the error using this method is negligible.

Once calculated the period with the short step, it is noticeable in Figure 3 (top), that a quantification step appears. In order to smooth it, a filter is applied on the raw period (middle) before converting it to a smooth range correction (bottom). a spline regression filter was preferred to a Lanczos filter low pass filter because it presents the strong advantage of filling small gaps of data taking into account the dynamic of the points apart from the gaps. It is shown to give better results than a Lanczos low pass filter near gaps and similar results elsewhere. To choose the spline smoothing factor a comparison between the two filtering methods was performed. The Lanczos cut-off frequency has indeed a real physical meaning, and is thus easier to estimate. Three complementary criteria were then observed to choose the final spline smoothing factor:

• Minimum standard deviation between the data filtered with he two metods

• Absence of strong non physical divergence for the spline

• Absence of local oscillations (this have been detected thanks to a relative comparison with a model method (see chapter on the comparison with the correction proposed by R Scharroo).

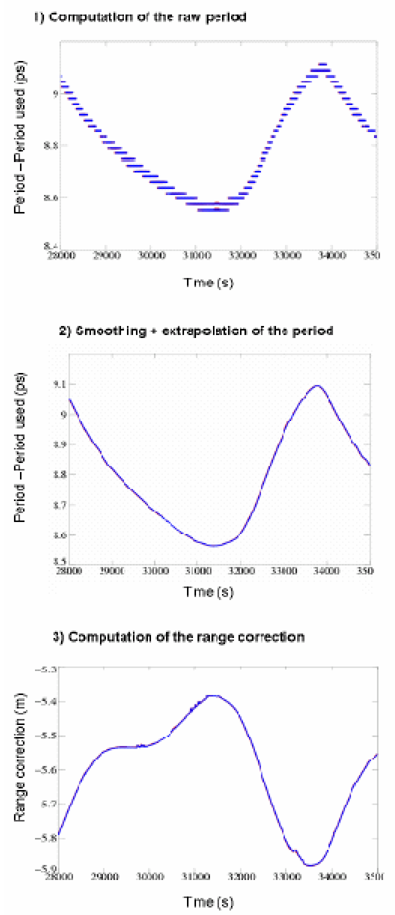

Figure 3. Raw period computation (top), filtering (middle) and conversion to range correction (bottom).

The USO range correction is then computed as follow with the equation:

$CorrUSO = Range.[Period(t) – Period_{GS}]/Period(t)$ (2)

where $Period_{GS}$ is the clock period used in the ground segment and equal to 12500ps for IPF versions up to V4.58. For data produced in more recent version before

11/03/2006, it is recomputed every 3 days to take into account the long term variations of USO clock period. After the 11/03/2006, this strategy was no more used and $Period_{GS}$ is set to 12499.999726000 ps.

4. QUALITY EVALUATION OF THE CORRECTED DATA OVER OCEANS

As seen in Figure 1, on the uncorrected SLA map, data are unusable without correction. The following monitoring shows that once corrected, data recover their nominal level of accuracy. Figure 4 shows an example of the SLA after correction. The monitoring of SLA (Figures 5) and SSH at crossovers (Figures 6) statistics shows a good consistency of the performances of corrected data before and after the anomaly. Another way of validating the correction consists in analysing relative performances of different corrections. The following part deals with a comparison between two possible approaches of correction.

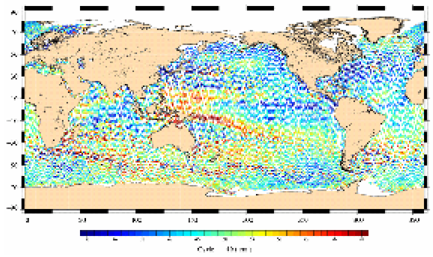

Figure 4. SLA corrected by the USO Correction on cycle 46 affected by the anomaly.

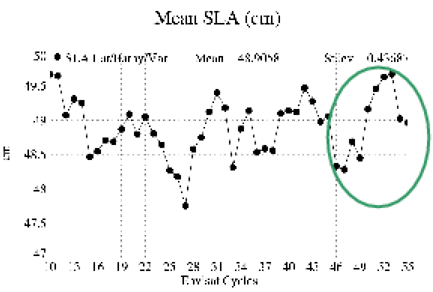

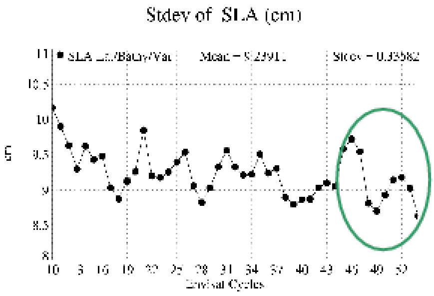

Figure 5. SLA average (top) and standard deviation (bottom) of corrected SLA. Cycles circled in green are affected by the anomaly.

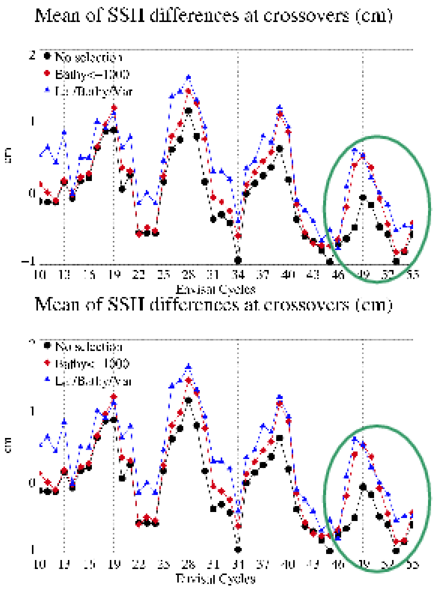

Figure 6. SSH at crossovers average (top) and standard deviation (bottom). Cycles circled in green are affected by the anomaly.

5. COMPARISON TO A MODEL BASED CORRECTION

Here, the operational correction is compared to a method based on a modelling of the USO period oscillation which was found to be strongly linked to the orbital period. It was proposed by Remko Scharroo and is detailed in [5]. This method is predictive, which can be a strong advantage in terms of operations for the generation of real time corrections. Because those methods are completely different, this relative comparison is a very good way for assessing the performance of the corrections. The performances are compared over the same data set over ocean using GDR data of Cycles 46 and 47. Thanks to either correction, the previously unusable altimetric data now have satisfactory performances. However, some fine differences are still evidenced. Figure 7 shows that the mean differences are weak (around 3mm). However, in case of strong variation of the USO period (after a switch off/on for example) this value can reach 10 cm (Figure 8).

Figure 9 shows that the geographical distribution of the difference between the two corrections is not homogeneous: the operational correction is slightly higher (of about 2-3 mm) than the predictive model's in the northern hemisphere whereas the situation is inverted in the Southern hemisphere. The variance of differences reaches 1cm2 around 40°S of latitude. Some higher values are also noticed along several passes. These passes corresponds to measurements just after a restart.

In order to compare the performance of the two methods, SSH differences at 10-day crossovers are computed. When looking at the mean SSH differences at crossovers, (see table 1), we see that the predictable model correction induces a strong bias compared to usual values whereas no bias is noticed when using the operational correction. This bias is due to some problems in the modelling method around 40°S of latitude. These errors implies systematic ascending/descending differences in these areas. The signature of these errors are also visible in Figure 9 (bottom).

Performance of SSH at crossovers	Operational Correction	Predictive model Correction
Cycle 46		
Number of Points	39406	39406
Mean	0.74 cm	1.55 cm
Standard Deviation	8.28 cm	8.41 cm
Mean Quadratic Error	8.31 cm	8.55 cm
Cycle 47		
Number of Points	26723	26723
Mean	-0.67 cm	-1.23 cm
Standard Deviation	7.93 cm	7.90 cm
Mean Quadratic Error	7.96 cm	8.00 cm

Table 1. Performance of SSH at crossovers for both Corrections. Cycles 46 and 47.

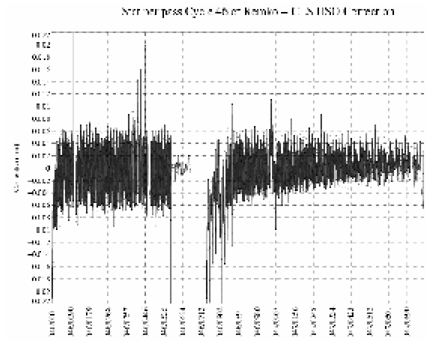

Figure 7. Average USO correction differences per pass for Cycle 46 and 47

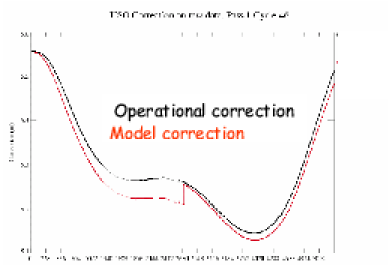

Figure 8. USO correction differences for the pass 1 of cycle 46.

To conclude, although the two corrections studied seem to have similar behaviours and to both provide a good correction of the data oscillations, the analysis presented here enables to lighten some differences. The predictive model, seems to need further tunings in order to better take into account rapid changes of the mean USO value in order to avoid the jumps between consecutive tracks. In addition to that, the bias it introduces between ascending and descending tracks should be further investigated and could probably be over turned with a different tuning of the model. Concerning the operational method, this study enabled to evidence very weak oscillations which drove to a refinement of the spline smoothing factor. After this refinement, the local oscillations are much smoothed and the performances of oceanographic parameters seem quiet close to the ones obtained before the anomaly period.

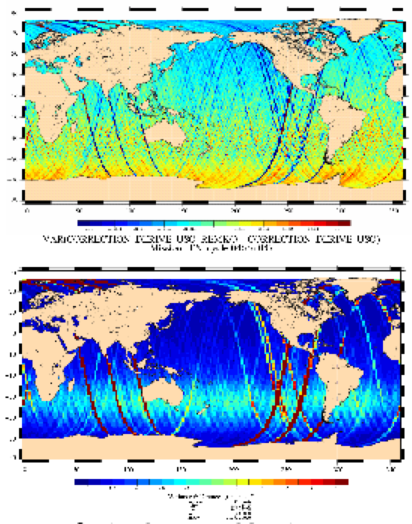

Figure 9. (Predictive model USO Correction - Operational USO Correction) mean differences (top) and standard deviation of differences

6. ANALYSIS OF THE VALIDITY OF THE LONG TERM DRIFT COMPONENT SEEN BY THE NEW CORRECTION

The aim of this section is to compare, on a non anomalous period, two methods of computing the USO corrections: a method using a step of 100s with a spline filter to the previous one, using a step of 86400s ([1]) with a three days interpolation of monthly averages. As expected, the first one is shown to follow more precisely the short terms variations such as recoveries after instrumental events. The other one is very much smoothed and only gives information on the long term drift.

As seen in Figure 10, for the analysed cycles, the drift can be approached by a linear increasing. The slopes of both methods are almost equal. Thanks to this study, it is therefore shown that the global long term drift is the same in both cases and that the short step method enables to recover the long term drift as well as the short term ones. This validates that a shorter step method does not loose any long term information.

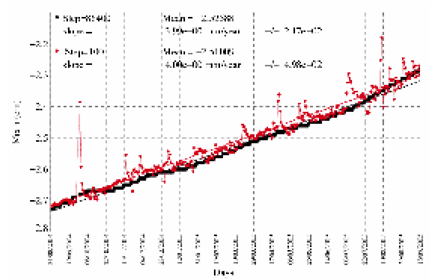

Figure 10. Mean per day of Correction Step=100s and Correction Step=86400s.

7. PRACTICAL USE OF THE TEMPORARY CORRECTION

This correction has been computed and developed operationally and delivered to the users since Cycle 46, see Figure 11). The correction concerning previous anomalies (Cycles 30, 44 and 45) were computed with the same method and also delivered to the users. There are three USO corrections for the different Envisat Level 2 altimetry data products:

• A NRT orbit basis USO correction for FDGDR products, available from http://earth.esa.int/pcs/envisat/ra2/auxdata/. The NRT USO correction is available from July 28, 2006 onwards.

• An Interim daily USO correction for IGDR products, available at the same F-PAC location as for IGDR, in the directory igdr ous corr.

• An OFL cycle USO correction for GDR products, available at the same F-PAC location as for GDR, in the directory gdr ous corr. Information on USO correction filename and format definition is available from: http://earth.esa.int/pcs/envisat/ra2/auxdata/NewCorrection.html. A software can be used to include the correction fields in the product themselves. It is available at the following address: http://earth.esa.int/pcs/envisat/ra2/auxdata/software/

This device is available under SUN and LINUX versions.

Note finally that users are advised to apply the correction auxiliary files even during the non-anomalous period in order to correct for the nominal ageing drift of the USO device.

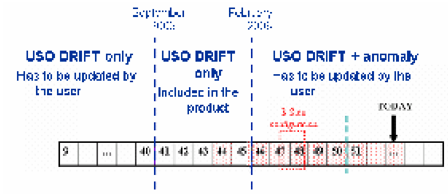

Figure 11. Chronology of USO Correction computation.

8. Conclusions

The USO anomaly is a major anomaly which strongly impacts the RA-2 quality data quality. An operational correction procedure has been implemented by the altimetry Data Processing and Quality Control (DPQC) team. Thanks to this temporary procedure the correction has allowed Ra-2 data to recover their nominal quality in real time since the 1st of August 2006.

An extensive validation was performed and enabled to show that the corrected data now had a nominal quality. The proposed method has also been validated by comparing to another method, a model based solution.

Soon, a finalized correction procedure will be implemented in the ground segment and the range will be directly corrected in the products themselves.

Acknowledgements

This work has been funded by ESA through Data Processing and Quality Control (DPQC) activities. The DPQC team would like to thanks Remko Scharroo who kindly provided the predictive model auxiliary files and who promptly sent fruitful feedbacks on the operational correction.

1. Celani, C.; Greco, B.; Martini, A.; Roca, M. Instruments corrections applied on RA-2 Level-1B Product. *Proceeding of the Envisat Calibration Workshop*. **2002**.

2. Faugere Y., A. Ollivier, Design and assessment of a method to correct the Envisat RA-2 USO *Technical Note OSME-DPQC-SEDA-TN-06-219*. **2006.**

3. Zanifé O.Z, Investigation on the USO range correction computation method. *Technical Note OSME-DPQC-SEDA-TN-06-XX*. **2006**.

4. Zanifé O.Z, Technical Note on Error on Delta Range Correction. *Technical Note OSME-DPQC-SEDA-TN-06-XX*. **2006**.

5. Scharroo Remko, RA-2 USO Anomaly: Predictive correction model. *Technical Note* . **2006.**